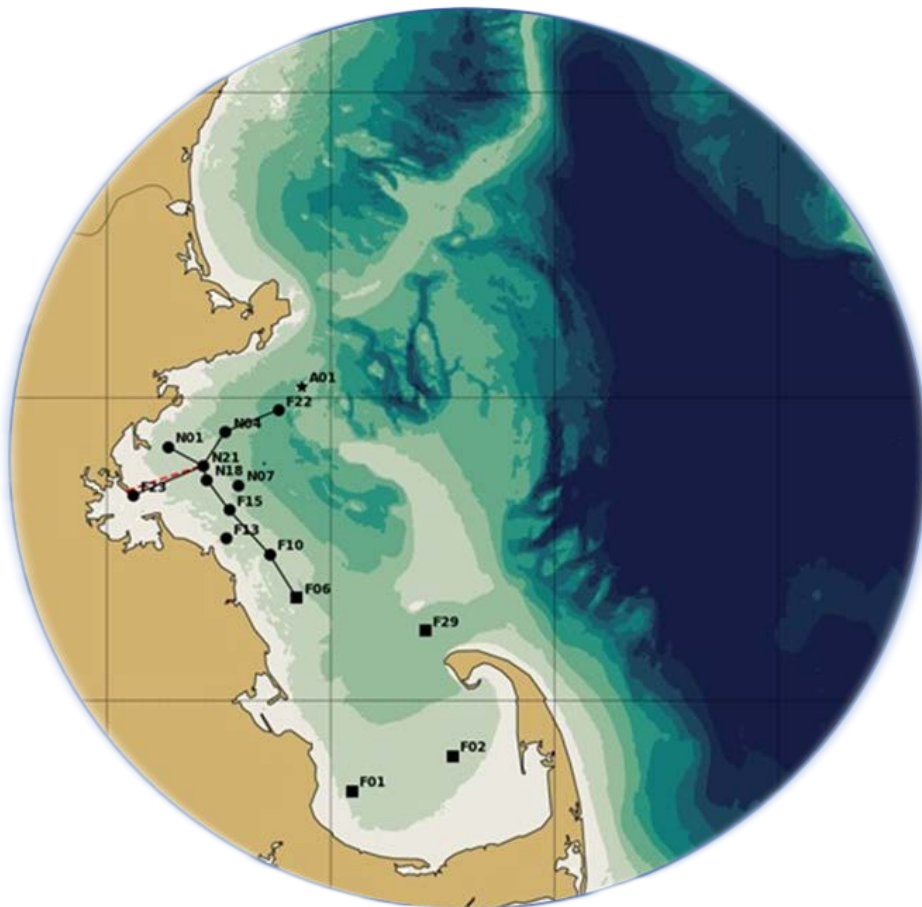




# Simulations of 2022 Hydrodynamics and Water Quality in the Massachusetts Bay System using the Bays Eutrophication Model



Massachusetts Water Resources Authority  
Environmental Quality Department  
Report 2024-07

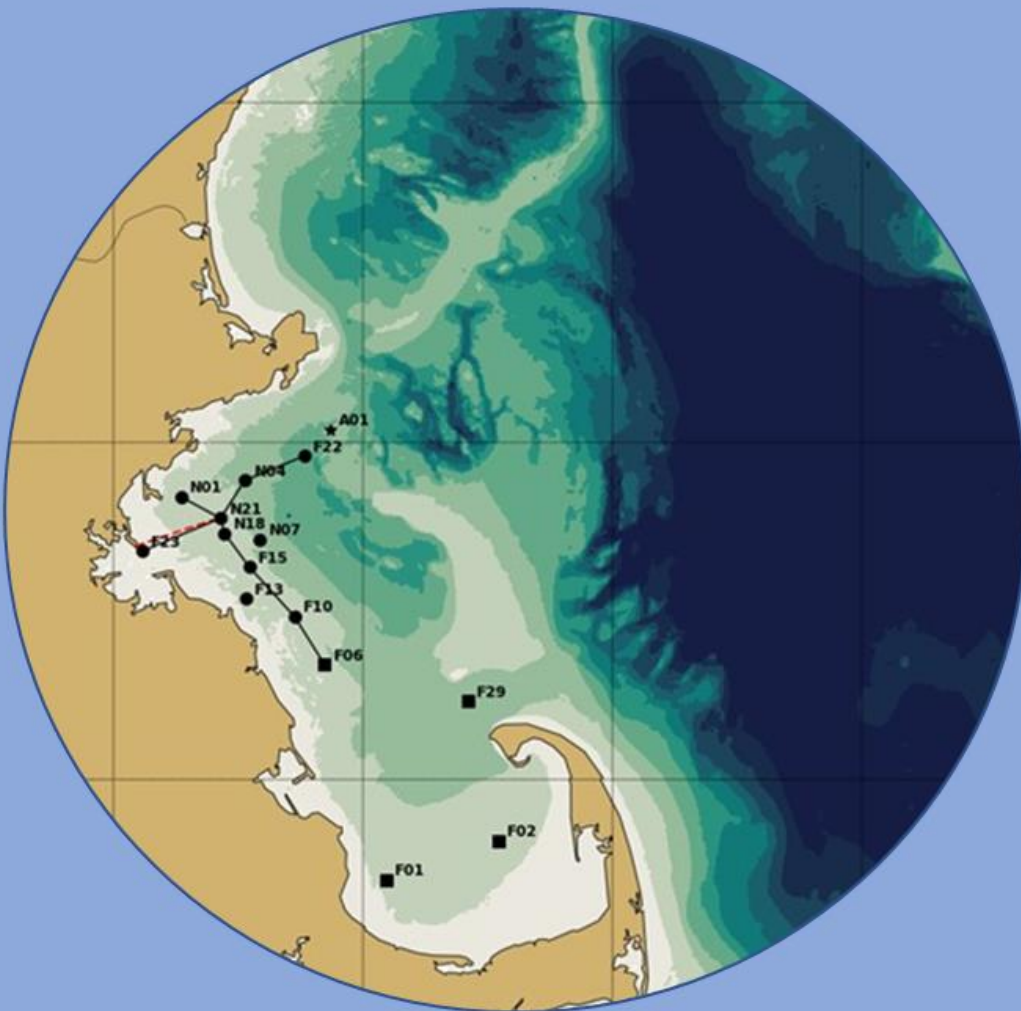


**Citation:**

Deltares, 2024. **Simulations of 2022 Hydrodynamics and Water Quality in the Massachusetts Bay System using the Bays Eutrophication Model.** Boston: Massachusetts Water Resources Authority. Report 2024-07. 82 p.

MWRA Environmental Quality Department reports can be downloaded from [www.mwra.com](http://www.mwra.com).

## Simulations of 2022 Hydrodynamics and Water Quality in the Massachusetts Bay System using the Bays Eutrophication Model



# Simulations of 2022 Hydrodynamics and Water Quality in the Massachusetts Bay System using the Bays Eutrophication Model

## Author(s)

Binglei Gong<sup>1</sup>  
Benjamin Munster<sup>1</sup>  
Lauriane Vilmin<sup>2</sup>  
Stendert Laan<sup>3</sup>  
Pradeep Mugunthan<sup>1</sup>

## Partners


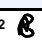
<sup>1</sup> Four Peaks Environmental and Data Solutions, AMHERST MA 01002, United States of America  
<sup>2</sup> Deltares, Delft, The Netherlands  
<sup>3</sup> Deltares USA, Silver Spring, MD, United States of America



|                  |  |
|------------------|--|
| <b>Client</b>    | MA Water Resources Authority - Massachusetts Water Resources Authority |
| <b>Contact</b>   | Ms Rogers  |
| <b>Reference</b> |  |
| <b>Keywords</b>  | updated BEM, 2022 simulations, hydrodynamics, water quality            |

| Document control   |                       |
|--------------------|-----------------------|
| <b>Version</b>     | 1.2                   |
| <b>Date</b>        | June 10, 2024         |
| <b>Project nr.</b> | 2243                  |
| <b>Document ID</b> | 11208511-002-ZKS-0002 |
| <b>Pages</b>       | 82                    |
|                    | final                 |

*The allowed use of this table is limited to check the correct order-performance by Deltares. Any other client-internal-use and any external distribution is not allowed.*

| Doc. version | Author   | Reviewer  | Approver   |
|--------------|--|---|--|
| 1.2          | Binglei Gong <sup>1</sup><br>Benjamin Munster <sup>1</sup><br>Stendert Laan <sup>3</sup><br>Lauriane Vilmin <sup>2</sup> W<br>Pradeep Mugunthan <sup>1</sup> | Jos van Gils <sup>2</sup>  | Toon Segeren <sup>2</sup> <br>Edwin Welles <sup>3</sup> |

#### Partners

<sup>1</sup> Four Peaks Environmental and Data Solutions, AMHERST MA 01002, United States of America

<sup>2</sup> Deltares, Delft, The Netherlands

<sup>3</sup> Deltares USA, Silver Spring, MD, United States of America

Deltares, 2024. Simulations of 2022 Hydrodynamics and Water Quality in the Massachusetts Bay System using the Bays Eutrophication Model, Deltares Ref. Nr. 11208511-002-ZKS-0001

Cover image: MWRA observation locations in Massachusetts Bay

# Summary

This report presents hydrodynamic and water quality model results for the Massachusetts Bays system (Massachusetts Bay, Cape Cod Bay, and Boston Harbor) during 2022. Treated effluent sent from the Massachusetts Water Resources Authority (MWRA) treatment plant through a 15 km (9.5 mi) long tunnel and released at an outfall offshore in Massachusetts Bay contains nutrients. Nutrients are necessary and important to support healthy and diverse marine ecosystems. However, excess nutrients can cause eutrophication, the overgrowth of phytoplankton (microscopic marine algae) that can degrade water quality and harm marine life by depleting oxygen when the phytoplankton decay. To address potential eutrophication and other concerns, MWRA maintains an extensive bay and harbor field monitoring program, which this modelling complements.

The hydrodynamic model simulates temperature, salinity, and currents, and is the foundation for the water quality model, which simulates key eutrophication parameters including nutrients, chlorophyll a (an indicator of the amount of phytoplankton), and oxygen. Deltares (2021) explains the methods. Hydrodynamic results for 2022 agree well with available observations and capture the geographic and vertical structure, and temporal variability, of temperature and salinity distributions and density stratification, as well as tidal and non-tidal currents. As in observations, temperature stratification in the 2022 simulation peaked in July and August. River flow in 2022 was lower than normal for most of the year and mid-June to mid-September saw the lowest flows of the 31-year monitoring program. Owing to this lower than typical summer river flow, observed and modeled salinity at the water surface (less than 5 m deep) was high.

The 2022 water quality simulation captured general patterns in observed seasonal variations, geographic distributions, and vertical structure for many variables. This included the late spring reduction in near-surface dissolved inorganic nitrogen (DIN) due to phytoplankton uptake, and its replenishment after mixing in fall due to cooling and storms. It also included seasonal dissolved oxygen variations, with peak values in spring at shallow depths due to colder water and phytoplankton growth, and late summer minima at depth where stratification inhibits reaeration by air-sea exchange. Modeled dissolved oxygen levels at the seafloor dropped at the end of the summer and beginning of fall, but not as low as observed dissolved oxygen levels, which were at historic minima at many stations by the end of the summer in 2022. Observations suggested there was a spring *Phaeocystis* bloom and in the model *Phaeocystis* appeared during this period. Additionally, a mid-summer dinoflagellate (*A. catenella*) bloom was observed in 2022 late June and was similarly predicted by the model. However, the modeled chlorophyll a levels were lower than the observed chlorophyll a levels.

The modeled DIN was elevated persistently within about 10 km (6 mi) of the outfall and intermittently as far as about 20 km (12 mi) away from the outfall, mainly due to ammonium in the treated effluent. The DIN projections were confirmed by observations. The model captured the observed vertical structure of the effluent influence, which reached the surface through the winter months and remained at depth from about April through October when the bay was stratified. During June through August, the highest simulated chlorophyll a concentrations occurred around the outfall indicating potential impact of the effluent. These higher concentrations were most likely enabled by exceptional 2022 summer environmental conditions in that area, such as weaker wind and less circulation than previous years. This pattern could not however be confirmed by the field data.

# Contents

|          |   |           |
|----------|---|-----------|
|          | <b>Summary</b>  | <b>5</b>  |
|          | <b>List of Figures</b>  | <b>8</b>  |
| <b>1</b> | <b>Introduction</b>   | <b>11</b> |
|          | 1.1 Background on oceanographic processes influencing water quality | 11        |
|          | 1.2 Summary of observed 2022 conditions                             | 13        |
| <b>2</b> | <b>Methods</b>  | <b>14</b> |
|          | 2.1 Updated methods   | 16        |
| <b>3</b> | <b>Forcing</b>  | <b>17</b> |
|          | 3.1 Wind, heat flux, solar radiation, and rivers                    | 17        |
| 3.1.1    | Wind  | 17        |
| 3.1.2    | Heat flux   | 17        |
| 3.1.3    | Solar radiation   | 18        |
| 3.1.4    | Rivers  | 18        |
|          | 3.2 Loading of organic carbon, nitrogen, and phosphorous            | 24        |
| <b>4</b> | <b>Hydrodynamic Model</b>   | <b>26</b> |
|          | 4.1 Verification of model performance                               | 26        |
|          | 4.2 Model-observation comparisons                                   | 29        |
| 4.2.1    | Time series of temperature and salinity                             | 29        |
| 4.2.2    | Spatial representation of temperature and salinity                  | 29        |
| 4.2.3    | Continuous measurements of temperature and salinity                 | 37        |
| 4.2.4    | Continuous measurements of non-tidal currents                       | 37        |
|          | 4.3 Model monthly-mean circulation                                  | 41        |
| <b>5</b> | <b>Water Quality Model</b>  | <b>44</b> |
|          | 5.1 Verification of model performance                               | 44        |
|          | 5.2 Model-observation comparisons                                   | 47        |
| 5.2.1    | Light extinction  | 47        |
| 5.2.2    | Dissolved inorganic nitrogen  | 49        |
| 5.2.3    | Chlorophyll a   | 53        |
| 5.2.4    | Particulate organic carbon (POC)                                    | 57        |
| 5.2.5    | Dissolved oxygen  | 61        |
| 5.2.6    | Primary production  | 66        |
| 5.2.7    | Fluxes to and from the sediment                                     | 68        |
|          | 5.3 Phytoplankton community composition                             | 71        |

|          |     |  |           |
|----------|-----|--|-----------|
|          | 5.4 | Conditions on West-East transect through outfall | 73        |
| <b>6</b> |     | <b>Synthesis/Application</b>                     | <b>77</b> |
| <b>7</b> |     | <b>Conclusion</b>                                | <b>78</b> |
|          |     | <b>References</b>                                | <b>80</b> |

# List of Figures

|  |    |
|--|----|
| Figure 1-1 Geography, bathymetry, schematic long-term mean circulation.  | 12 |
| Figure 2-1 Model grid of the entire model domain (left) and zoomed-in for Massachusetts Bay (right)  | 14 |
| Figure 2-2 Model bathymetry of the entire model domain (left) and zoomed-in for Massachusetts Bay (right)  | 14 |
| Figure 2-3 Schematic overview of all state variables and processes. Reproduced from Deltares (2021). Note that Inorganic Matter, Algae and Detritus affect light extinction in the water column.   | 15 |
| Figure 2-4 Location of MWRA monitoring locations (circles=Northern stations, squares=Southern stations, triangles=Harbor stations). The red dashed line indicates the tunnel to the outfall diffusers. The black lines are the West-East and North-South transects used for model-observation comparisons. The horizontal black dashed line represents the transect through the outfall on which model results are presented in later figures.   | 16 |
| Figure 3-1 Surface wind forcing, monthly averages, compared to prior 20-year period.   | 19 |
| Figure 3-2 Surface heat flux, compared to prior 10-year period.  | 20 |
| Figure 3-3 Solar radiation, compared to prior 20-year period.  | 21 |
| Figure 3-4 Merrimack River daily/cumulative discharge and anomaly relative to previous 20 years.   | 22 |
| Figure 3-5 Summed discharge of all modeled rivers (Saugus, Mystic, Charles, Neponset, North, and Jones) flowing directly in to Massachusetts and Cape Cod Bays.  | 23 |
| Figure 3-6 Organic Carbon (OC), Total Nitrogen (TN) and Total Phosphorus (TP) loads to Massachusetts and Cape Cod Bays in 2022. In the TN and TP plots, the darker sections of the bars represent the organic fractions. Left: loads from non-oceanic sources; percent of total is shown at top of each bar, and percent oceanic input (offshore boundary) shown at upper right. (Percentages correspond to summed organic and inorganic fractions.) Right: Deer Island Treatment Plant loads since 2017. OC=organic carbon; TN=total nitrogen; TP=total phosphorus. | 25 |
| Figure 4-1 Taylor diagrams of model quality for MWRA vessel-based survey observations.   | 28 |
| Figure 4-2 Temperature time series, model-observation comparison near surface (black) and seafloor (cyan).   | 31 |
| Figure 4-3 Temperature time series, model-observation comparison in water column (between surface and seafloor).   | 32 |
| Figure 4-4 Salinity time series, model-observation comparison near surface (black) and seafloor (cyan).  | 33 |
| Figure 4-5 Salinity time series, model-observation comparison in water column (between surface and seafloor).  | 34 |

|  |    |
|--|----|
| Figure 4-6 Temperature spatial structure, at/near sea surface, model-observation comparison.   | 35 |
| Figure 4-7 Temperature spatial structure, at/near seafloor, model-observation comparison.  | 35 |
| Figure 4-8 Salinity spatial structure, at/near sea surface, model-observation comparison.  | 36 |
| Figure 4-9 Salinity spatial structure, at/near seafloor, model-observation comparison.   | 36 |
| Figure 4-10 Time series of Mooring A01 temperature and salinity model-observation comparison (3-day means), at three depths (top two panels), and temperature and salinity differences between the 1m and 20m depths and 1m and 50m depths, as an indication of the stratification within the water column (lower two panels). | 38 |
| Figure 4-11 Currents time series model-observation comparison, Jan – Jun.  | 39 |
| Figure 4-12 Currents time series model-observation comparison, Jul – Dec.  | 40 |
| Figure 4-13 Model currents, monthly-mean spatial structure, at sea surface.  | 42 |
| Figure 4-14 Model currents, monthly-mean spatial structure, 15 m deep.   | 43 |
| Figure 5-1 Taylor diagrams for MWRA vessel-based survey observations. Top panels show the parameter Extinction and bottom panels Dissolved Inorganic Nitrogen. Left panels show results for the simulation period 2012-2016 and right panels for the year 2022.  | 45 |
| Figure 5-2 Taylor diagrams for MWRA vessel-based survey observations. Top panels show the parameter Chlorophyll a and bottom panels Dissolved Oxygen. Left panels show results for the simulation period 2012-2016 and right panels for the year 2022.   | 46 |
| Figure 5-3 Extinction time series, model-observation comparison for 2022. Model: lines. MWRA vessel-based survey observations: symbols.  | 48 |
| Figure 5-4 Dissolved Inorganic Nitrogen time series, model-observation comparison near surface (black) and seafloor (cyan). Model results: lines. MWRA vessel-based survey observations: symbols.  | 50 |
| Figure 5-5 Dissolved Inorganic Nitrogen time series, model-observation comparison within water column (between surface and seafloor). Model results: lines and full symbols. MWRA vessel-based survey observations: open symbols.  | 51 |
| Figure 5-6 Dissolved Inorganic Nitrogen ( $\mu\text{M}$ ) for 2022 along North-South (N-S) and West-East (W-E) transects (Figure 2-4). MWRA measurements are plotted with round symbols. Model results are 5-day averages around sampling date.  | 52 |
| Figure 5-7 Chlorophyll a time series, model-observation comparison near surface and seafloor. Model results: lines. MWRA vessel-based survey observations: symbols.  | 54 |
| Figure 5-8 Chlorophyll a time series, model-observation comparison within water column (between surface and seafloor). Model results: lines and full symbols. MWRA vessel-based survey observations: empty symbols.  | 55 |

|   |    |
|---|----|
| Figure 5-9 Chlorophyll a ( $\mu\text{g/L}$ ) for 2022 along North-South (N-S) and West-East (W-E) transects (Figure 2-4). MWRA measurements are plotted with round symbols. Model results are 5-day averages around the sampling date.  | 56 |
| Figure 5-10 Particulate Organic Carbon time series, model-observation comparison near surface and seafloor. Model results: lines. MWRA vessel-based survey observations: symbols.   | 58 |
| Figure 5-11 Particulate Organic Carbon time series, model-observation comparison within water column (between surface and seafloor). Model results: lines and full symbols. MWRA vessel-based survey observations: empty symbols.   | 59 |
| Figure 5-12 Particulate Organic Carbon ( $\mu\text{M}$ ) for 2022 along North-South (N-S) and West-East (W-E) transects (Figure 2-4). MWRA measurements are plotted with round symbols. Model results are 5-day averages around the sampling date. Frames without field observations are ARRS (Alexandrium) survey dates (7/6, 7/13, 7/20). | 60 |
| Figure 5-13 Dissolved Oxygen time series, model-observation comparison near surface and seafloor. Model results: lines. MWRA vessel-based survey observations: symbols.   | 62 |
| Figure 5-14 Dissolved Oxygen time series, model-observation comparison in water column. Model results: lines and full symbols. MWRA vessel-based survey observations: open symbols.   | 63 |
| Figure 5-15 Dissolved Oxygen time series 50.5m deep at A01 mooring site, model-observation comparison for 2022.   | 64 |
| Figure 5-16 Dissolved Oxygen ( $\text{mg/L}$ ) for 2022 along North-South (N-S) and West-East (W-E) transects (Figure 2-4). MWRA measurements are plotted with round symbols. Model results are 5-day averages around the sampling date.  | 65 |
| Figure 5-17 Simulated (lines; 2022) and observed (box-whiskers; 1995-2010) primary production.  | 67 |
| Figure 5-18 Simulated (line; 2022) and observed (box-whiskers; 2001-2010) sediment flux of ammonium. Note change of scale between the Boston Harbor stations (left) and Mass Bay stations (right).  | 69 |
| Figure 5-19 Simulated (line; 2022) and observed (box-whiskers; 2001-2010) sediment oxygen demand. Note change of scale between the Boston Harbor stations (left) and Mass Bay stations (right).   | 70 |
| Figure 5-20 Simulated phytoplankton biomass time-series. Biomasses of the 4 simulated species groups (dinoflagellates, other flagellates, diatoms and Phaeocystis) are stacked.   | 72 |
| Figure 5-21 Dissolved Inorganic Nitrogen ( $\mu\text{M}$ ) for 2022 along west-east transect (Figure 2-4). Horizontal axis is distance eastward from coast; black triangle indicates the location of the outfall on the seafloor.   | 74 |
| Figure 5-22 Chlorophyll a ( $\mu\text{g/L}$ ) for 2022 along west-east transect (Figure 2-4). Horizontal axis is distance eastward from coast; black triangle indicates the location of the outfall on the seafloor.  | 75 |
| Figure 5-23 Dissolved Oxygen for 2022 along west-east transect (Figure 2-4). Horizontal axis is distance eastward from coast; black triangle indicates the location of the outfall on the seafloor.   | 76 |



# 1 Introduction

The Massachusetts Water Resources Authority (MWRA) has established a long-term monitoring program to evaluate the impact of its sewage treatment plant effluent on the water quality and ecosystem function of Massachusetts Bay, Cape Cod Bay, and Boston Harbor. The monitoring program primarily consists of a series of ongoing field observation surveys and includes complementary water quality modeling as required by the discharge permit (No. MA0103284). The water quality simulations are carried out using the Bays Eutrophication Model (BEM, Deltares, 2021). This report presents simulation results for the 2022 calendar year.

## 1.1 Background on oceanographic processes influencing water quality

Massachusetts Bay and Cape Cod Bay (Figure 1-1) comprise a temperate coastal embayment system. Readers unfamiliar with the geography and/or the current understanding of the physical and biological oceanographic processes characterizing the system are referred to the introductory summaries found in sections 1.2 and 1.3 of MWRA Technical Report 2011-13 (Zhao et al., 2012), in the annual MWRA water column monitoring reports (e.g., for calendar year 2022, Libby et al., 2023), and in references cited by them. All MWRA Technical Reports, including those just cited, are available online at <http://www.mwra.state.ma.us/harbor/enquad/trlist.html>. A brief summary follows here. In this subsection, the focus is on processes and influences other than effluent from the MWRA outfall, which has been shown in past studies to have a minor system-wide effect.

System hydrodynamics are characterized by a persistent general circulation pattern driving the flow of offshore Gulf of Maine waters into Massachusetts Bay via the Western Maine Coastal Current off Cape Ann, then southward before returning offshore just to the north of Cape Cod, with a portion of the flow first passing through Cape Cod Bay to the south (Figure 1-1). Rough estimates of the water residence time are about a month based on the surface currents, somewhat longer at mid-depth or deeper, where currents are weaker, and also longer in Cape Cod Bay than in Massachusetts Bay. While this slow general circulation is important in determining long-term average transport pathways, superposed on it are stronger and more variable wind-driven currents, and oscillatory tidal motions. Temperatures follow the characteristic temperate seasonal pattern of minima in late winter and peaks in late summer. Salinities are freshest inshore and in the upper several meters; in addition to the influence of offshore oceanographic conditions, salinities vary mainly in response to riverine inputs including primarily those brought by the Western Maine Coastal Current and the Merrimack River outflow to the north, and to a lesser extent the smaller amounts delivered via Boston Harbor. There is a seasonal cycle in vertical structure that includes transitions between well-mixed conditions, present from fall through early spring due to higher winds and atmospheric cooling, and strong density stratification during the late spring and summer due mainly to increased surface temperatures resulting from atmospheric heating.

The biology of the system is plankton-based and exhibits clear seasonal cycles that are tied closely to those hydrodynamic features, but with more pronounced spatial and interannual variability. Phytoplankton abundance typically peaks most strongly during bloom-favorable conditions in the late winter and early spring, as temperatures rise, light increases, and nutrients remain plentiful near the surface due to the active vertical mixing. Following the transition from spring to summer, near-surface nutrient concentrations become depleted as density stratification impedes the vertical mixing that replenishes them. Zooplankton abundance and biomass generally peak in late summer, following the

spring increase in phytoplankton prey levels. Primary productivity is commonly sustained at modest levels through summer and typically there is a second increase in phytoplankton during fall, when vertical mixing increases again and delivers nutrients to the surface while temperature and light conditions are still favorable before winter. Dissolved oxygen (DO) concentrations are influenced by a combination of biological and physical processes. There is a seasonal DO peak in late spring, which occurs from a combination of phytoplankton production and strong reaeration of the water during the winter months. Then, DO concentrations decrease to a late summer minimum due to respiration and reduced reaeration. The summer oxygen minimum is lower at depth, where stratification limits reaeration.

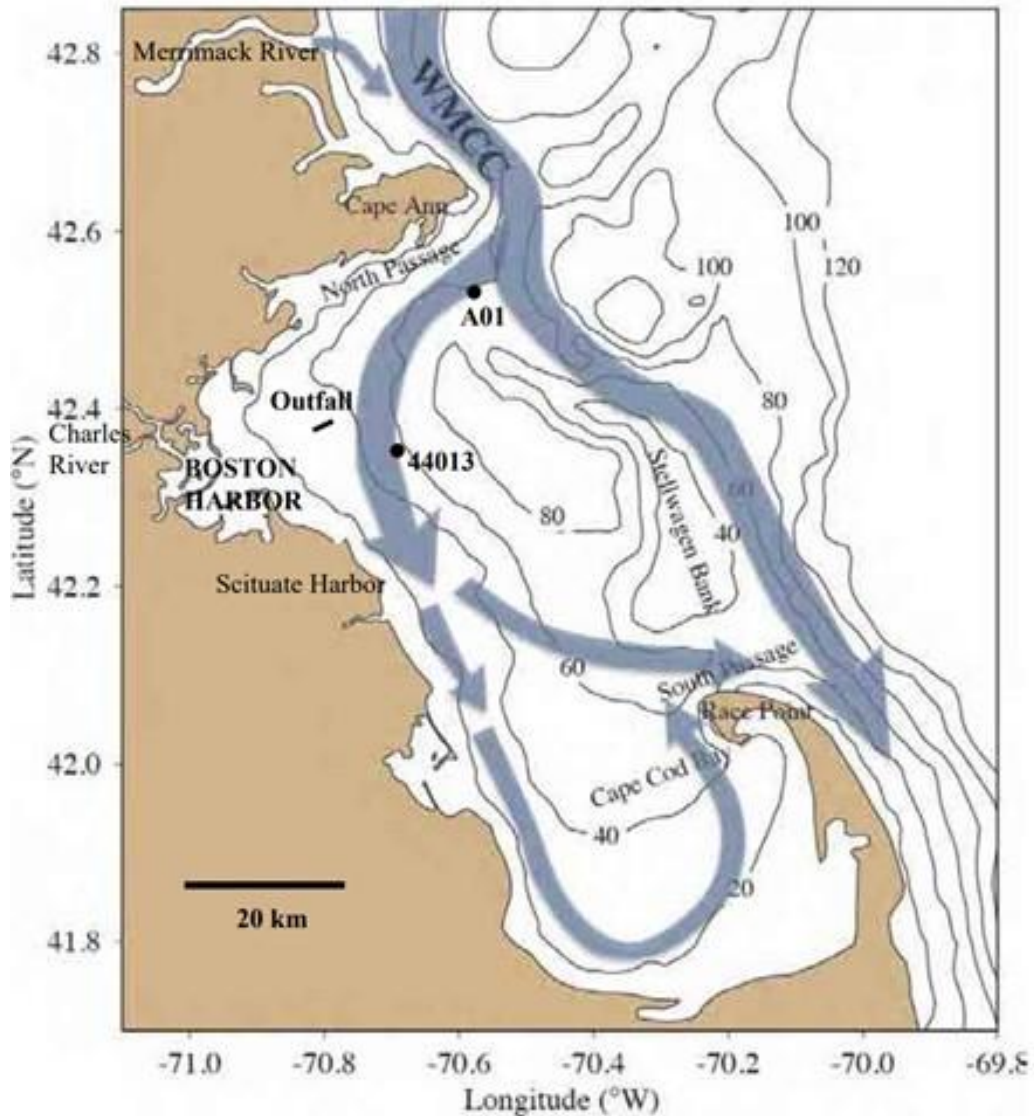


Figure 1-1 Geography, bathymetry, schematic long-term mean circulation.

WMCC = Western Maine Coastal Current. A01 = Oceanographic mooring (Northeastern Regional Association of Coastal and Ocean Observing Systems). 44013 = Weather buoy (National Data Buoy Center). Contours = water depth in meters. Figure from Zhao et al. (2017), adapted from Xue et al. (2014).

## 1.2 Summary of observed 2022 conditions

To provide context for descriptions of model simulations of 2022 throughout this report, a brief summary is given here of observed 2022 conditions based on monitoring results (Libby et al., 2023). In February, fewer measurements were collected than usual due to staff reductions during the COVID pandemic.

- River flow in 2022 was relatively high during the winter, but the river flows during June through October were among the lowest flows of the 31-year monitoring program, resulting in unusually high surface salinities.
- Surface temperatures were generally above historical levels but dropped in July and August due to upwelling.
- Total phytoplankton abundances were at or above long-term levels, mainly due to a winter/spring bloom of *Skeletonema* and *Pseudo-nitzschia*, followed by a May bloom of *Prorocentrum* and an October bloom of mixed centric diatoms. Dinoflagellates are the only phytoplankton functional group that appears to be increasing in recent years, mainly due to *Karenia mikimotoi* (not included in the model), but there was not a significant bloom of *Karenia* in 2022. A large *Alexandrium catenella* bloom peaked in late June and was observed to decline in abundance through late July.
- Chlorophyll concentrations were relatively low aside from elevated levels observed during the March survey.
- Bottom water (within 5m of the sea floor) dissolved oxygen (DO) concentrations were low throughout Massachusetts Bay, declining through the summer with no wind-driven mixing events. Strong wind events were not seen consistently until mid-November, so bottom water DO continued to decline to historic minima at many stations in September and October.

## 2 Methods

A complete model description is documented in MWRA's technical report 2021-02 and its appendices (Deltares, 2021). The model is set up in the Delft3D Flexible Mesh Suite, developed by Deltares. Technical details on the model set-up, its grid and forcing is presented in Appendix A of Deltares (2021). A description of the software package and underlying hydrodynamic and water quality equations are available in Section A1 of Deltares (2021), and in Deltares (2019a, b). The model was calibrated using the years 2012-2016, as described in Appendix B of Deltares (2021). The results of the model validation are given in the main report body of Deltares (2021).

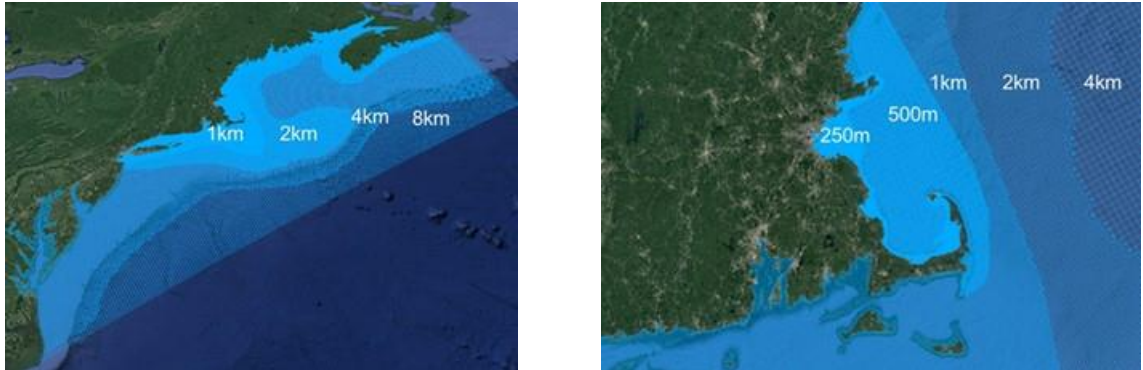


Figure 2-1 Model grid of the entire model domain (left) and zoomed-in for Massachusetts Bay (right)

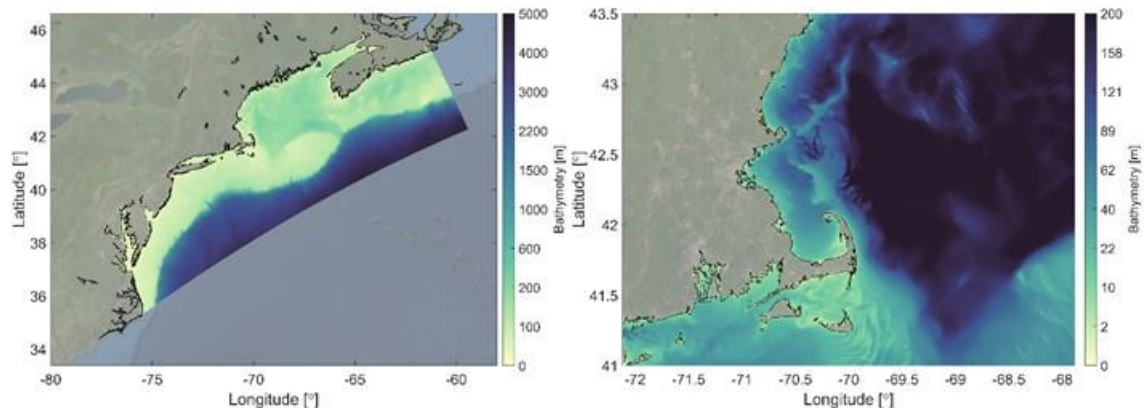


Figure 2-2 Model bathymetry of the entire model domain (left) and zoomed-in for Massachusetts Bay (right)

The model domain is large in order to best handle influences of offshore boundaries, as explained in Deltares (2021); it covers the entire Gulf of Maine region as well as the coastal region to the south, down to and including Chesapeake Bay (Figure 2-1 and Figure 2-2). Model performance in comparison to field measurements has been demonstrated most carefully in the area of Massachusetts Bay nearest the outfall, using MWRA observations (Deltares, 2021). The horizontal resolution is roughly 8km at the open ocean and is gradually refined toward the coast, with the highest minimum resolution of 250m in Boston Harbor and along the surrounding coastline, which includes the outfall location.



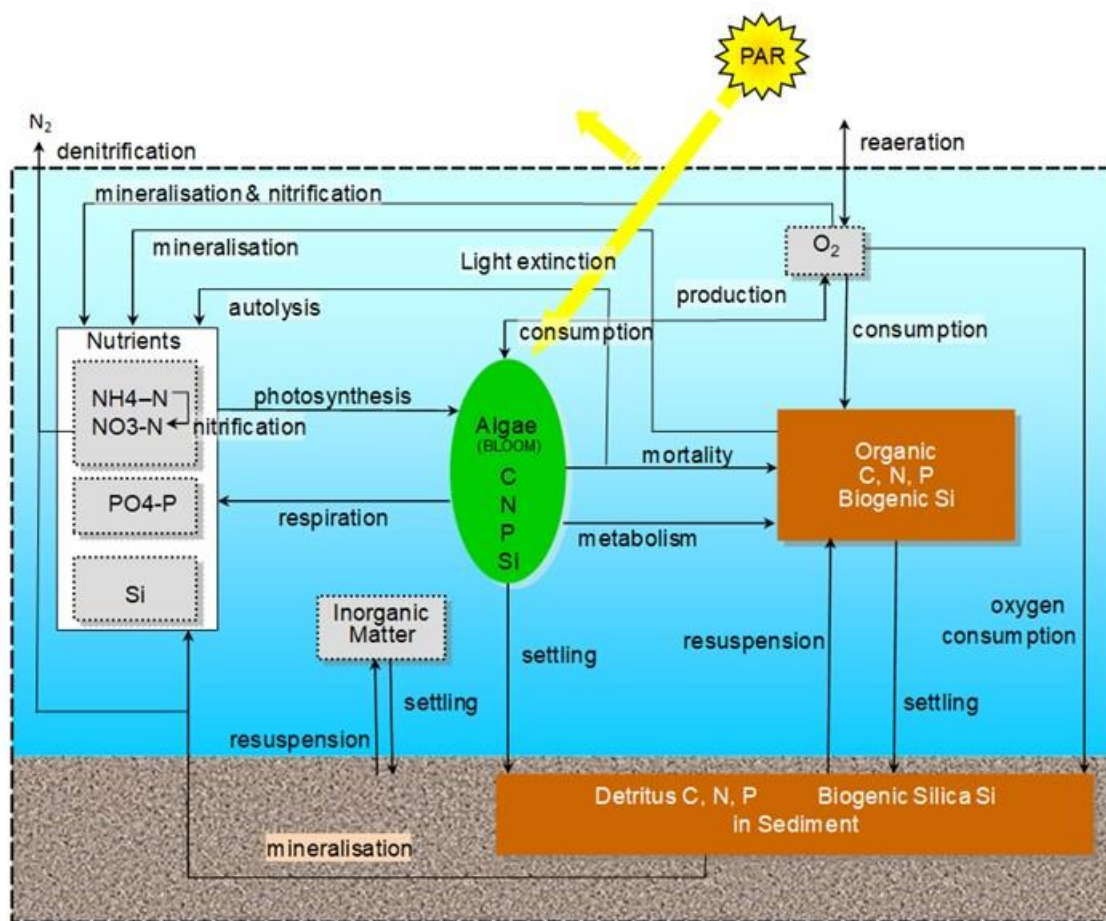


Figure 2-3 Schematic overview of all state variables and processes. Reproduced from Deltares (2021). Note that Inorganic Matter, Algae and Detritus affect light extinction in the water column.

Figure 2-3 provides an overview of the simulated state variables and processes for the water quality component. Four functional groups of pelagic phytoplankton are simulated (“Algae” in the figure): diatoms, dinoflagellates, other flagellates, and *Phaeocystis*.

The monitoring stations used to assess model performance and the transects along which water quality variables are examined are mapped in Figure 2-4. Model-observation comparison time-series are plotted for a representative selection of eight stations: N01 in the Northern Mass Bay, F22 with a greater oceanic influence, F23 near the outlet of Boston Harbor, N18 close to the MWRA outfall, N07 southeast of the outfall, F13 and F06 toward the south shore, and F02 in Cape Cod Bay.

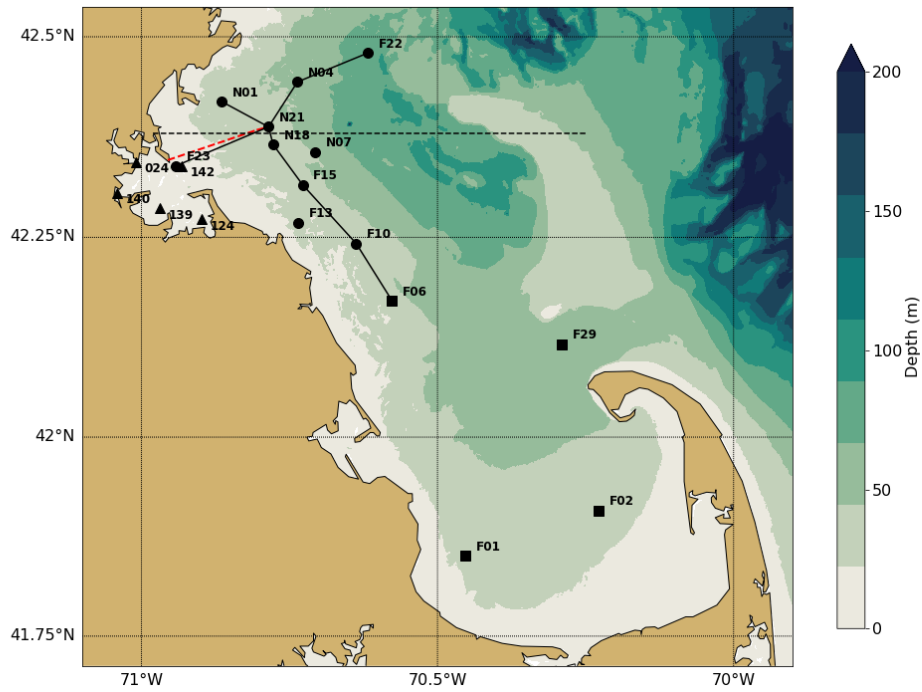


Figure 2-4 Location of MWRA monitoring locations (circles=Northern stations, squares=Southern stations, triangles=Harbor stations). The red dashed line indicates the tunnel to the outfall diffusers. The black lines are the West-East and North-South transects used for model-observation comparisons. The horizontal black dashed line represents the transect through the outfall on which model results are presented in later figures.

## 2.1 Updated methods

In the 2022 BEM run, no changes to the methods were implemented. The same model set-up and data handling as used for the 2021 BEM run (Deltares, 2023) was applied.

# 3 Forcing

## 3.1 Wind, heat flux, solar radiation, and rivers

### 3.1.1 Wind

In Figure 3-1, the main characteristics of the monthly-mean wind forcing for the simulated year 2022 are compared to the means of the previous 20 years (2001-2021) for the A01 mooring location off Cape Ann (Figure 1-1). Ranges of the standard deviation and of the minimum and maximum values are also shown.

The seasonal pattern of the vector-averaged velocities (top frame) largely followed the long-term mean. Notable differences were visible in the months of March, September, and October. In March winds were directed more north-eastward compared to long-term average direction of south-eastward. In September and October, the winds were largely oriented southward, while the long-term average directions were southwest and southeast in September and October, respectively.

Wind speeds (second frame) were comparable to, or lower than, the long-term mean in February, June through August, and October through December. In January, March through May, and September the wind speeds were higher than the long-term mean. Monthly-mean wind stress magnitudes (third frame) show a similar pattern to wind speeds (second frame). The mean wind stresses were comparable to the 20-year maximum in January and May. North-south wind stresses (bottom frame) are an indicator for upwelling. North-south wind stress was comparable to or weaker than normal in nearly all 2022 except for November and December. North-south wind stress was comparable to, or even weaker, than the 20-year minimum in January and May. This is in agreement with 2022 observations of weaker upwelling than typical until mid-November.

### 3.1.2 Heat flux

A comparison between time series of the calculated net air-sea heat flux (including solar radiation) for 2022 and for the previous years is given in Figure 3-2. A moving average with a window of 3 days is applied to visualize the instantaneous values. A positive net flux value indicates the net heat exchange is from air to sea. The time series of the net flux includes ranges of the standard deviation from the mean and of the minimum and maximum values. The cumulative flux (middle frame) is presented without any filtering.

The seasonal pattern in 2022 (top frame) showed an overall negative heat flux in winter (loss of heat from the surface, cooling of the ocean) and an overall positive heat flux in summer (heating of the ocean). The 2022 net flux was generally comparable to the long-term patterns and within one standard deviation of the long-term mean for most of the year except for portions of late January (more heat loss than usual) and mid-July to mid-August (more heat gain than usual).

The cumulative flux (middle frame) In 2022 was slightly lower than the long-term mean from mid-January to mid-August. From mid-August to the end of 2022, the cumulative flux has a similar value as the long-term mean. The same pattern was visible in the cumulative anomaly of the heat flux (bottom frame).

### 3.1.3 Solar radiation

The solar radiation from the meteorological forcing product is given in Figure 3-3. The solar radiation was similar to the long-term mean in most months. It was above average for most of August and September, causing an increase in the cumulative flux, which remained at about  $+0.1 \text{ GJ m}^{-2}$  until the end of the year. So, on an annual-mean basis, 2022 had slightly more incident surface solar radiation than a typical year.

The slightly higher than average net surface heat flux in 2022 was consistent with the slightly higher than average incident radiation in 2022. Every year there is a net influx of solar radiation of about  $5.5 \text{ GJ m}^{-2}$  (Figure 3-3, middle frame). Since the net air-surface heat flux was about  $0.5 \text{ GJ m}^{-2}$  in 2022 (Figure 3-2, middle frame), around  $5.0 \text{ GJ m}^{-2}$  was lost through other air-sea heat fluxes. These fluxes consist of evaporative and convective turbulent fluxes or long wave radiation.

### 3.1.4 Rivers

In Figure 3-4 the volume transport for Merrimack River is presented. The figures include the daily-averaged discharges (top frame) for the simulated year 2022 and for the previous 20 years (2001-2021). Ranges of the standard deviation and of the minimum and maximum values are also given.

The discharge in the Merrimack River was mostly comparable to the long-term mean in the first three months of the year except for a runoff event in late February that produced flows higher than one standard deviation above the long-term mean. From April to November, flow was mostly lower than average with flows as low as one standard deviation below the long-term mean from mid-June to mid-September. In December there were several runoff events including one in late December that produced flows that exceeded the long-term maximum flow. This was visible in the total discharged volume (middle frame), which was comparable to the long-term mean in January, then slightly above the long-term mean due to the runoff event in late February, and remained lower than the long-term mean from May to the end of year. The deviation (from the long-term mean) gradually increased starting in May due to the sustained lower-than-average flow conditions from April to November. The largest anomaly of the discharged volume (bottom frame) in 2022 was negative with a value of about  $-2.0 \text{ km}^3$  in mid-December. By the end of 2022 the anomaly was about  $-1.6 \text{ km}^3$ .

The combined volume transport for the rivers discharging directly to Massachusetts Bay and Cape Cod Bay is presented in Figure 3-5. These rivers are Saugus, Mystic, Charles, Neponset, North, and Jones. The pattern of the combined discharge was similar to the pattern of discharge from the Merrimack River. The discharged volume was lower than the long-term mean from May to the end of the year. This resulted in a maximum negative anomaly of the discharged volume (bottom frame) of  $-0.3 \text{ km}^3$  in mid-December. By the end of 2022 the anomaly was about  $-0.28 \text{ km}^3$ .



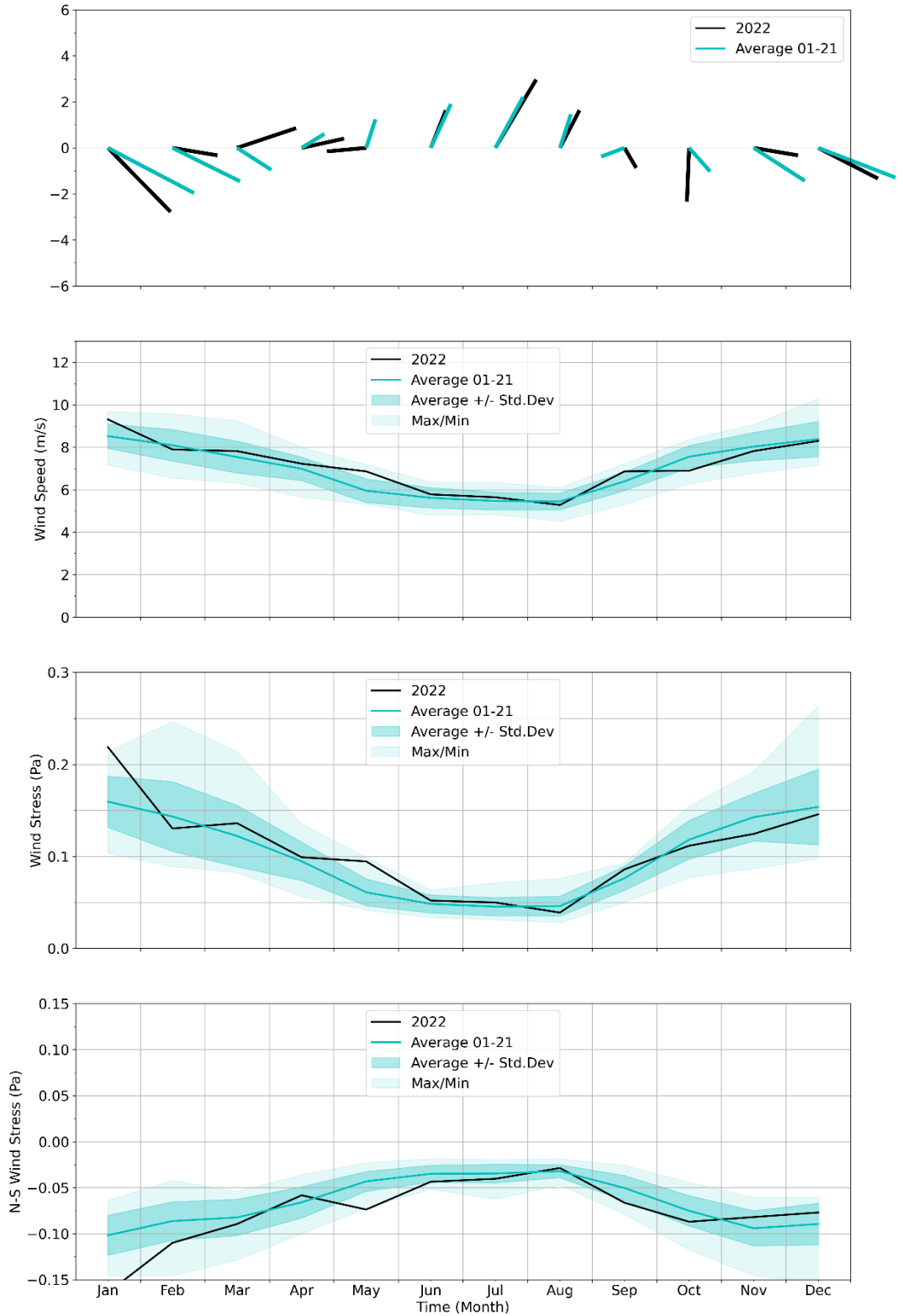


Figure 3-1 Surface wind forcing, monthly averages, compared to prior 20-year period.

Top frame: Vector-averaged wind velocities. Second frame: Wind speed. Third frame: Wind stress magnitude. Bottom frame: North-south component of wind stress, an indicator for wind-driven upwelling.

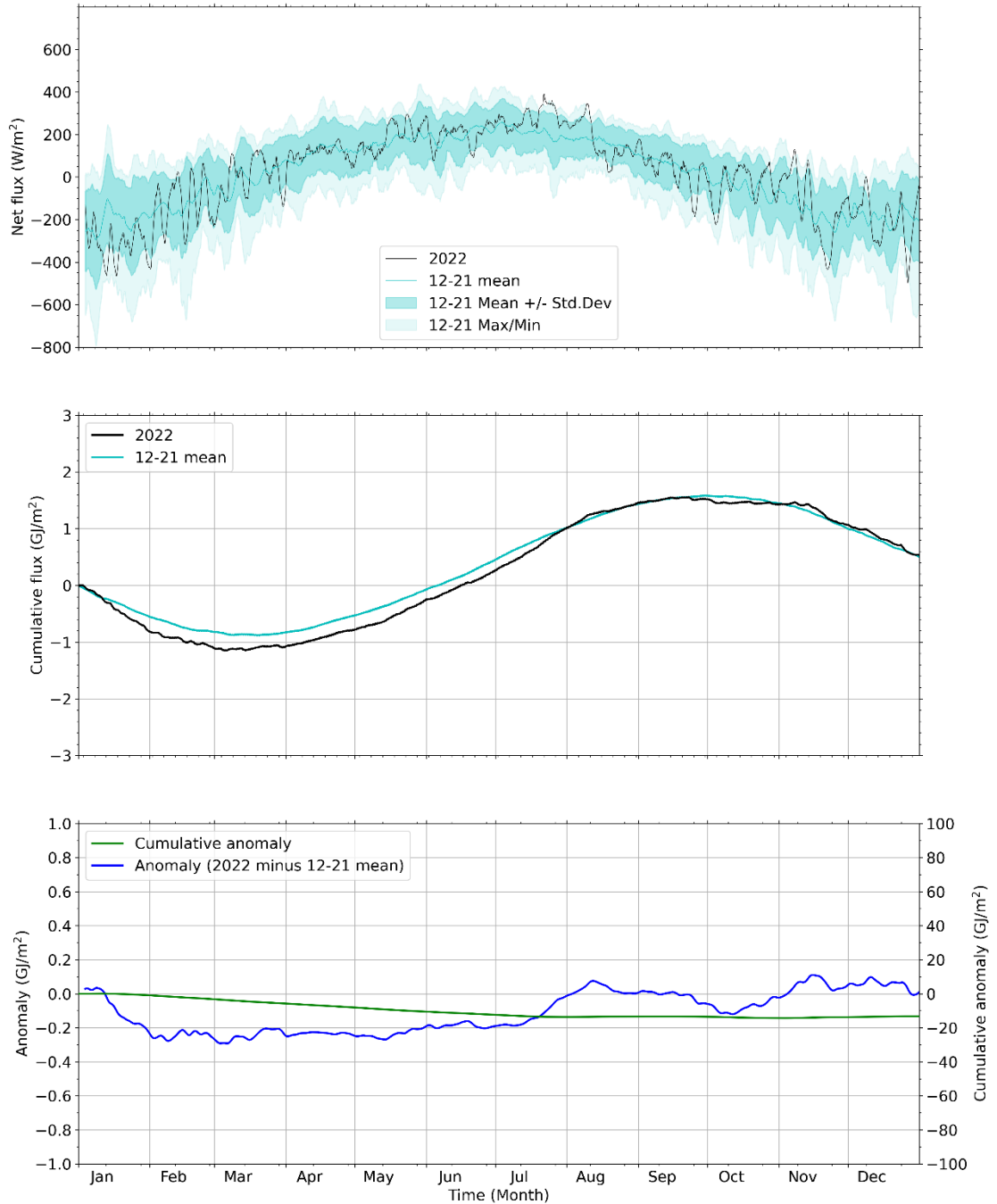


Figure 3-2 Surface heat flux, compared to prior 10-year period.

Top frame: Net heat flux into ocean. Middle frame: Cumulative net heat flux starting from January 1. Bottom frame: Anomaly (blue, left axis) and cumulative anomaly (cumulative sum of daily mean anomaly; green, right axis) of 2022 net cumulative heat flux relative to 2012-2021 average. The 2012-2021 reference period has been used because direct simulation output is available; it is shorter than the 20 years used for the long-term mean.

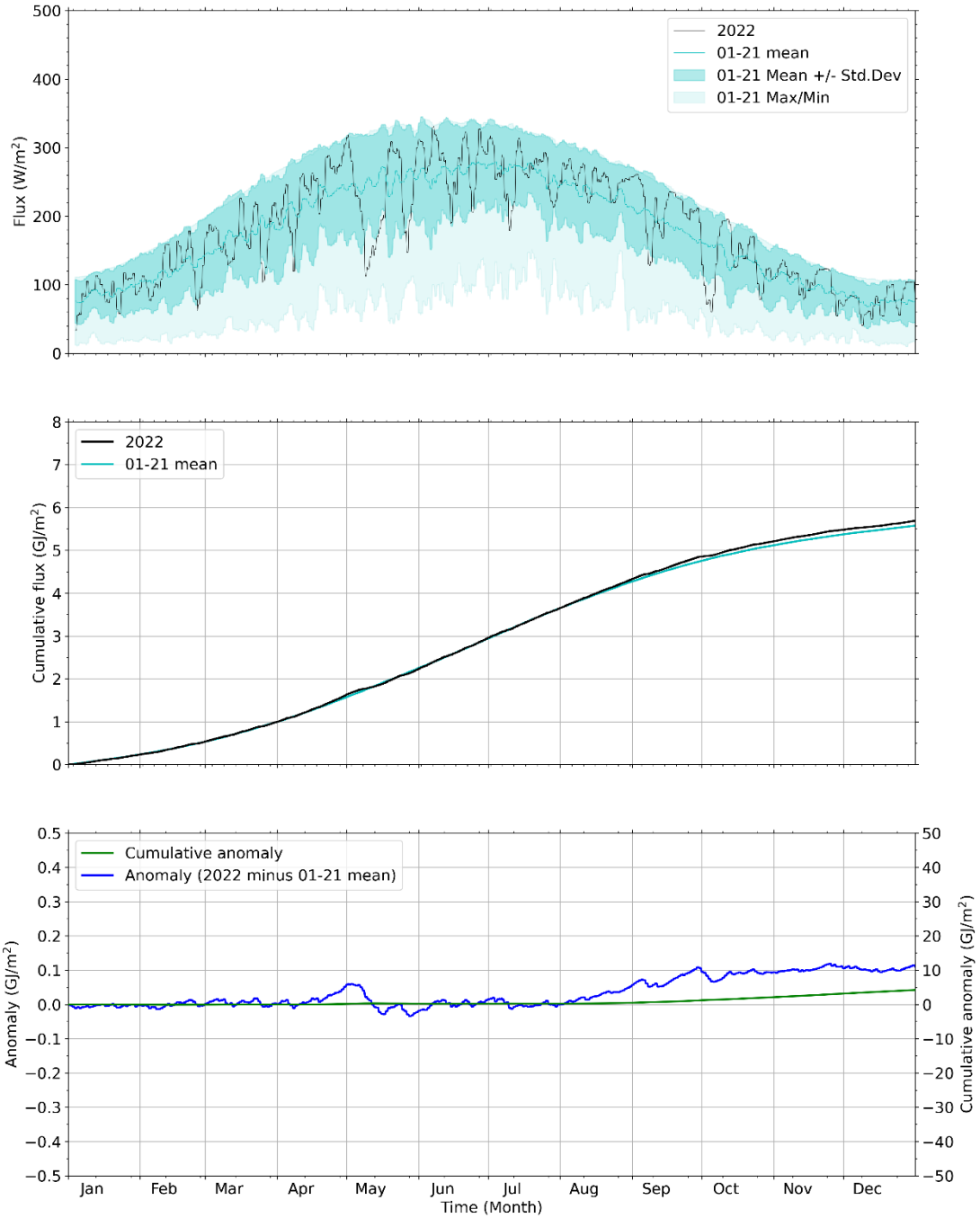


Figure 3-3 Solar radiation, compared to prior 20-year period.

Top frame: Solar radiation into ocean. Middle frame: Cumulative solar radiation starting from January 1. Bottom frame: Anomaly and cumulative anomaly (cumulative sum of daily mean anomaly) of 2022 cumulative solar radiation relative to 2001-2021 average.

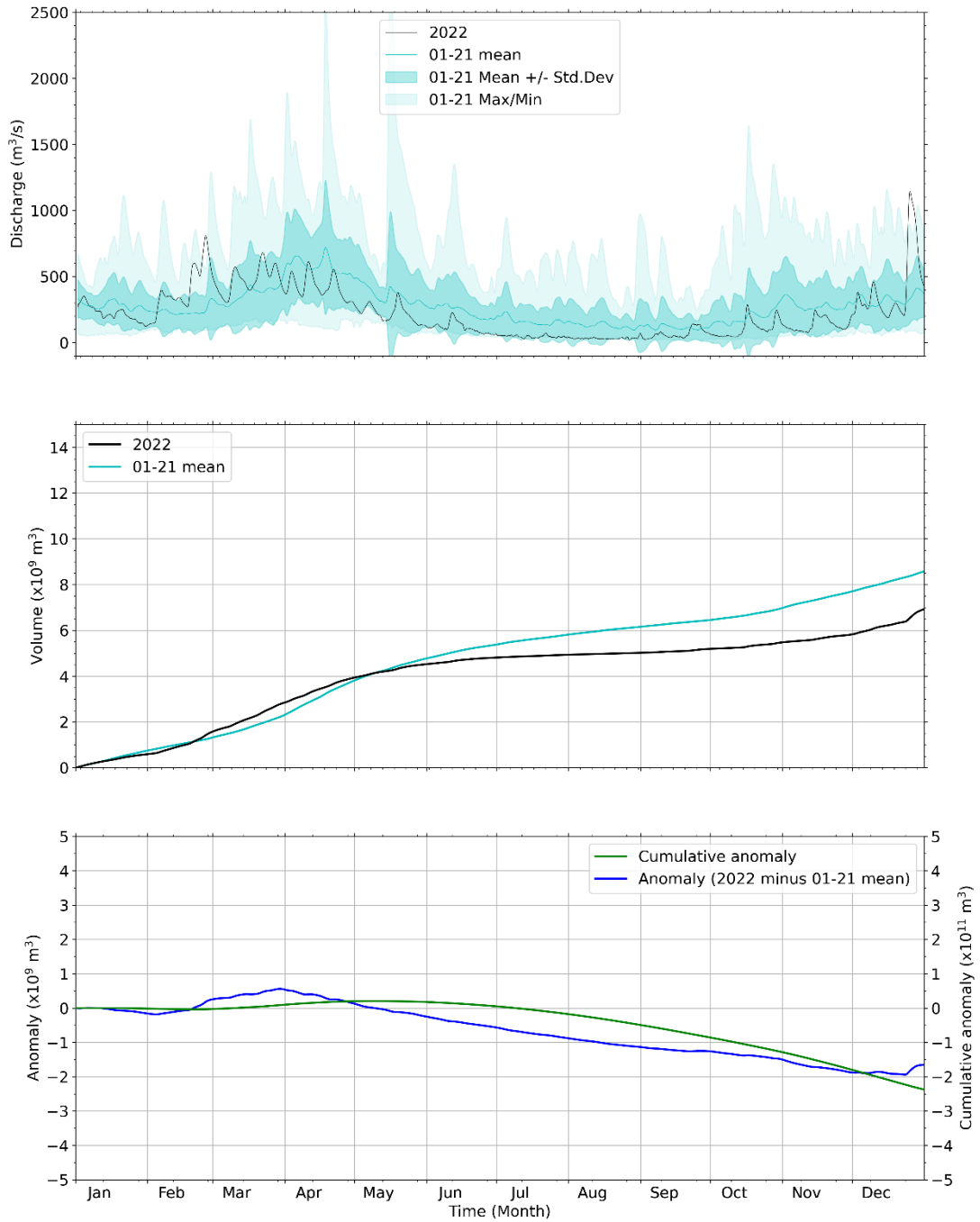


Figure 3-4 Merrimack River daily/cumulative discharge and anomaly relative to previous 20 years.

Top frame: Merrimack River discharge. Middle frame: Cumulative discharge relative to January 1. Bottom frame: Anomaly and cumulative anomaly (cumulative sum of daily mean anomaly) of discharge in 2022 relative to 2001-2021 average.

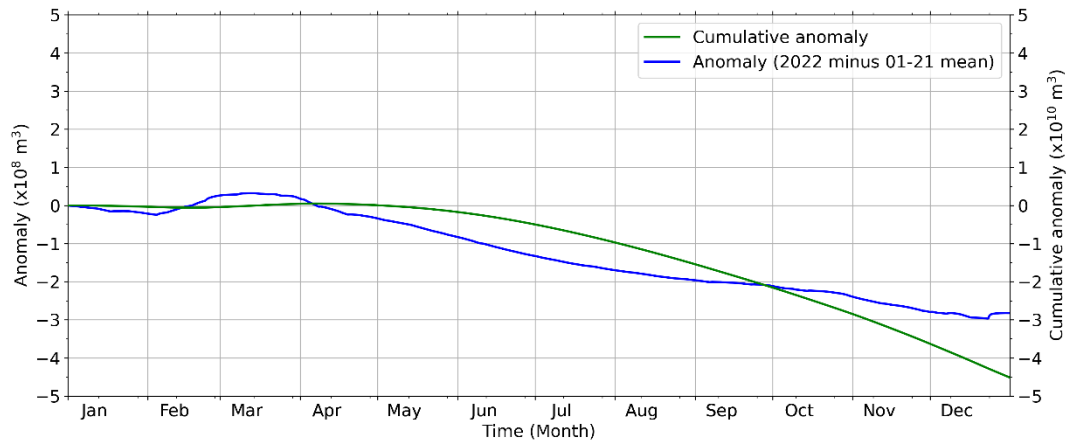
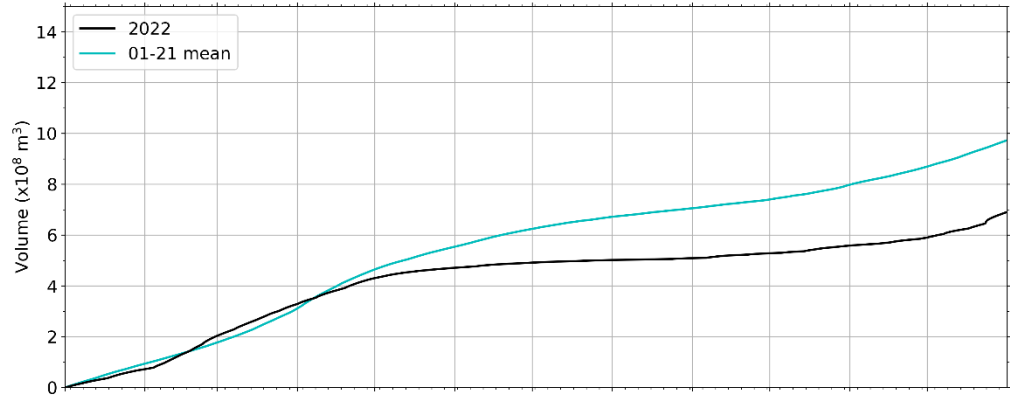
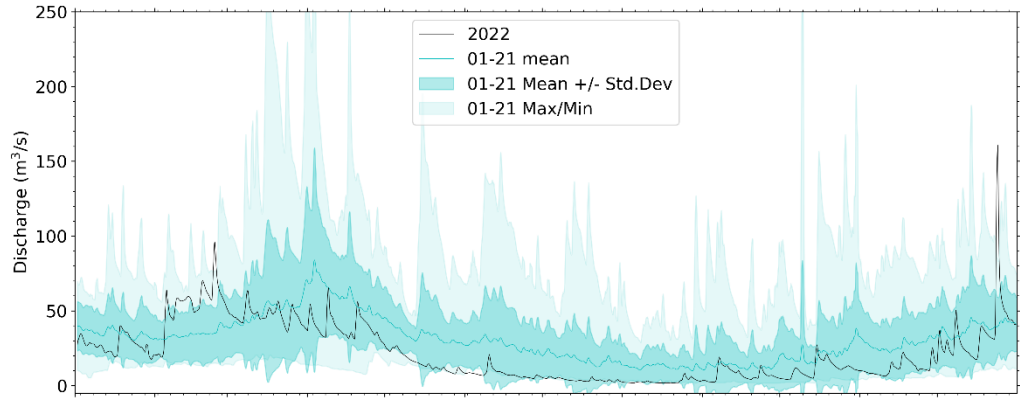


Figure 3-5 Summed discharge of all modeled rivers (Saugus, Mystic, Charles, Neponset, North, and Jones) flowing directly in to Massachusetts and Cape Cod Bays.

Presented as in Figure 3-4.

## 3.2 Loading of organic carbon, nitrogen, and phosphorous

Loads directly entering Massachusetts and Cape Cod Bays from rivers, the Deer Island treatment plant, and the atmosphere are shown in Figure 3-6. Loads entering the system through its offshore boundary are marked “oceanic input”, which include the northern Gulf of Maine and rivers to the north like the Merrimack. Loads entering the system from local rivers flowing into Massachusetts Bay and Cape Cod Bay are marked as “rivers”. These local rivers are Saugus, Mystic, Charles, Neponset, North, and Jones.

### **Oceanic input**

Model results show that oceanic input was the dominant source of organic carbon (OC), nitrogen, and phosphorus (both in organic and inorganic forms), accounting for 99%, 90%, and 96% of their total inputs, respectively (Figure 3-6). The simulated oceanic inputs of total nitrogen (TN) and total phosphorus (TP) were comparable to years 2017-2021 (within ~3 and 1 percentage points for TN and TP respectively). Oceanic TN inputs were slightly on the low side compared to previous years, which could be caused by lower flows from the rivers north of Massachusetts Bay, including the Merrimack. TN input was however comparable to the estimates based on the simulation of 1992 conditions from Hunt et al. (1999), reported by Zhao et al. (2017). Hunt et al. (1999) indicated that 93% of the TN entering the Massachusetts Bay originated from the Gulf of Maine.

### **Rivers**

Rivers were the second largest source of OC, accounting for 75% of the non-oceanic input. Rivers are the smallest source of TN and TP to Massachusetts and Cape Cod bays, representing 5% and 3% of their non-oceanic inputs, respectively. The contributions of river inputs to total OC, TN, and TP loads in 2022 were on the lower side of the ranges of those from previous years (2017-2021). This is most likely due to the lower-than-average river discharges for more than half of the year.

### **MWRA Effluent**

MWRA loads constitute the main non-oceanic source of TN and TP. These occur mainly in the inorganic form. The 2022 OC loads from the MWRA effluent were with 25% of the non-oceanic inputs in the middle of the range of loads from the preceding years 2017-2021. The 2022 TN effluent loads were comparable to 2017-2021 and on the low side for TP, representing 85% and 97% of their non-oceanic inputs, respectively. The organic fraction of TN effluent loads was relatively high compared to the years 2017-2018 but slightly lower than 2019-2021.

### **Atmospheric deposition**

Atmospheric deposition accounted for approximately 11% of the non-oceanic TN inputs.

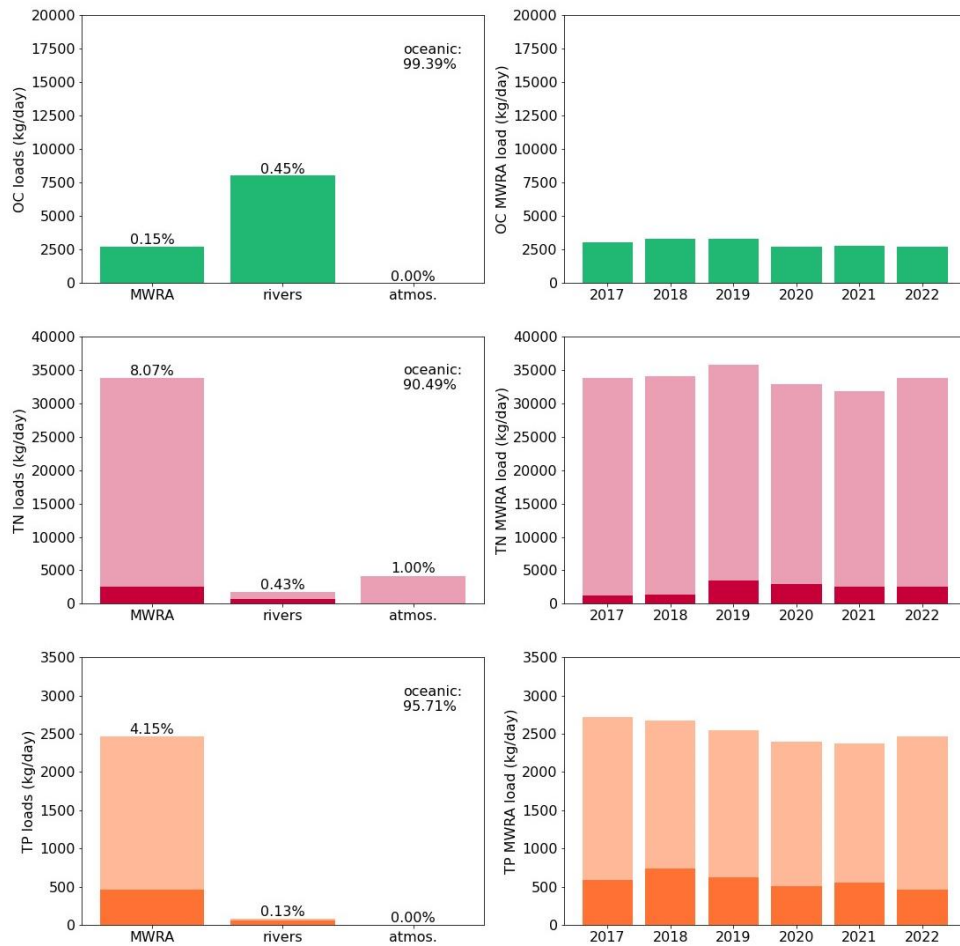


Figure 3-6 Organic Carbon (OC), Total Nitrogen (TN) and Total Phosphorus (TP) loads to Massachusetts and Cape Cod Bays in 2022. In the TN and TP plots, the darker sections of the bars represent the organic fractions. Left: loads from non-oceanic sources; percent of total is shown at top of each bar, and percent oceanic input (offshore boundary) shown at upper right. (Percentages correspond to summed organic and inorganic fractions.) Right: Deer Island Treatment Plant loads since 2017. OC=organic carbon; TN=total nitrogen; TP=total phosphorus.

## 4 Hydrodynamic Model

In this section the performance of the hydrodynamic model is discussed, and model results are compared to measurements.

### 4.1 Verification of model performance

The model skill was assessed for surface and bottom temperature and salinity by means of a statistical analysis. Three quantitative skill measures (correlation, normalized standard deviation Std\*, and normalized unbiased root mean square error uRMSE\*) were determined, based on simulation results and vessel-based observations by MWRA surveys. The result is presented in four sets of Taylor diagrams in Figure 4-1. The left column shows the 2012-2016 validation period (Deltares, 2021) and the right column shows the 2022 simulation. See also the box on the next page for further details and an explanation of the statistics in the diagrams.

Modeled and observed temperatures had correlations of over 0.97 and 0.93, Std\* of 0.90-1.08 except for three locations around 0.75, and uRMSE\* of under 0.25 and 0.38, at the surface and bottom respectively (Figure 4-1, first row and second row of panels, respectively). The performance at both the surface and bottom were comparable to the validation result. The performance at the bottom shows a larger spread compared to the averaged results of the multi-year validation period, but it does not deviate from the results of previous years.

The skill of simulated salinity varied more per observation station, compared to temperature. Modeled and observed salinities had correlations of 0.45-0.9 and 0.5-0.87, Std\* of 0.55-1.35 and 0.8-1.75, and uRMSE\* of under 0.9 and 1.0, except for stations F02 and F29 going as high as 1.1 and 1.3, at the surface and bottom respectively (Figure 4-1, third row and last row of panels, respectively). The performance at the surface and at the bottom is mostly similar to the validation result and previous years. The normalized standard deviations Std\* are slightly improved compared to the validation results for the bottom salinity but with slightly worse normalized unbiased root mean square error uRMSE\*. This is acceptable, considering that 2022 was a very dry year with extremely low river discharges that were not part of the calibration of the model.

Overall, the figures presented here serve to verify that the performance of the hydrodynamic model in the simulations of 2022 did not deviate substantially from its performance during the 5-year validation period. For completeness, Taylor diagrams broken out for individual years 2012-2016, are presented in Appendix A of the Annual BEM Report on 2017 (Deltares, 2022).



### How to read a Taylor diagram

A Taylor diagram consists of a combination of three quantitative skill measures:

- Correlation Coefficient, represented in the plot by the azimuthal angle or dashed blue lines.
- Normalized Standard Deviation (Std\*), the Standard Deviation of the model results, normalized (\*) by the standard deviation of the corresponding measurements. This ratio represents the relative amplitude of the modeled and observed variations, with a value of less than one indicating less modeled variability. It is represented in the plot by the radial distance from the origin (0,0).
- Unbiased Root-Mean-Square Error or standard deviation of the error, normalized with the standard deviation of the corresponding measurements (uRMSE\*). It is represented in the plot by the grey contours, whose values are proportional to the radial distance from the target (black star).

A model with a perfect skill would have a Correlation Coefficient of 1.0, resulting in a point on the horizontal axis, a Normalized Standard Deviation of 1.0, resulting in a point on the dashed black line, and a Unbiased Root-Mean-Square Error of 0.0, resulting in a point at the center of the grey contours. Summing up the ideal value of these skill measures, the target point is located at  $\text{Std}^*=1.0$  on the horizontal axis. This position, representing observations, is indicated with a black star. The closer a station is located to this target, the better its skill.

In practice, a perfect skill does not occur, because every model and the measurements themselves contain a certain degree of error. When assessing the skill of the current simulated year, the point cloud of the calibration and validation simulation for 2012-2016 should be compared to the current year. If this last point cloud is on average closer to the target, the model skill is higher. However, some more scatter can be expected, because Figure 4-1 compares the model skill of an individual year to the average of the multiple years of the 2012-2016 reference simulation.

A more detailed description of Taylor diagrams including the underlying equations can be found in the official publication by Taylor (2001) or Karl Taylor's simple description of the diagram<sup>1</sup>.

---

<sup>1</sup> Taylor diagram primer: [https://pcmdi.llnl.gov/staff/taylor/CV/Taylor\\_diagram\\_primer.pdf](https://pcmdi.llnl.gov/staff/taylor/CV/Taylor_diagram_primer.pdf)

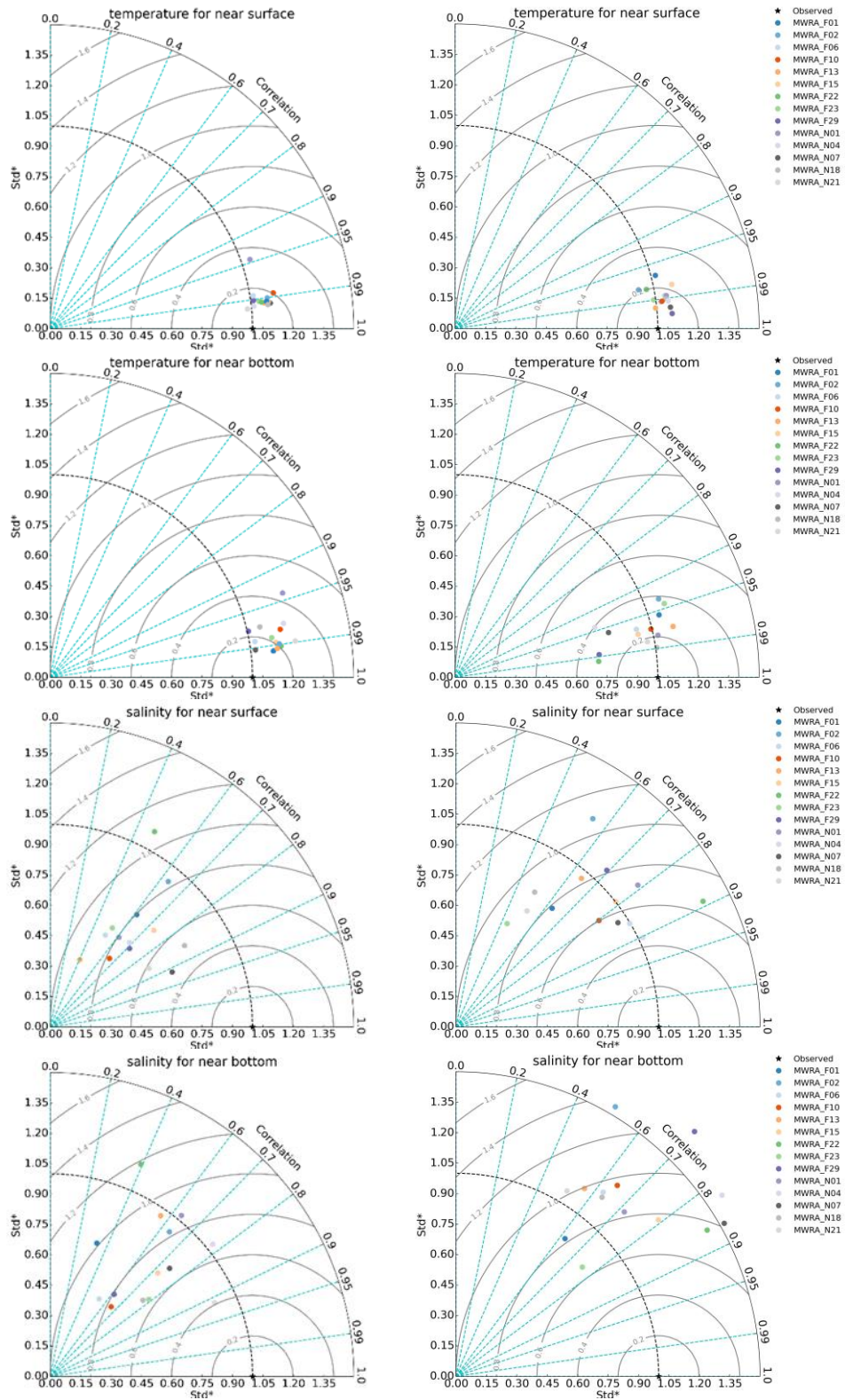


Figure 4-1 Taylor diagrams of model quality for MWRA vessel-based survey observations.

Temperature (upper 4 frames), salinity (lower 4 frames); 2012-2016 validation period (left column) and 2022 simulation (right column)

## 4.2 Model-observation comparisons

The simulation for 2022 was compared to observations to assess the level of agreement between them for temperature and salinity, both in time and space.

### 4.2.1 Time series of temperature and salinity

For eight observation stations in the Massachusetts Bay and Cape Cod Bay, simulation timeseries of the surface (less than 5 m deep) and bottom (within 5 m of seafloor) temperature and salinity are presented in Figure 4-2 and Figure 4-4, respectively. Additionally, a comparison at three levels within the water column, between the surface and seafloor, is given for temperature and salinity in Figure 4-3 and Figure 4-5 (described below), respectively.

In these figures, vessel-based observations by MWRA surveys are included as individual symbols. The locations of the observation stations are given on a bathymetric map in the upper left frame. They include four stations generally surrounding the outfall (N01, N07, N18, and F13), one station to the south (F06), one station farther offshore (F22), one station at the mouth of Boston Harbor (F23), and one station in central Cape Cod Bay (F02).

In Figure 4-3 and Figure 4-5, showing results from within the water column, the depths vary by station and by survey but are nominally at 25%, 50%, and 75% of the water depth. The model output between surveys is not shown on these figures because the depths used, set by the observations, differ from survey to survey.

Overall, the seasonal cycle and most events were well captured by the model. Simulated stratification was in line with observations. At most stations, the onset of temperature stratification was in April with a maximum in July and August. The water column started to become mixed again over the course of November. Spikes with higher than usual bottom temperatures in September and October are not always captured by the model. An increase in surface temperature was observed in late-July in the observations (N01, N18, F13, and F23), which was also reproduced by the model (Figure 4-2). In most cases model-observation differences for temperature were less than 1°C at the surface and seafloor and slightly larger within the water column. The seasonal variations in salinity and salinity stratification in 2022 were largely limited. At most stations, particularly those to the north or closer to the shoreline (e.g., F22, N01, N18, and F13), surface salinities were high in June to August based on the observed data (Libby et al., 2023; Figure 2-2). This can be attributed to the unusually low river flows observed in summer 2022, visible in the timeseries of river discharges in Figure 3-4 and Figure 3-5. This higher salinity observation was reproduced by the model (Figure 4-4). Simulated salinity showed a bias similar to previous years throughout the water column for most samples in 2022.

### 4.2.2 Spatial representation of temperature and salinity

To assess the simulation spatially, maps have been plotted for surface and seafloor conditions, with the mean of the modeled results averaged over a period of 5 days centered on the observation dates. The five presented periods span the seasonal cycle of stratification. This is given in Figure 4-6 and Figure 4-7 for temperature and in Figure 4-8 and Figure 4-9 for salinity. For the model-observation comparison, the available observations are plotted over the simulation fields as colored symbols. Note that the presented simulation fields are the average over 5 days, where the observations are instantaneous values, usually measured in the morning. This might introduce a bias.

These figures show a good agreement between the simulation and observations. The spatial variation at both the surface and bottom was comparable, with near-shore temperatures warmer in summer and colder in winter. Model-observation differences for surface and seafloor temperatures were at most

1°C. At both depths, salinities were generally fresher near the coast. Similar to 2021, 2020 and 2018 (and in contrast with other years), no large freshwater plume was present in the spring or early summer of 2022. This can be explained by the low discharge from the Merrimack River in the first 6 months of 2022 (Figure 3-4). Additionally, 2022 flows were unusually low for the rest of the summer, and the simulated surface salinities reproduced the observations reasonably well (Figure 4-8, August frame). The model shows an overestimation of salinity of about 0.5 PSU at both the seafloor and the sea surface.

**Black:** Near-surface

**Cyan:** Near-seafloor

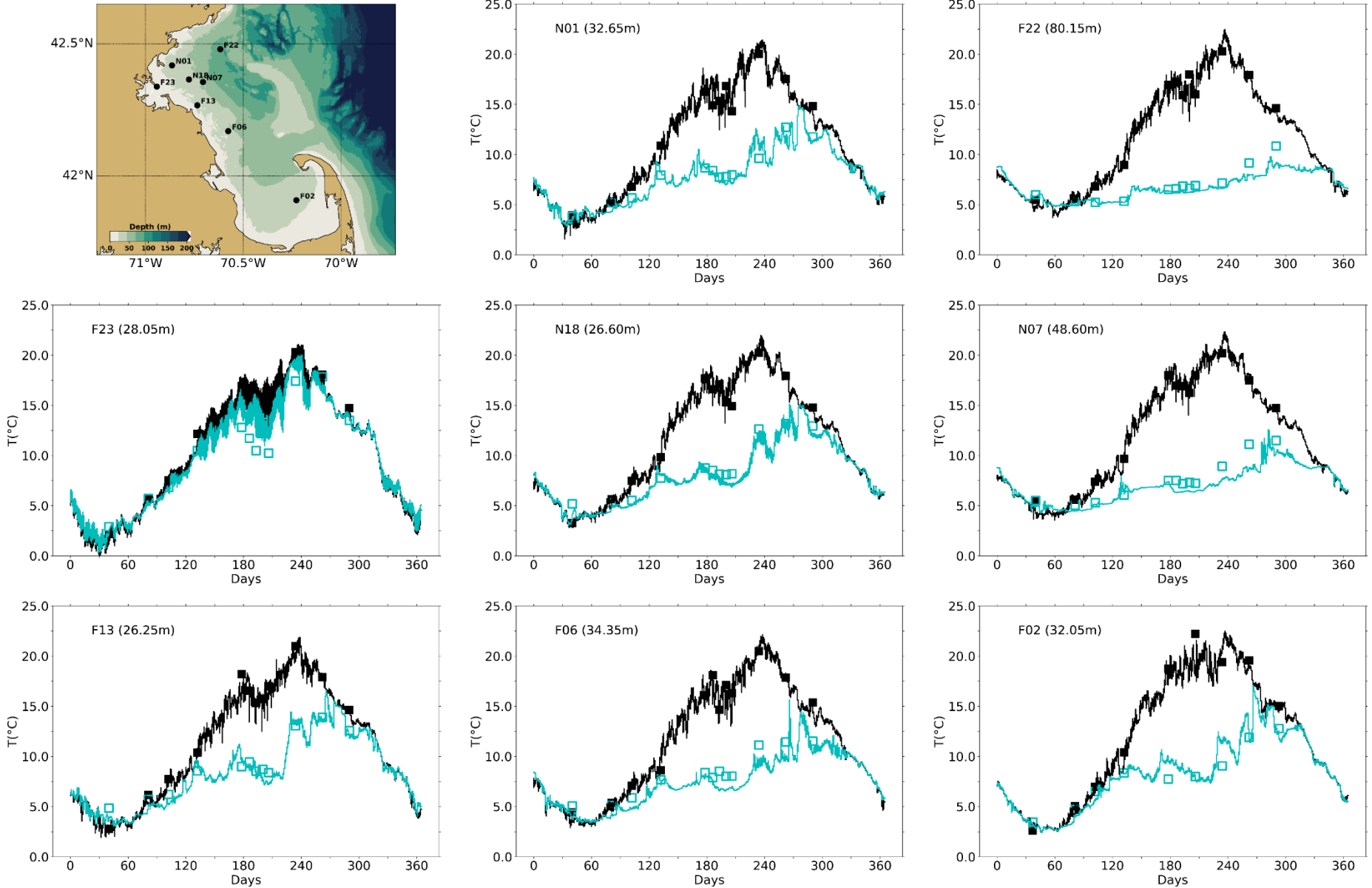


Figure 4-2 Temperature time series, model-observation comparison near surface (black) and seafloor (cyan).

Model results: lines. MWRA vessel-based survey observations: symbols.

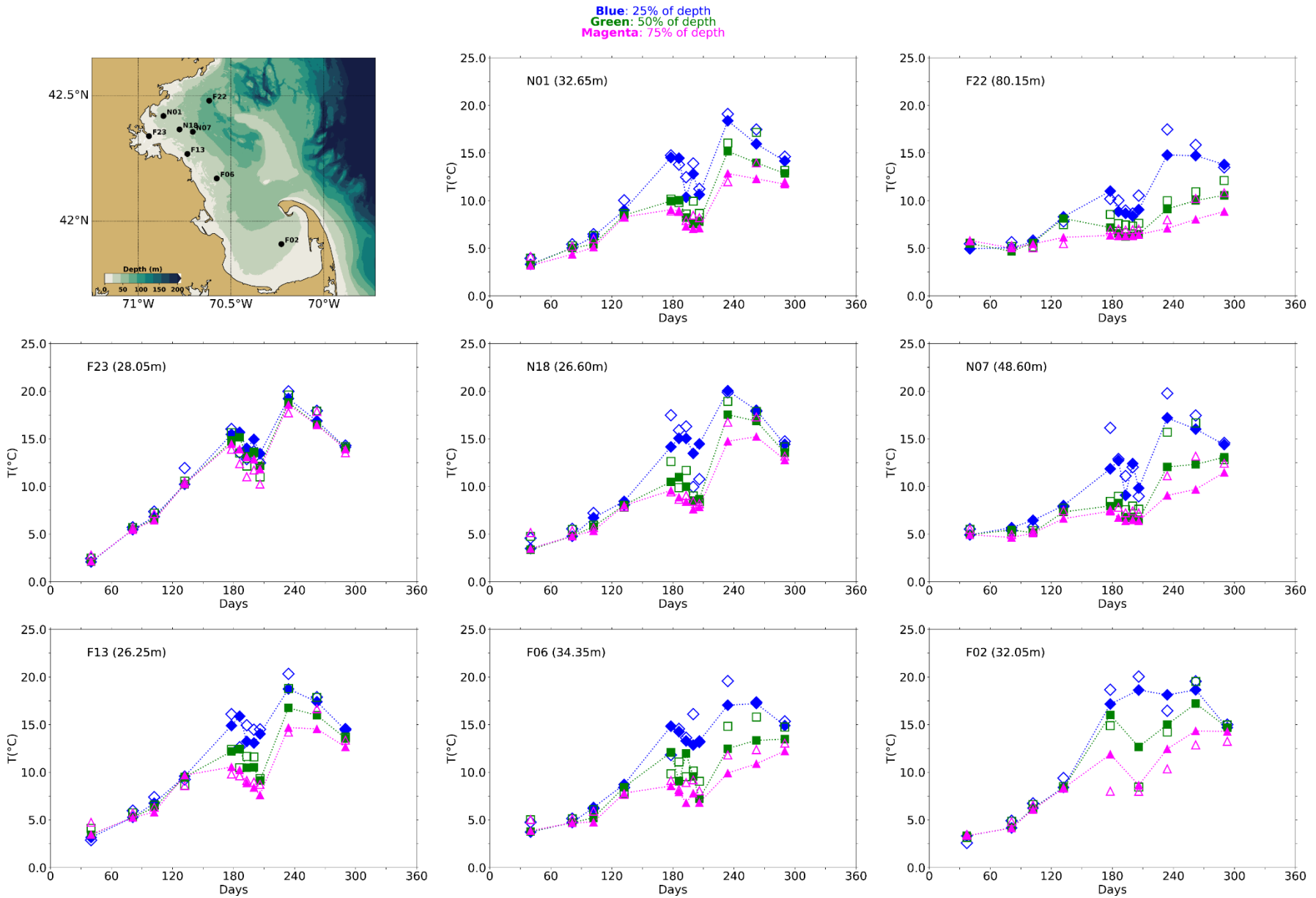


Figure 4-3 Temperature time series, model-observation comparison in water column (between surface and seafloor).

Model results: lines with filled symbols. MWRA vessel-based survey observations: open symbols.



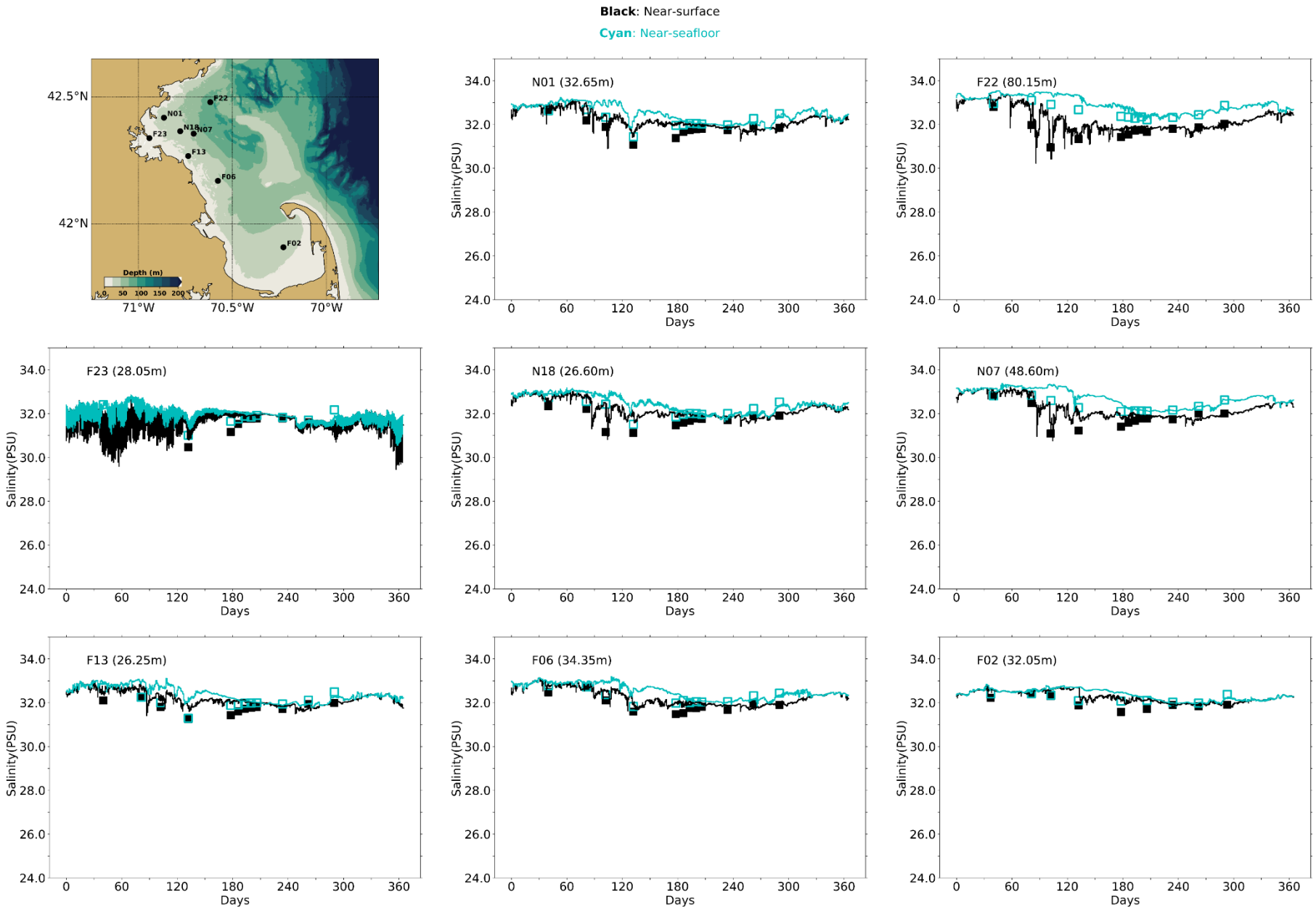


Figure 4-4 Salinity time series, model-observation comparison near surface (black) and seafloor (cyan).

Model results: lines. MWRA vessel-based survey observations: symbols.

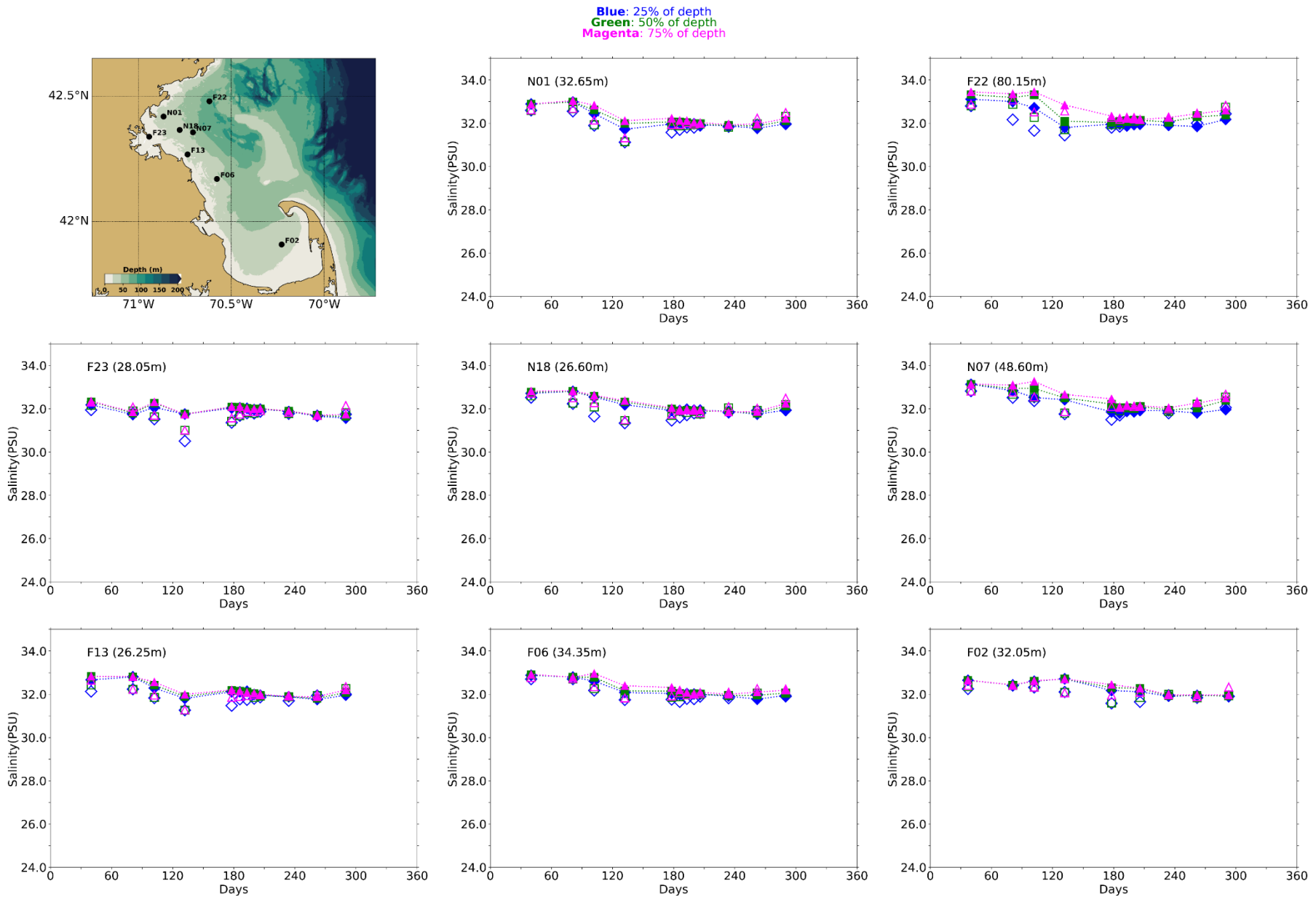


Figure 4-5 Salinity time series, model-observation comparison in water column (between surface and seafloor).

Model results: lines with filled symbols. MWRA vessel-based survey observations: open symbols.



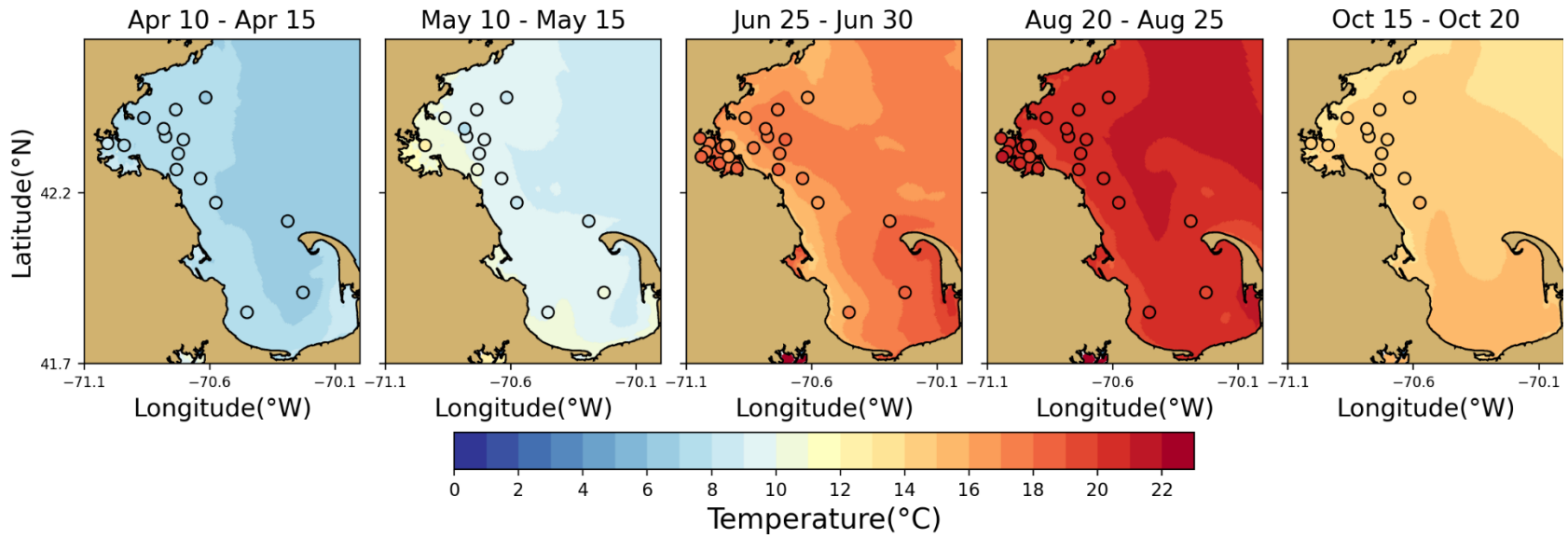


Figure 4-6 Temperature spatial structure, at/near sea surface, model-observation comparison.

Model results: background. MWRA vessel-based survey observations: symbols. Model results are averaged over the 5-day period centered on the measurement date.

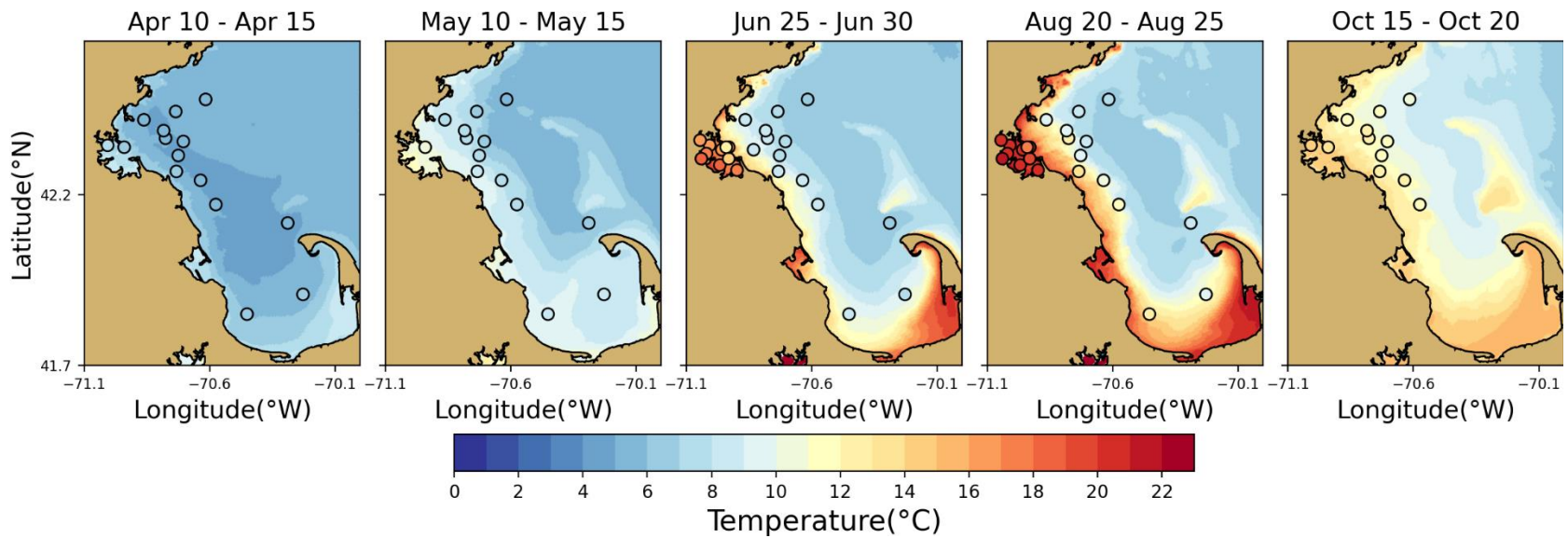


Figure 4-7 Temperature spatial structure, at/near seafloor, model-observation comparison.

Model results: background. MWRA vessel-based survey observations: symbols. Model results are averaged over the 5-day period centered on the measurement date.

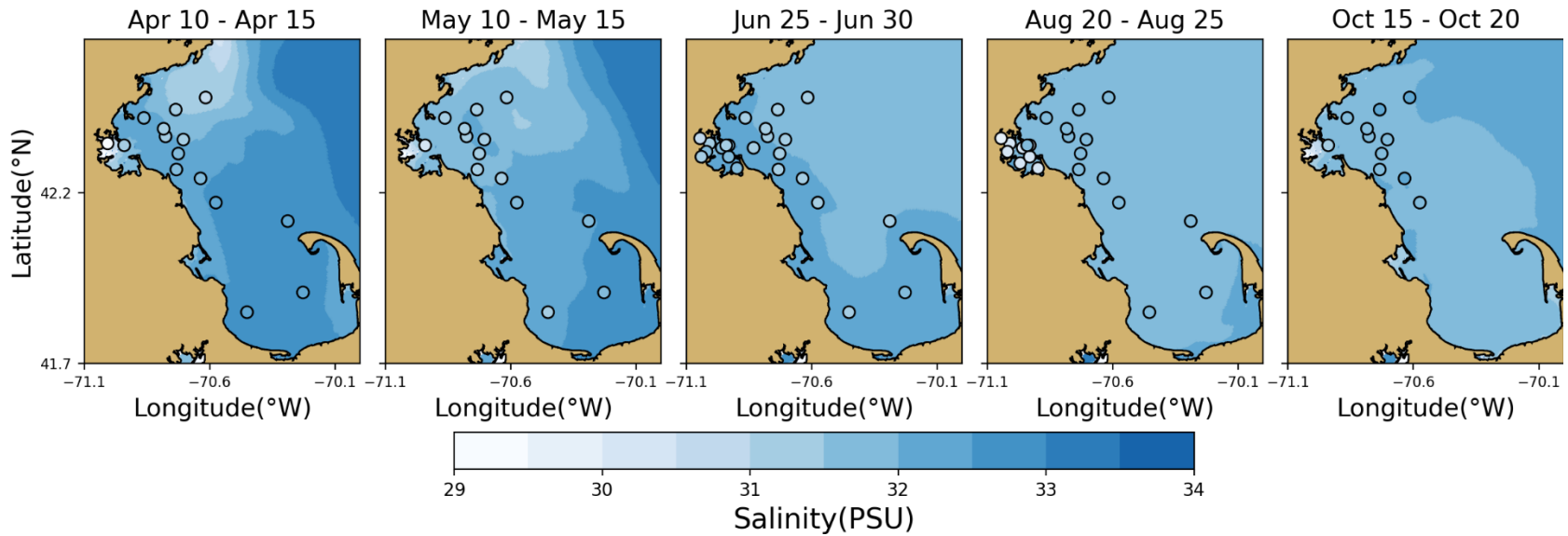


Figure 4-8 Salinity spatial structure, at/near sea surface, model-observation comparison.

Model results: background. MWRA vessel-based survey observations: symbols. Model results are averaged over the 5-day period centered on the measurement date.

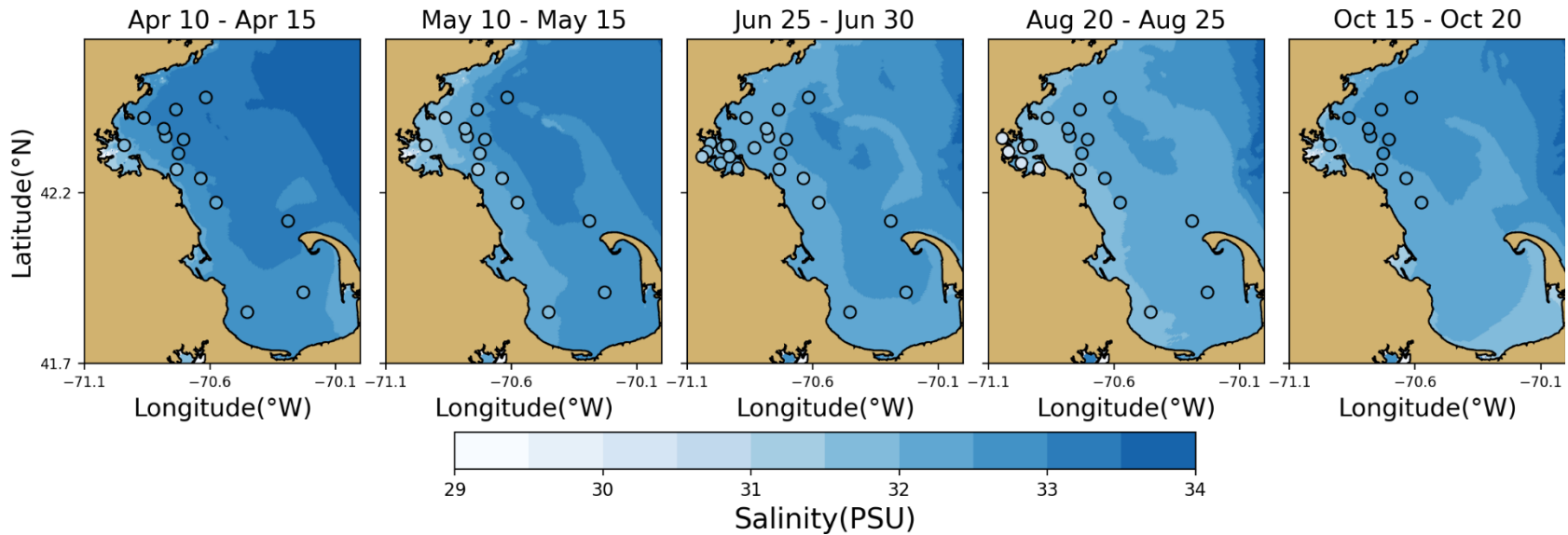


Figure 4-9 Salinity spatial structure, at/near seafloor, model-observation comparison.

Model results: background. MWRA vessel-based survey observations: symbols. Model results are averaged over the 5-day period centered on the measurement date.

### 4.2.3 Continuous measurements of temperature and salinity

Hourly measurements were available from Mooring A01 at multiple depths. This station is located south of Cape Ann, northeast from MWRA station F22. To provide a more complete assessment of the model-observation comparison in time, timeseries for this station are presented in Figure 4-10. This figure shows the simulated and observed temperature and salinity at three depths (1m, 20m, and 50m; top panels of Figure 4-10) and the salinity and temperature differences between the 1m and 20m depths and 1m and 50m depths (bottom panels of Figure 4-10), as an indication of the stratification within the water column. Observation data at the surface were only available during the summer months and from November onward. Consequently, large gaps are present in the 1m time series and vertical difference time series of both temperature and salinity.

The available data showed a good result of the model-observation comparison for temperature and salinity and different depths. In the summer months, simulated temperature at the surface and at 20m showed good agreement with the monitored data and was slightly overestimated at 50m. Temperature stratification was well represented in the model. Individual events were captured, but in summer months, an overestimation of approximately 1°C occurred at the 50m depth. The bias in salinity of about 0.50-0.75 PSU throughout the water column, as explained in Deltares (2021), is clear in the second frame of the figure. The typical seasonal cycle of less saline near-surface waters in the summer was not pronounced in 2022 due to the unusually low discharge from Merrimack River from June through September. The salinity stratification showed a good comparison between model and observations for the 1m-20m stratification and slightly underestimated the 1m-50m stratification in the summer. Overall, the model captures features of observed stratification well, as is important for the water quality simulation because stratification is a main influence on vertical transport.

### 4.2.4 Continuous measurements of non-tidal currents

For Mooring A01 observed currents were available, although currents from mid-September through the end of 2022 were missing. In Figure 4-11 and Figure 4-12 a model-observations comparison is presented for the first and second halves of the year, respectively. In the top frame, time series of wind from the meteorological product used to force the model is given for context. In the frames below, simulated and observed time series of non-tidal currents at four depths (2m, 10m, 22m and 50m) are given alternately. To remove the tidal variability, time series have been filtered using a low-pass filter with a 33 hour filter half amplitude (Alessi, 1985). The resulting signal consists mainly of weather-related and seasonal changes. For plotting this has been subsampled to a 6 hour resolution.

The time series of the filtered wind showed wind in all directions. Winds were generally changing on timescales of multiple days. In general, the wind speeds were lower during the summer months. Winds included a dominantly eastward component year-round, with a dominant southward component in winter and a dominant northward component in summer.

Simulated and observed non-tidal currents showed a similar pattern with a prevailing direction to the south and west. The simulated currents showed less variability in direction than observed, but the order of magnitude of their amplitudes was similar. Strong currents occurred in late-April and May due to a strong south-westward wind. Throughout the year, some small events occurred, but these were not persistent. These events were well represented in the model. This model-observation comparison at a specific location is a challenging test of the hydrodynamic simulation performance. The agreement between the two was sufficient to conclude that the representation of processes in the hydrodynamic model was adequate to support water quality modelling.

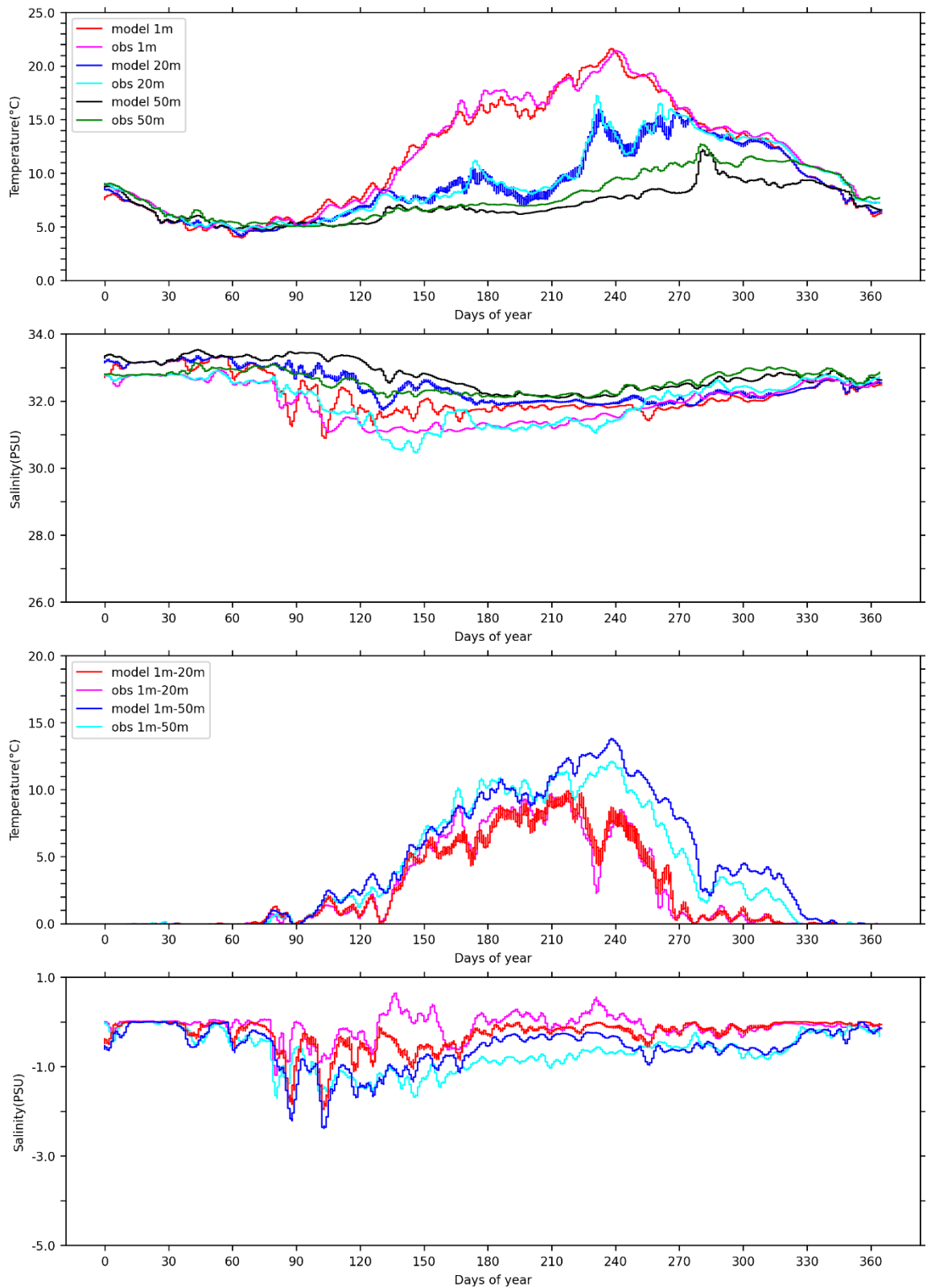


Figure 4-10 Time series of Mooring A01 temperature and salinity model-observation comparison (3-day means), at three depths (top two panels), and temperature and salinity differences between the 1m and 20m depths and 1m and 50m depths, as an indication of the stratification within the water column (lower two panels).

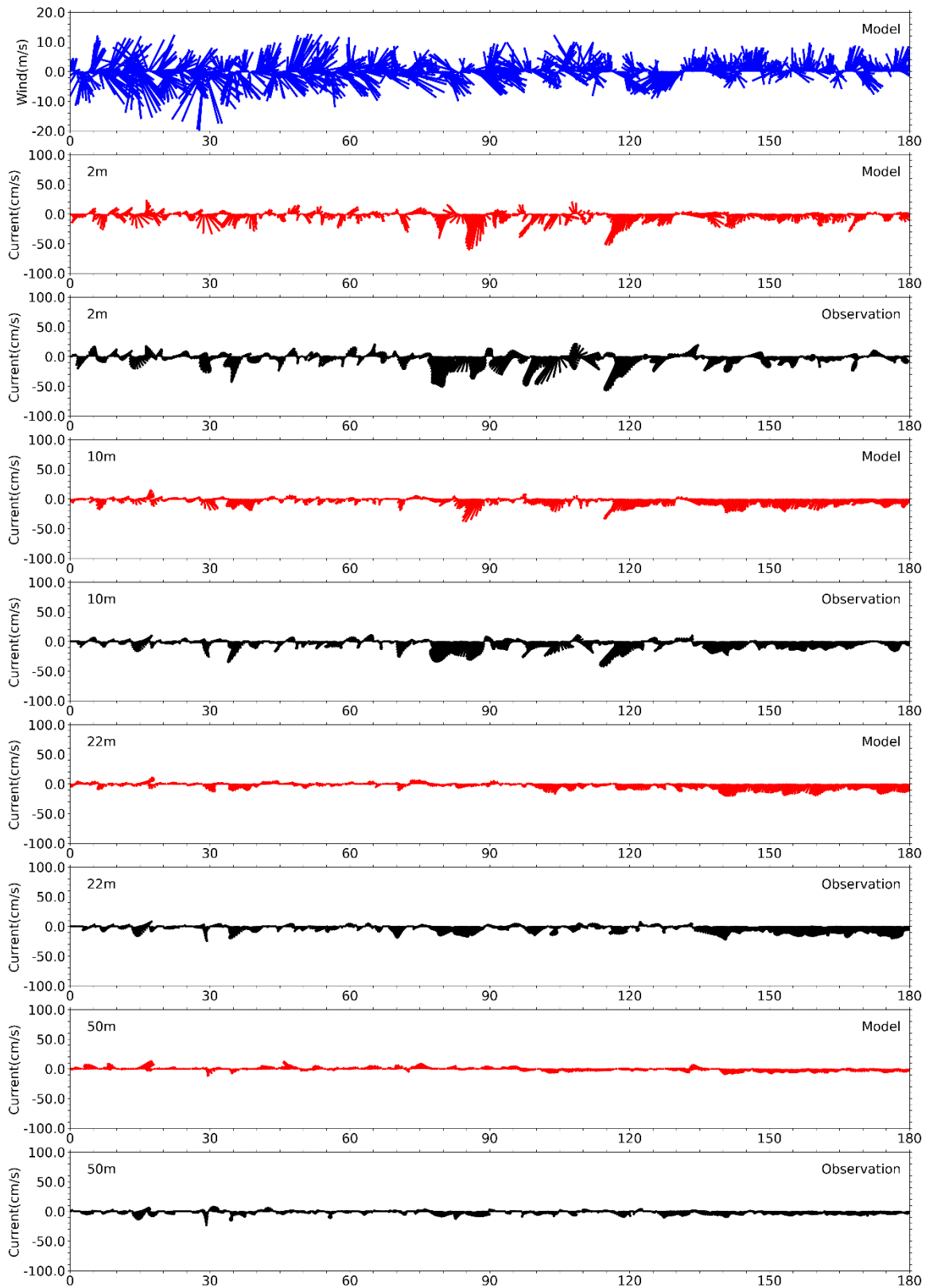


Figure 4-11 Currents time series model-observation comparison, Jan – Jun.

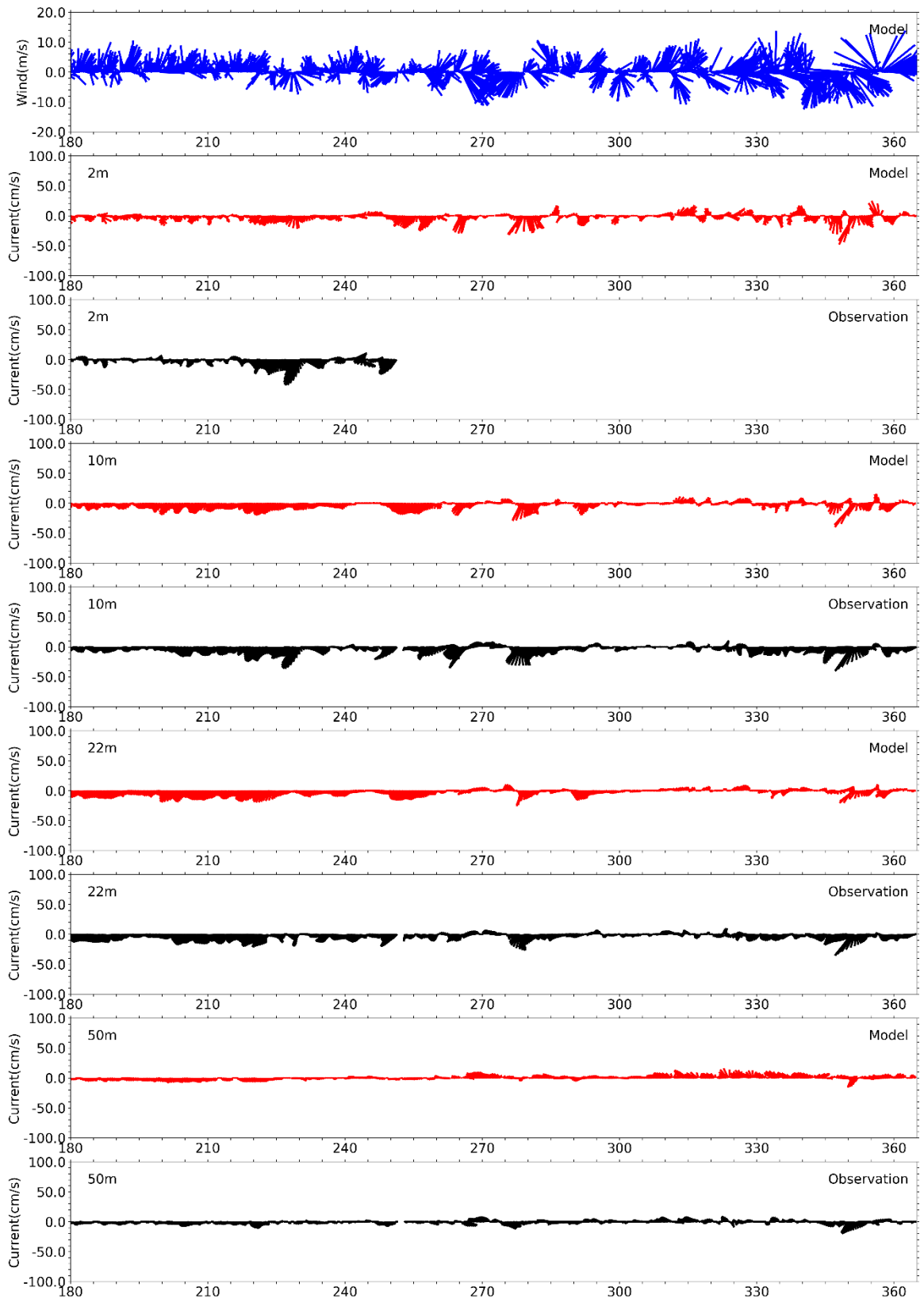


Figure 4-12 Currents time series model-observation comparison, Jul – Dec.

### 4.3 Model monthly-mean circulation

Figure 4-13 and Figure 4-14 present the simulated monthly-mean currents at the surface and at a depth of 15m. Flow was largely consistent with the general circulation pattern recognized to hold (Figure 1-1).

This schematic pattern was apparent in the residual surface currents during most of the year. In October the circulation in Cape Cod Bay was partially reversed, although with low velocities.

Surface currents near the Massachusetts Bay were strongest off Cape Ann and Cape Cod with the largest magnitudes in May and July respectively, reaching up to  $0.20\text{m s}^{-1}$ . Residual currents within Massachusetts Bay were strongest in July with magnitudes up to  $0.15\text{m s}^{-1}$  in the center of the bay (see Figure 4-13). During the rest of the year surface currents were calmer and did not exceed  $0.10\text{m s}^{-1}$ . The strongest north-eastward currents in North Passage occurred in November, reaching up to  $0.15\text{m s}^{-1}$ .

In general, the circulation pattern at 15m depth (Figure 4-14) was somewhat similar to the general circulation pattern of Figure 1-1, including a flow directed into northern Massachusetts Bay from offshore, and changed little from month to month. Current magnitudes were lower than at the surface, with maxima in May of up to  $0.2\text{m s}^{-1}$  at Cape Anne. Within Massachusetts Bay, residual currents were smaller than at the surface, reaching up to  $0.2\text{m s}^{-1}$  at North Passage in May. In Cape Cod Bay, residual current magnitudes at this level were weaker, due to its limited depth and sheltered geometry.



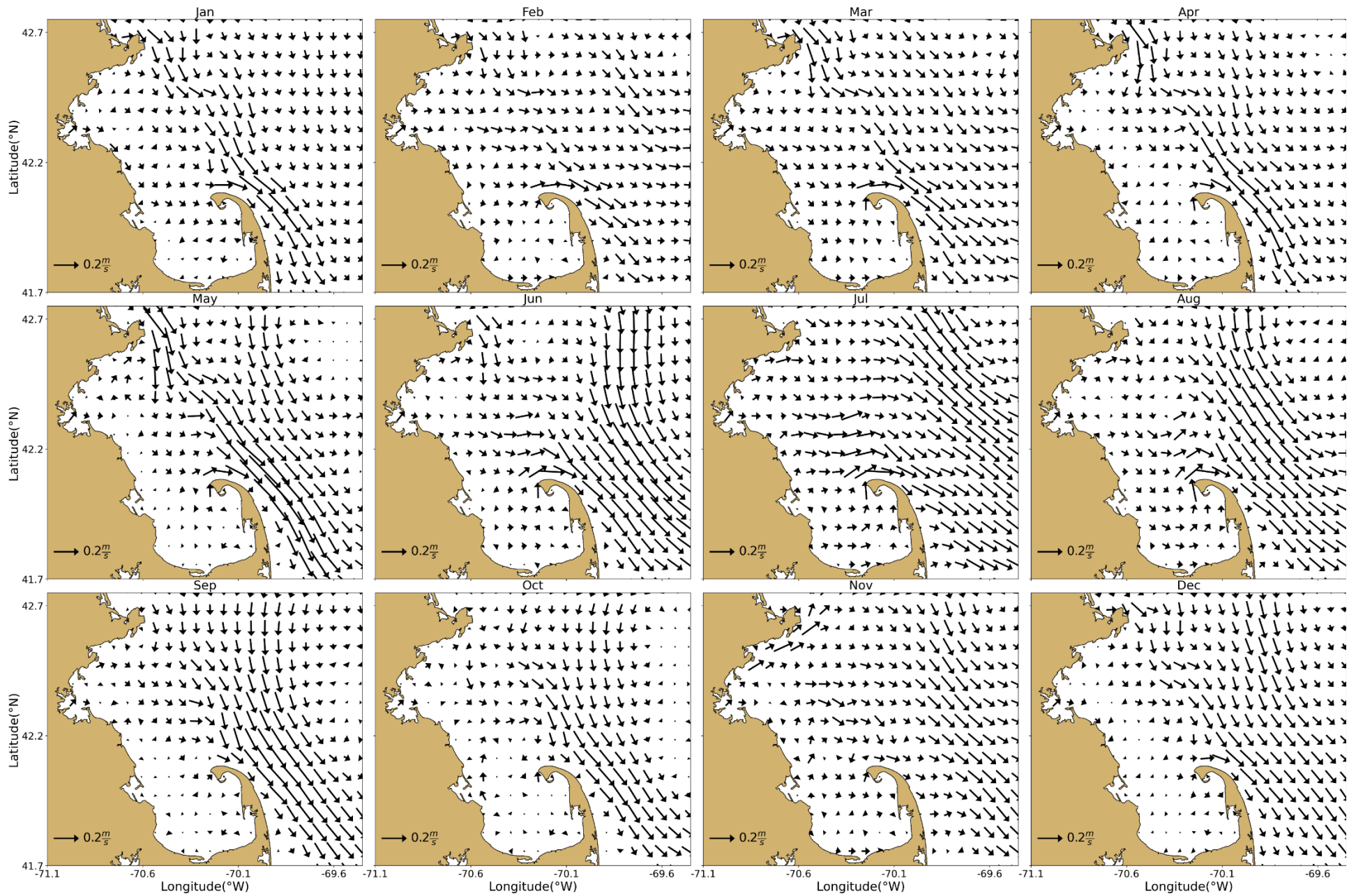


Figure 4-13 Model currents, monthly-mean spatial structure, at sea surface.



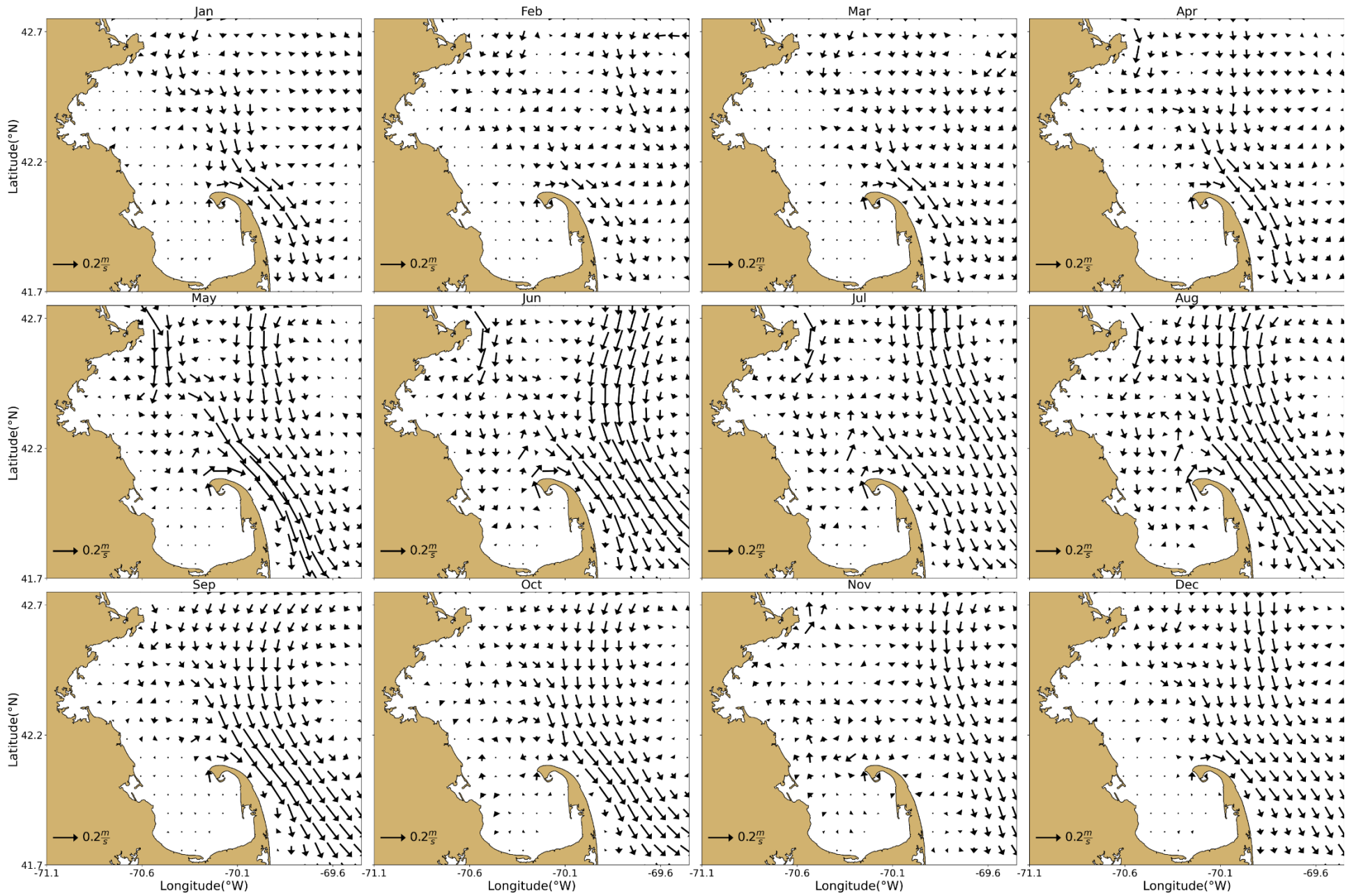


Figure 4-14 Model currents, monthly-mean spatial structure, 15 m deep.

# 5 Water Quality Model

## 5.1 Verification of model performance

To demonstrate that the water quality model performance during 2022 was comparable to the performance for the calibration and validation period 2012-2016, skill metrics were calculated and plotted on Taylor diagrams as in Section 4. Station N21, directly on top of the outfall, was excluded, as the BEM model equations do not resolve the necessary physics so close to the outfall and as operational constraints may have affected the precise sampling location relative to position of the plume. For a further discussion, reference is made to Deltares (2021). Information on how to interpret Taylor diagrams can be found in section 4.1 (box “How to read a Taylor diagram”).

Taylor diagrams are plotted for the light extinction coefficient and dissolved inorganic nitrogen (DIN) in Figure 5-1, and for chlorophyll a and DO in Figure 5-2. These parameters were selected because they are key drivers of ecosystem functioning. Statistics for the period 2012-2016 are plotted on the left side and statistics for 2022 on the right side. For reference, the 2017 simulation report (Deltares, 2022) provides, in its Appendix A, similar diagrams for the individual years 2012 to 2016. The plots show statistics for three clusters of monitoring stations: Northern Bay stations (F22, N01, N04, N07, F10, N18, F15, F13 and F23), Southern Bay and Cape Cod stations (F06, F29, F01 and F02), and harbor stations (024, 140, 142, 139 and 124) (see Figure 2-4 for station locations).

Extinction skill metrics (Figure 5-1) for 2022 show slightly higher correlation coefficients compared to the calibration period 2012-2016. Variability in 2022 is slightly underestimated and unbiased RMSE values are slightly improved compared to the validation period (individual years 2012-2016).

Skill metrics for DIN (Figure 5-1) are more variable than the calibration period 2012-2016. In 2022, correlations for observed and modeled DIN were not as strong as during 2012-2016 for most stations, especially bottom concentrations. The model performance for predicting bottom concentrations of DIN for 2022 is largely similar to 2012-2016, while variability tends to be more overestimated for near-surface concentrations, especially at Southern stations. Unbiased RMSE values are mostly in the range of those calculated for individual years 2012-2016.

Skill metrics for chlorophyll a (Figure 5-2) in 2022 are in the range of those from individual validation years 2012-2016 for most bottom chlorophyll a though with slightly weaker correlations in 2022. Variability of near-surface concentrations is generally underestimated, as it was for model predictions in years 2017-2019. This was not the case for validation years 2012-2016, for which variability of near-surface chlorophyll a was overestimated at some stations, especially those from Northern Massachusetts Bay.

DO skill metrics (Figure 5-2) are similar to 2012-2016. The model performs very well for surface DO concentrations and in terms of correlation and unbiased RMSE for bottom DO concentrations. Variability is generally underestimated by the model near the seabed, more than for the 2012-2016 validation period. This was also the case for the most recent simulated years (e.g. 2020-2021).

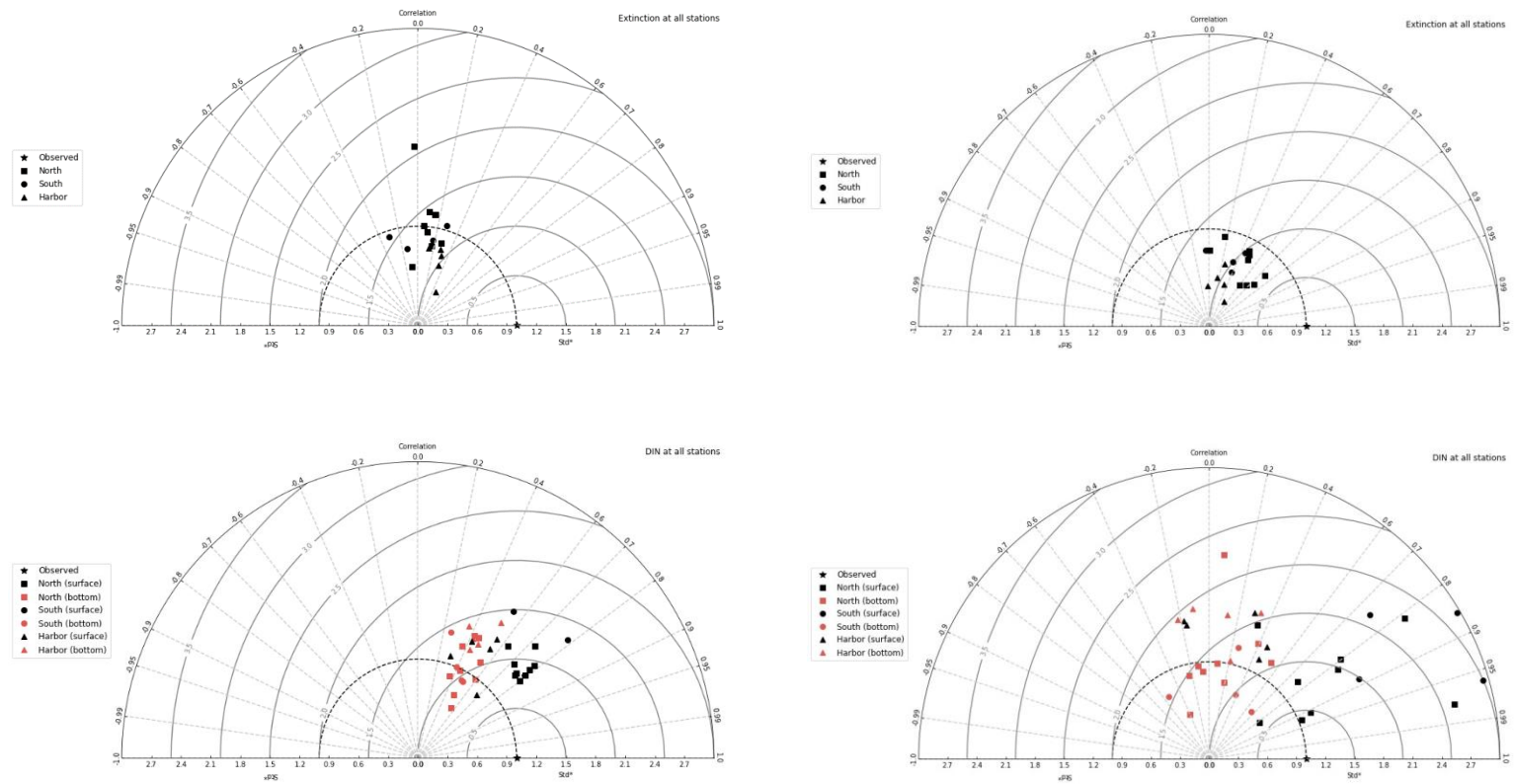


Figure 5-1 Taylor diagrams for MWRA vessel-based survey observations. Top panels show the parameter Extinction and bottom panels Dissolved Inorganic Nitrogen. Left panels show results for the simulation period 2012-2016 and right panels for the year 2022.

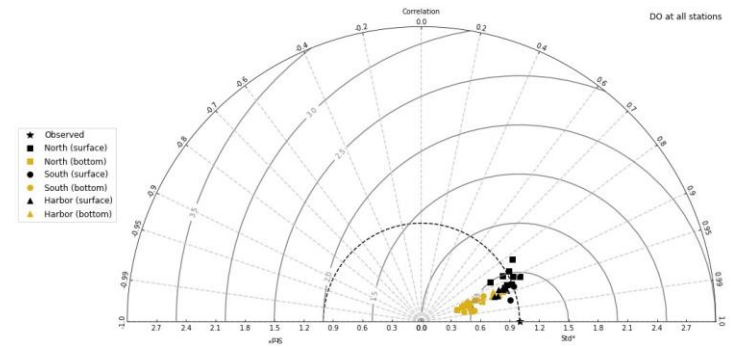
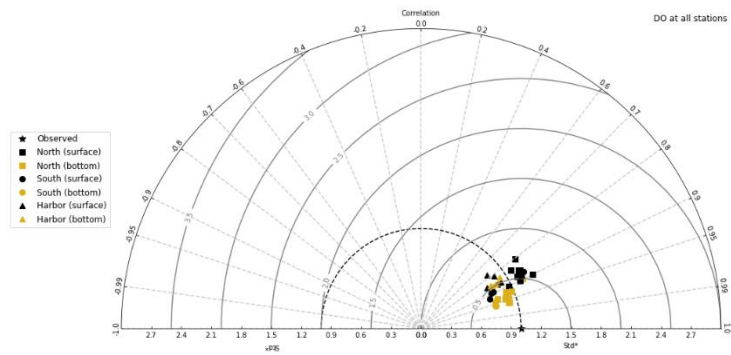
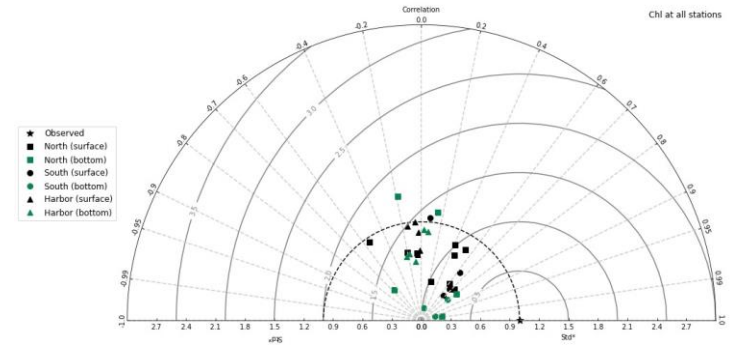
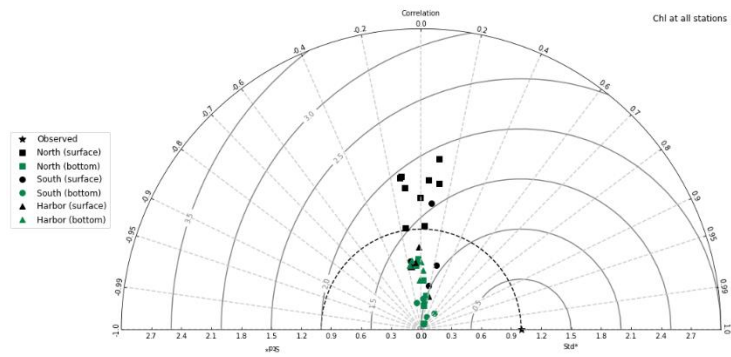


Figure 5-2 Taylor diagrams for MWRA vessel-based survey observations. Top panels show the parameter Chlorophyll a and bottom panels Dissolved Oxygen. Left panels show results for the simulation period 2012-2016 and right panels for the year 2022.

## 5.2 Model-observation comparisons

In this section model-observation comparisons in the same format as for the hydrodynamic model (Section 4) are provided. For time series plots, a 3-day moving average is applied to the model outputs to smooth high-frequency variability.

To assess the simulation spatially, vertical transects have been plotted along North-South and West-East transects (Figure 2-4). Model results in these figures are 5-day averages centered around the sampling date indicated in each plot.

### 5.2.1 Light extinction

Measured extinction for the year 2022 (Figure 5-3) ranged from 0.1 to 0.5 per m at all stations, except at F23, near the harbor, where it ranged between 0.3 and 0.6. These ranges were similar to previous years, even though average extinction was overall slightly higher. The model seems to slightly underestimate extinction values all year round, which was not the case for previous years. Extinction variability is reproduced well at most stations. The relatively narrow range of light extinction coefficients indicates that light penetration is generally high (approximately 10 m or greater, when  $K_d$  is lower than 0.5 per m). Conditions near the harbor tend to be more variable, likely influenced by both wind-induced resuspension and suspended sediments loading from freshwater inflows. The model does a reasonable job of capturing these events. For example, the light extinction coefficient observations at F13 and F23 were higher around Days 120 and 280, and the model reproduced this pattern. The latter moment follows a period of sustained wind gust (see Figure 4-12), and higher extinction therefore most likely resulted from a wind-induced resuspension event. Simulated peaks are higher than measured light extinction coefficient values around these days, but it is not possible to compare these one-to-one, due to the lower time resolution of the observations and since the measurements were not carried out on the simulated maximum peak day.

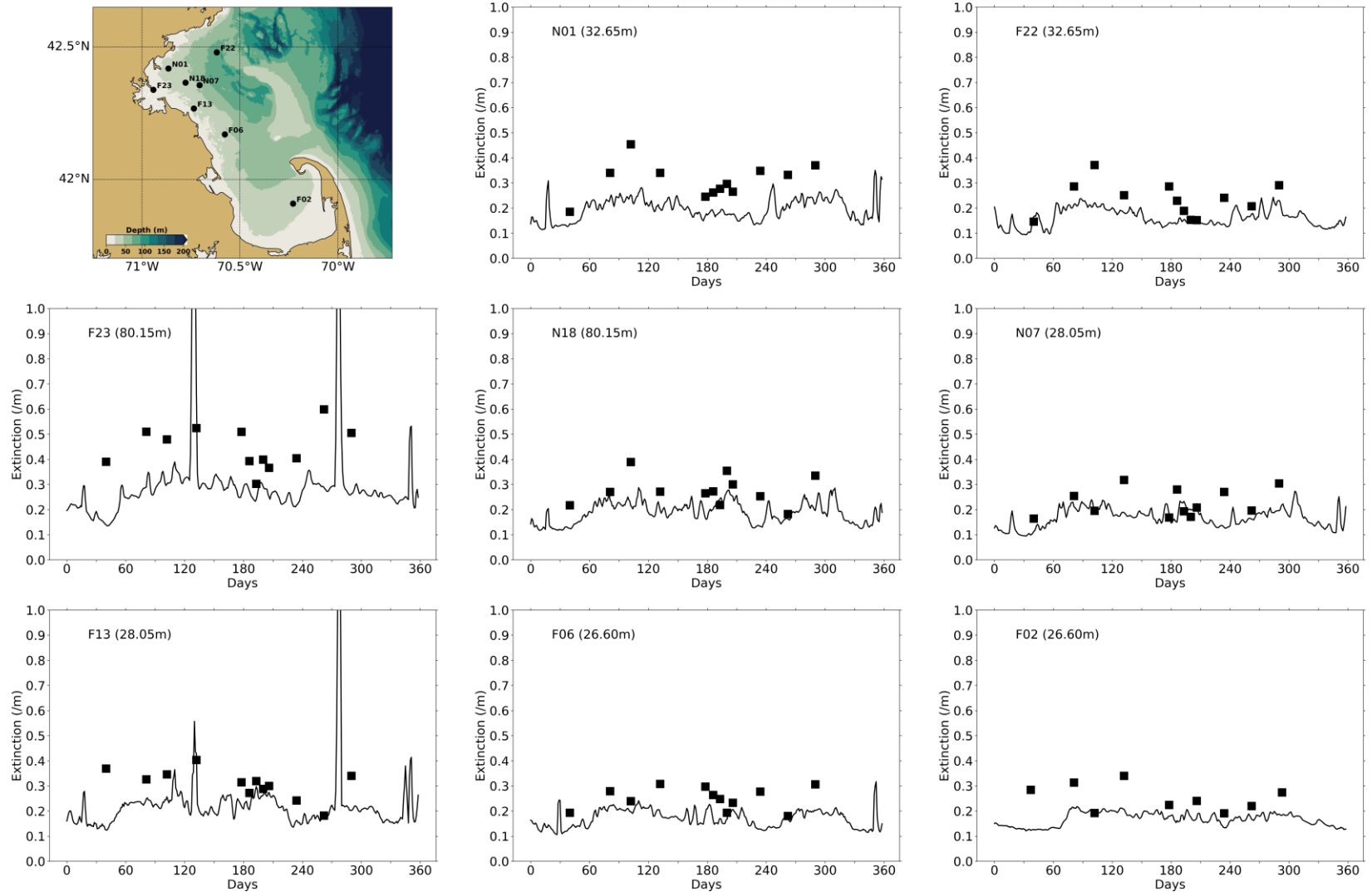


Figure 5-3 Extinction time series, model-observation comparison for 2022. Model: lines. MWRA vessel-based survey observations: symbols.



### 5.2.2 Dissolved inorganic nitrogen

Seasonal variations of surface and bottom DIN concentrations in 2022 were similar to those observed and simulated for previous years (Figure 5-4), even though depletion of near-surface DIN seems to have occurred slightly later than for previous years at some stations (F22, N18, N07). Surface and bottom concentrations were similar in winter, when the water column was well mixed. Surface DIN concentrations declined at the end of winter and were depleted from April to October, before increasing again mid-fall. Bottom concentrations remained around winter levels in the locations farther offshore (F22, N07), but nearshore locations (F23) followed a similar pattern as the surface concentrations. The model generally reproduced these observed seasonal variations and vertical differences. Observed variations at intermediate depths in the water column were generally well reproduced by the model including at N18 where the model captured a few deeper observations of higher DIN concentrations in August and September (Figure 5-5).

The model overall reproduced the outfall DIN signature that was evident in the data. Both model results and observations showed elevated concentrations at depth near the outfall during the stratified months of June through October (Figure 5-6). Stratification seems to occur earlier in the model: in April and May, simulated high DIN concentrations remain “trapped” at lower depths, while higher concentrations were measured all the way up to the surface. During the other months, higher DIN concentrations were evident throughout the water column in vicinity of the outfall (station N21). This was similar to observations and simulations from previous years. In the model during stratified periods, the highest concentrations at N21 (directly over the outfall) were always simulated at the bottom of the water column, while the highest measured concentrations were sometimes higher up in the water column (e.g., June 28). This aspect of the model directly over the outfall was discussed in a previous report by Deltares (2021).

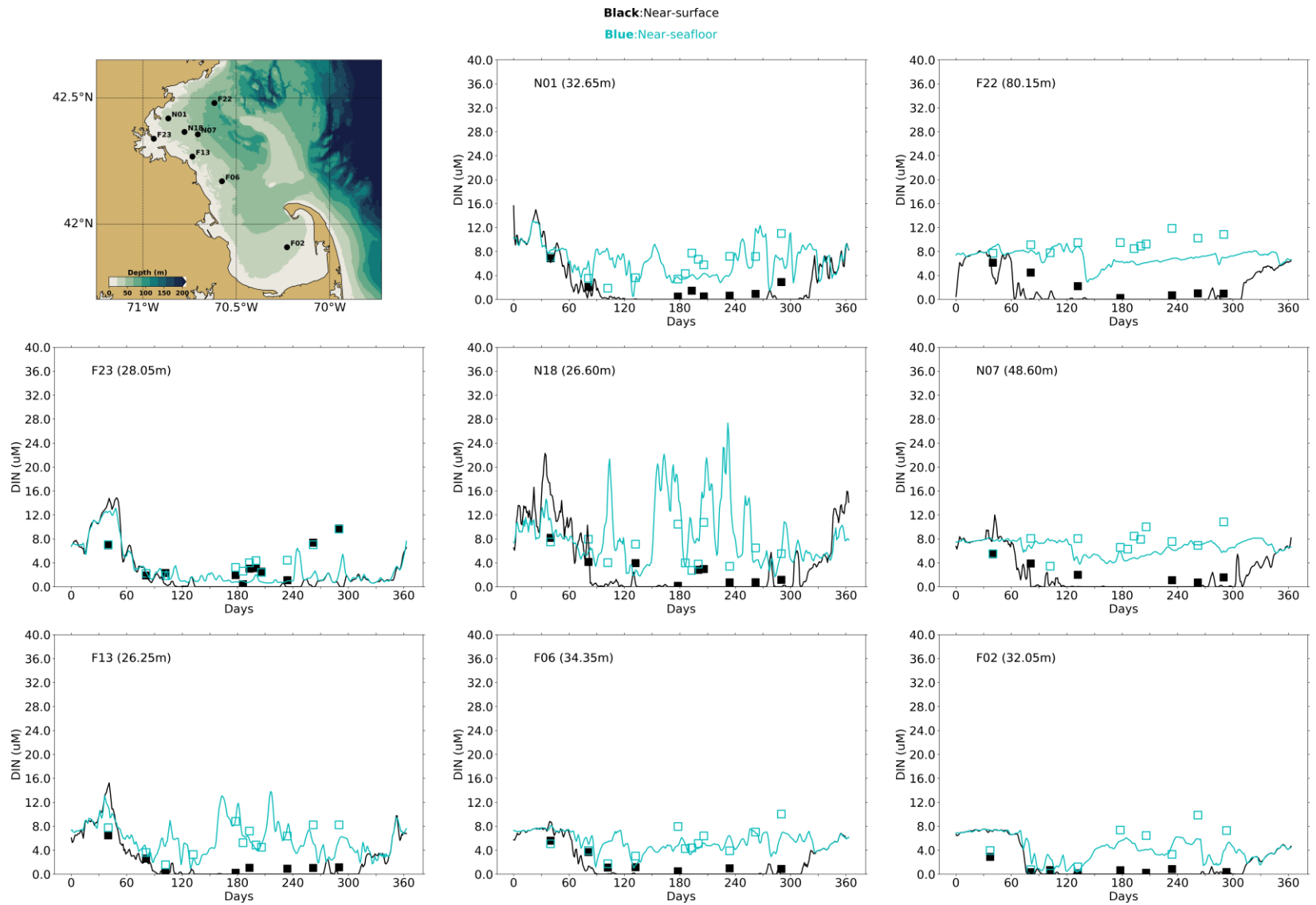


Figure 5-4 Dissolved Inorganic Nitrogen time series, model-observation comparison near surface (black) and seafloor (cyan). Model results: lines. MWRA vessel-based survey observations: symbols.



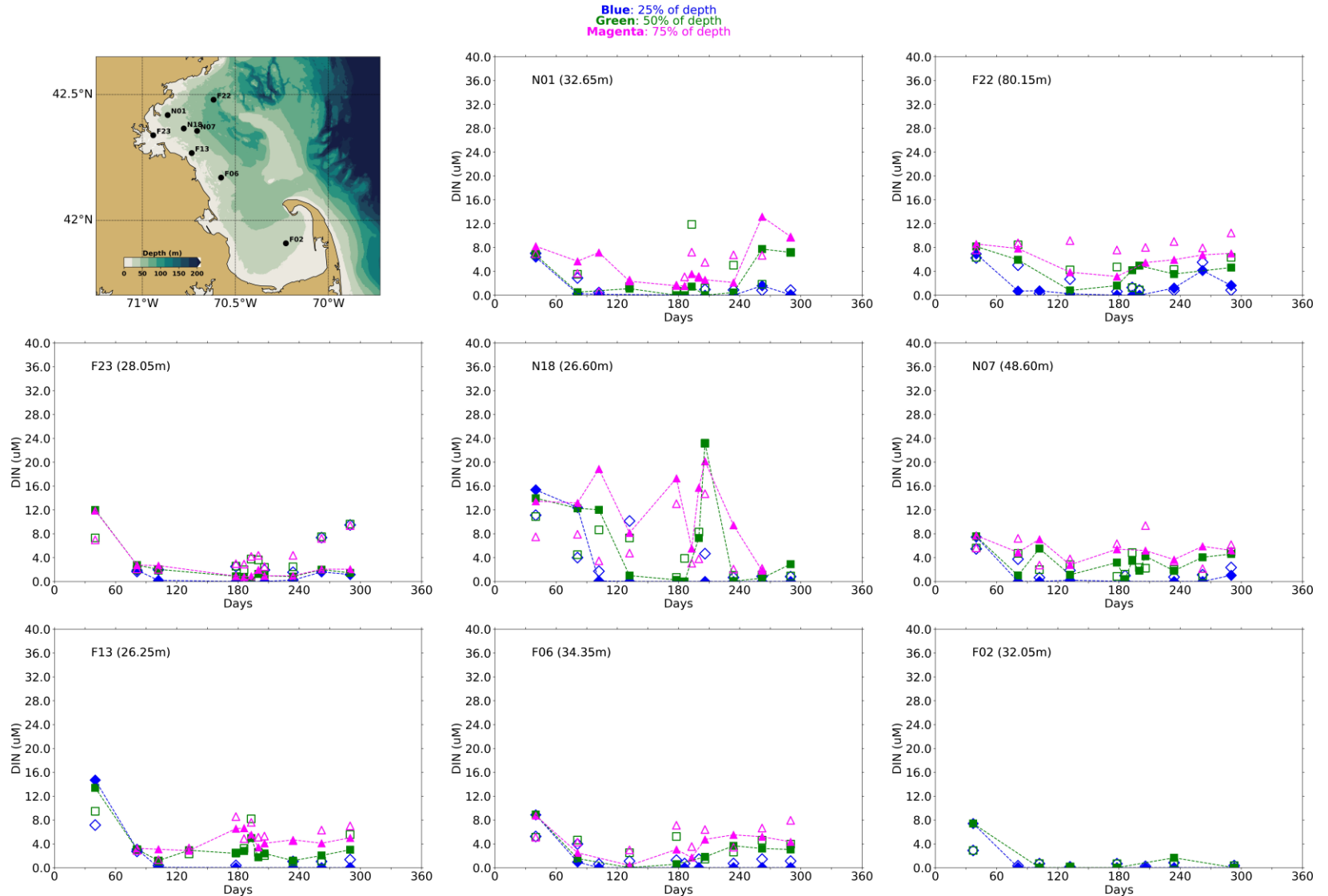


Figure 5-5 Dissolved Inorganic Nitrogen time series, model-observation comparison within water column (between surface and seafloor). Model results: lines and full symbols. MWRA vessel-based survey observations: open symbols.

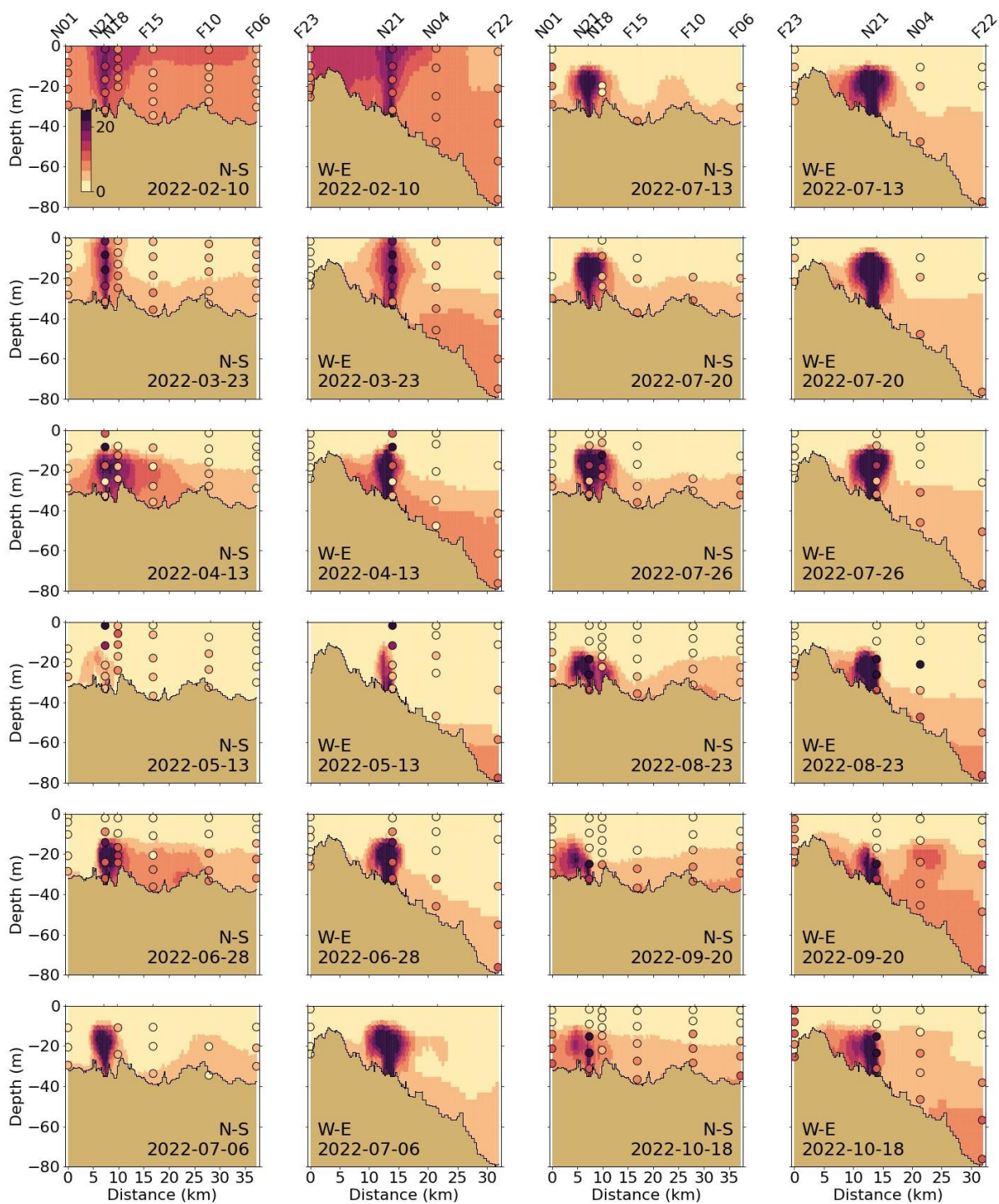


Figure 5-6 Dissolved Inorganic Nitrogen ( $\mu\text{M}$ ) for 2022 along North-South (N-S) and West-East (W-E) transects (Figure 2-4). MWRA measurements are plotted with round symbols. Model results are 5-day averages around sampling date.

### 5.2.3

#### Chlorophyll a

There were two to three peaks in chlorophyll a at most locations in 2022, one in late winter/early spring centered around mid-March (e.g. stations N01, F22, F13, F06, and F02 in Figure 5-7), and another in mid-summer (around July) or late summer (September) (e.g. stations N01, F23, N18 and N07 in Figure 5-7). In the spring months, biomass production is evident throughout the water column in the nearshore locations and extends deeper than 20 m farther offshore (see Figure 5-8 and Figure 5-9). These are consistent with the observations of the photic depth discussed earlier with the light extinction coefficient (see Section 5.2.1). Once stratification sets in around late spring to early summer, the top 10 to 15 m are devoid of nutrients because of the spring production. Therefore, biomass production in summer months is largely limited to the lower edge of the photic zone where DIN still diffuses up from the lower portions of the water column (compare Figure 5-6 and Figure 5-9).

The model reproduced the higher observed chlorophyll a peaks in late winter/early spring and in the summer, but did not fully capture the magnitude of the observed chlorophyll a peak in the Cape Cod Bay area (F02) (Figure 5-7). As observed in 2019 to 2021, the late summer bloom was dominated by dinoflagellates, but unlike previous years there was not a significant bloom of *Karenia mikimotoi* in 2022 (Libby et al., 2023). Figure 5-20 shows that the model does simulate a peak of dinoflagellates biomass in late summer, but at a smaller magnitude for peak biomass or duration compared to 2021, showing good agreement with 2022 observations. As for previous years, near-surface simulated concentrations were usually in the same range as observations. Bottom chlorophyll a measurements appear similar to previous years. In Cape Cod Bay (station F02), some observed bottom concentrations in spring and summer were higher than near the surface. The observed chlorophyll a spring peak concentrations at station F02 were higher than previous years and the model underestimated the spring peak concentrations. Chlorophyll a concentrations in summer and fall were slightly underestimated at the observation stations at intermediate depths as well (Figure 5-7 and Figure 5-8). The mid-summer peaks observed at stations N01, F22, F23 and N18 were not reproduced by the model.

Simulated chlorophyll a concentrations decreased eastward from the coast (Figure 5-9). The early spring increase (March 23) occurred throughout the water column (~30-40 m) as it was relatively well mixed. During the months in which stratification occurred, simulated bottom chlorophyll a remained low and highest values occurred in the subsurface, near the bottom edge of the photic depth. In the summer, the highest measured concentrations were slightly shallower than the modeled depth of peak concentrations (e.g., July 26). In July, highest simulated concentrations occurred in the subsurface in the vicinity of the outfall (station N21), which was not clearly confirmed by the field data.

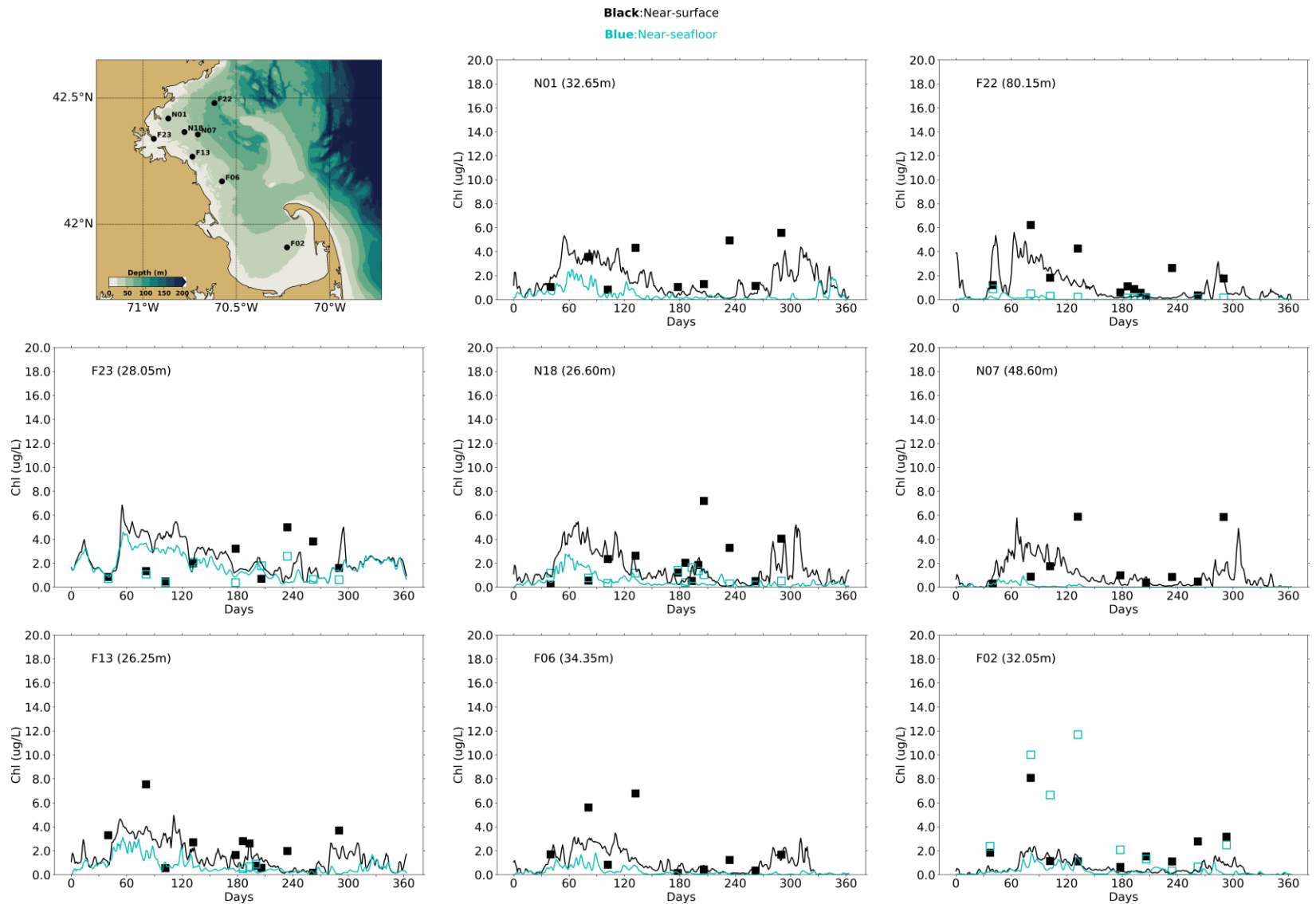


Figure 5-7 Chlorophyll a time series, model-observation comparison near surface and seafloor. Model results: lines. MWRA vessel-based survey observations: symbols.

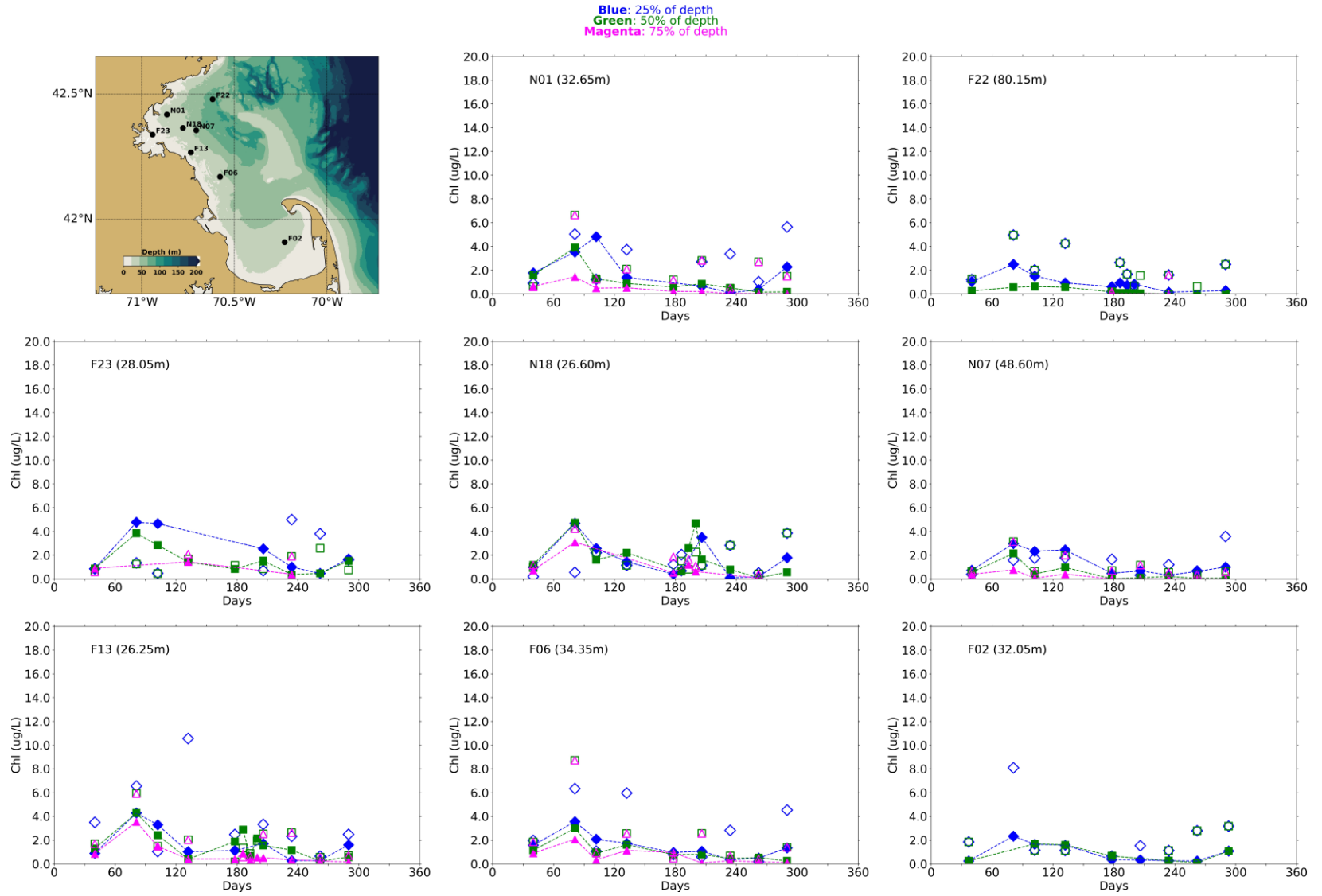


Figure 5-8 Chlorophyll a time series, model-observation comparison within water column (between surface and seafloor). Model results: lines and full symbols. MWRA vessel-based survey observations: empty symbols.



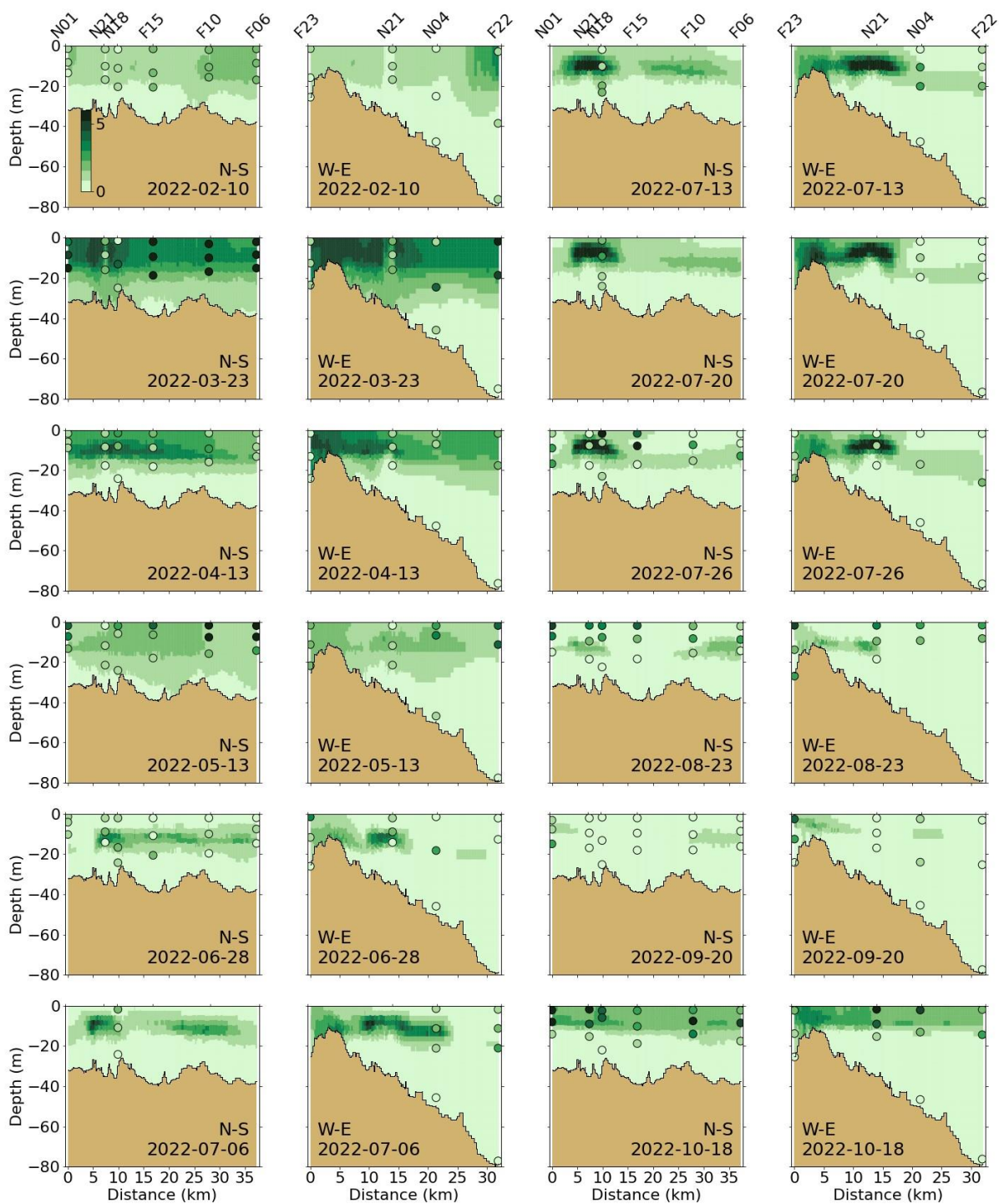


Figure 5-9 Chlorophyll a ( $\mu\text{g/L}$ ) for 2022 along North-South (N-S) and West-East (W-E) transects (Figure 2-4). MWRA measurements are plotted with round symbols. Model results are 5-day averages around the sampling date.

#### 5.2.4 **Particulate organic carbon (POC)**

Observations of POC showed higher concentrations in spring and summer months with the upper layers exhibiting higher concentrations than the bottom (Figures 5-10 through 5-12). Particulate organic carbon peaks are consistent with the timing of the runoff events and the biomass production discussed in the previous section.

The model seemed to generally capture POC concentration ranges and vertical gradients at the plotted locations (Figure 5-10 and Figure 5-11). As for previous years, POC concentrations were overestimated at F23, closer to the harbor, and the model moreover underestimates summer near-surface concentrations at several locations (e.g. N01, F22) and does not capture the observed peak end of July at stations N18. This is consistent with the discussion in Section 5.2.3 about the model potentially missing or underestimating the phytoplankton peak in that period.

Model predicted POC concentrations decreased from the coast eastward (Figure 5-12). The signature of the outfall was not visible in the deeper layers along either the North-South or the West-East transects. This was consistent with the fact that the MWRA outfall only represented a small part of the total non-oceanic OC inputs to the study area (Figure 3-6). During periods of stratification, concentrations are higher in the subsurface, most likely due to higher phytoplankton biomass. Highest simulated concentrations occurred in the subsurface in July in the NorthWest, directly in the vicinity of the outfall (station N21). This coincides with highest simulated chlorophyll a concentrations.

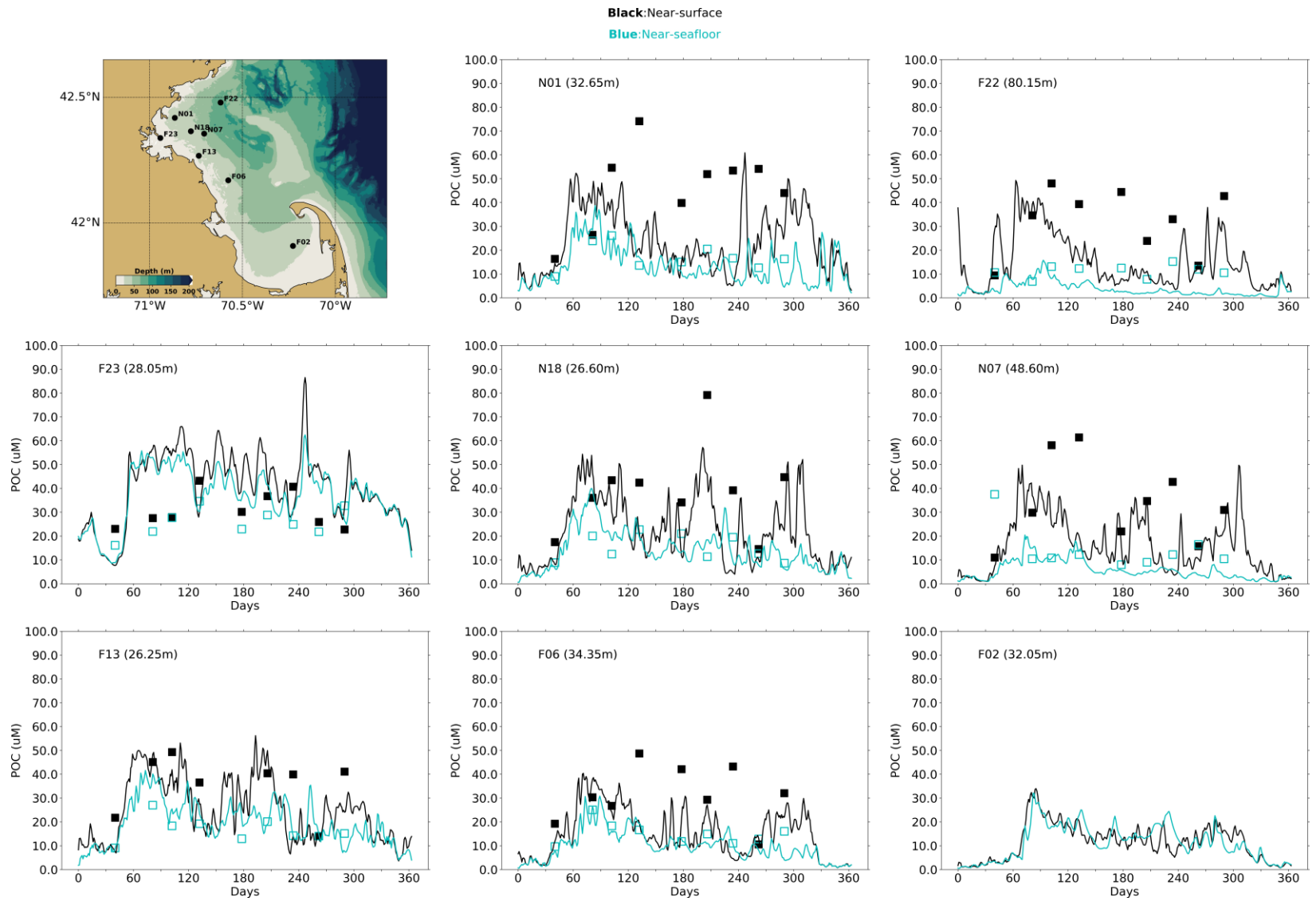


Figure 5-10 Particulate Organic Carbon time series, model-observation comparison near surface and seafloor. Model results: lines. MWRA vessel-based survey observations: symbols.



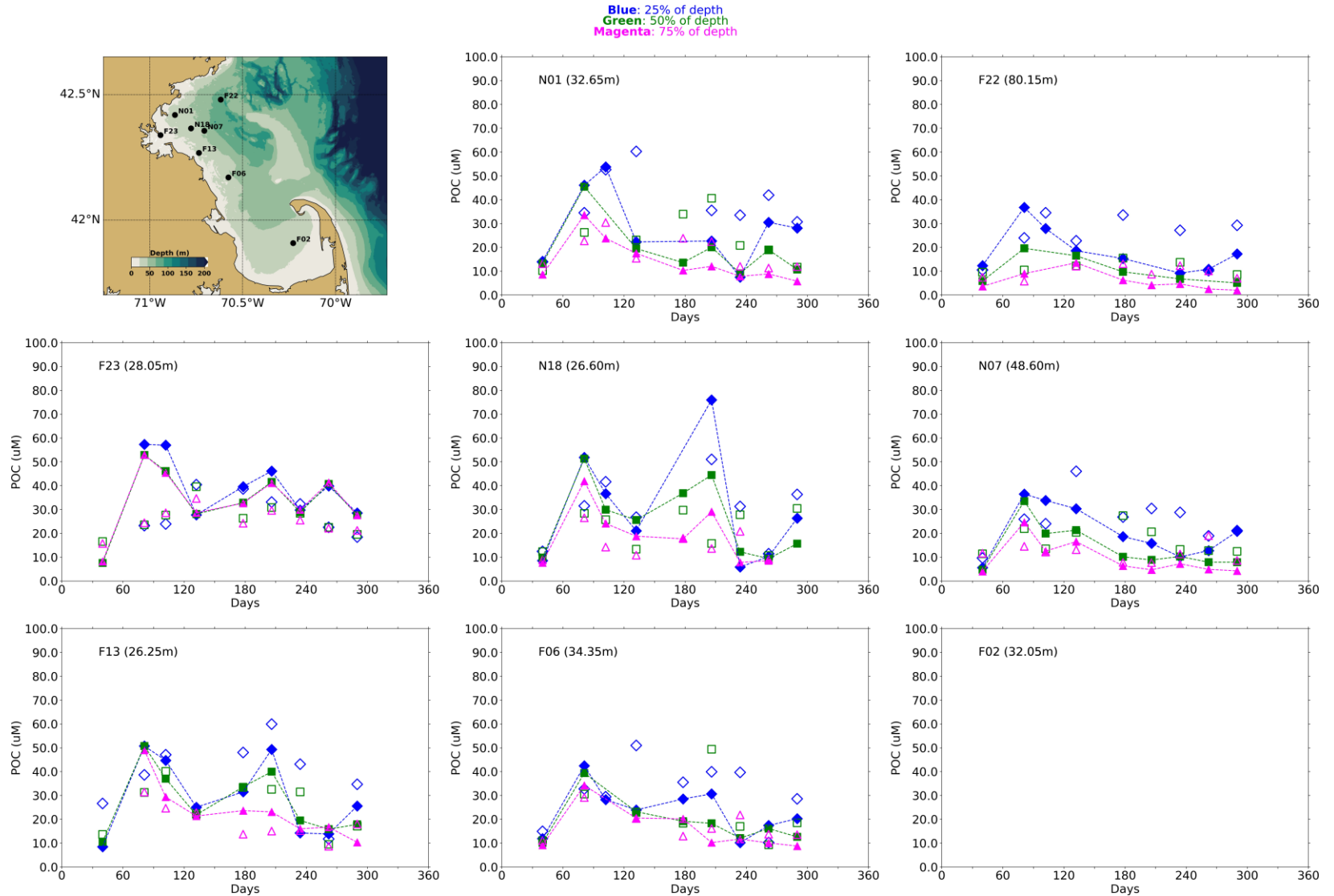


Figure 5-11 Particulate Organic Carbon time series, model-observation comparison within water column (between surface and seafloor). Model results: lines and full symbols. MWRA vessel-based survey observations: empty symbols.

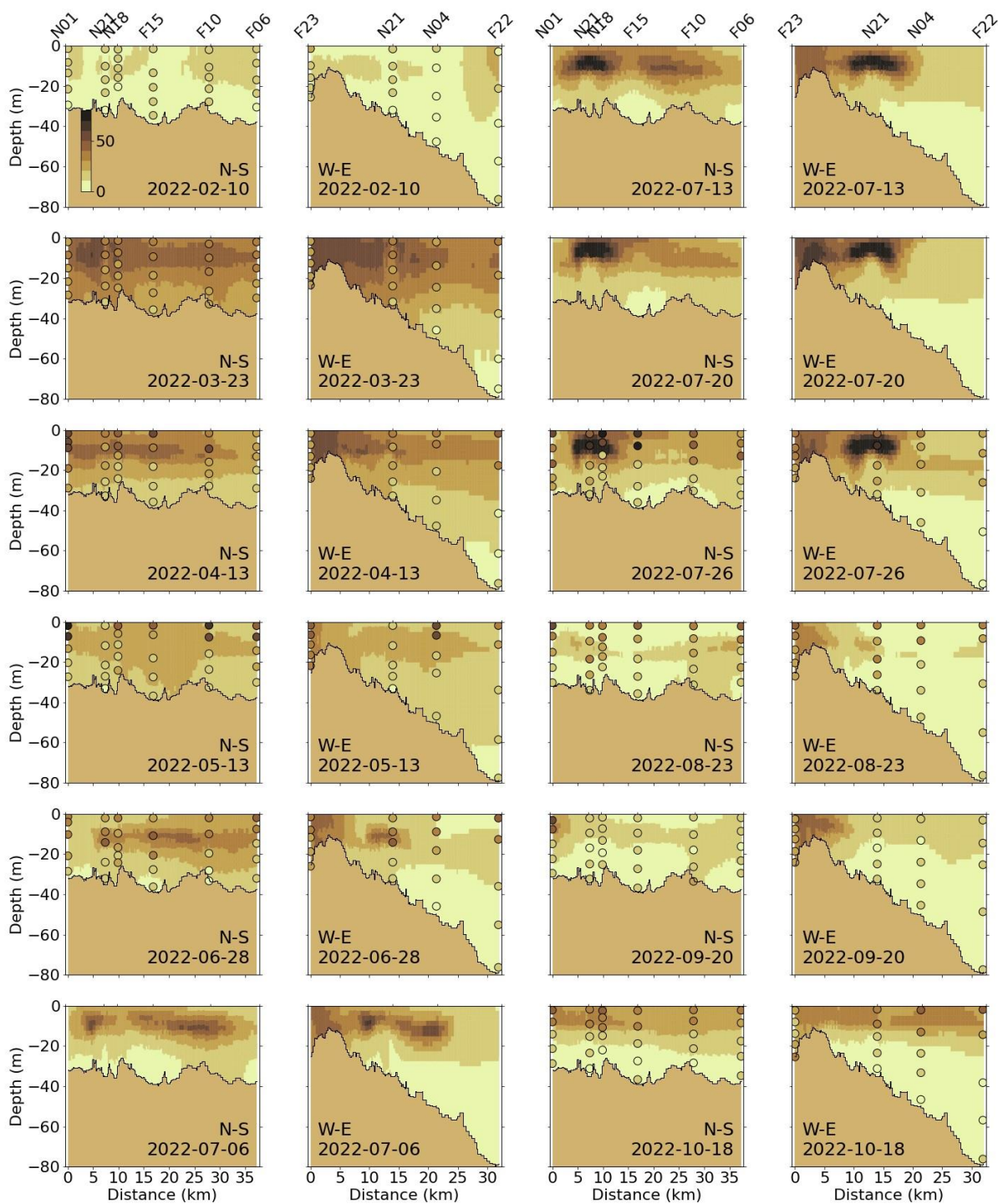


Figure 5-12 Particulate Organic Carbon ( $\mu\text{M}$ ) for 2022 along North-South (N-S) and West-East (W-E) transects (Figure 2-4). MWRA measurements are plotted with round symbols. Model results are 5-day averages around the sampling date. Frames without field observations are ARRS (Alexandrium) survey dates (7/6, 7/13, 7/20).

### 5.2.5 Dissolved oxygen

The 2022 seasonal variations of near-surface DO concentrations were well reproduced, with maximum concentrations observed at the end of winter or beginning of spring and decreasing until the end of summer before rising again (Figure 5-13). While winter concentrations at the surface and the bottom were comparable, bottom concentrations dropped lower at the end of the summer and beginning of fall. Differences between top and bottom observed concentrations reached about  $3 \text{ mg L}^{-1}$  at the end of October at several stations. Field measurements reported historic minima of DO at many stations in September and October. The field measurements included unusually low bottom DO concentrations at stations N01, F22, N07, F13, and F06 at the end of the summer/beginning of fall. The model does not capture these lowest concentrations at the plotted stations. The slope of the bottom DO concentration decrease in summer and fall is underestimated by the model at all stations and is even smaller than the slope modelled for near-surface concentrations, leading to a slight overestimation of bottom DO concentrations in summer and a strong overestimation of bottom DO concentrations in the fall. The model-observation comparison at intermediate water depths showed similar behavior (Figure 5-14).

At the A01 mooring station, the model reproduced the general seasonal pattern in the observed DO well. However, the model underestimated the slope of DO decrease in summer and the beginning of fall and, as a consequence, overestimated the end-of-fall minimum by about  $2.2 \text{ mg L}^{-1}$  (Figure 5-15).

As for previous years, the North-South and West-East cross-section plots show that DO generally had weak vertical gradients (Figure 5-16). Concentrations were higher at the end of winter and beginning of spring and decreased until fall. The model reproduced the elevated DO observations in the subsurface, where phytoplankton biomass was present, at the end of spring or early summer. It overestimated the DO concentration directly above the outfall. Several low DO observations (lower than  $6 \text{ mg L}^{-1}$ ) in deep water were not fully captured by the model in September and October. The overestimation of DO in late summer and fall may reflect the model's underestimation of the summer dinoflagellate bloom event in the offshore locations when the bloom termination and subsequent detrital decomposition in the water column likely caused the lower observed DO. It is noted that this seems to be a phenomenon occurring not just in Massachusetts Bay but also in the larger Gulf of Maine area.

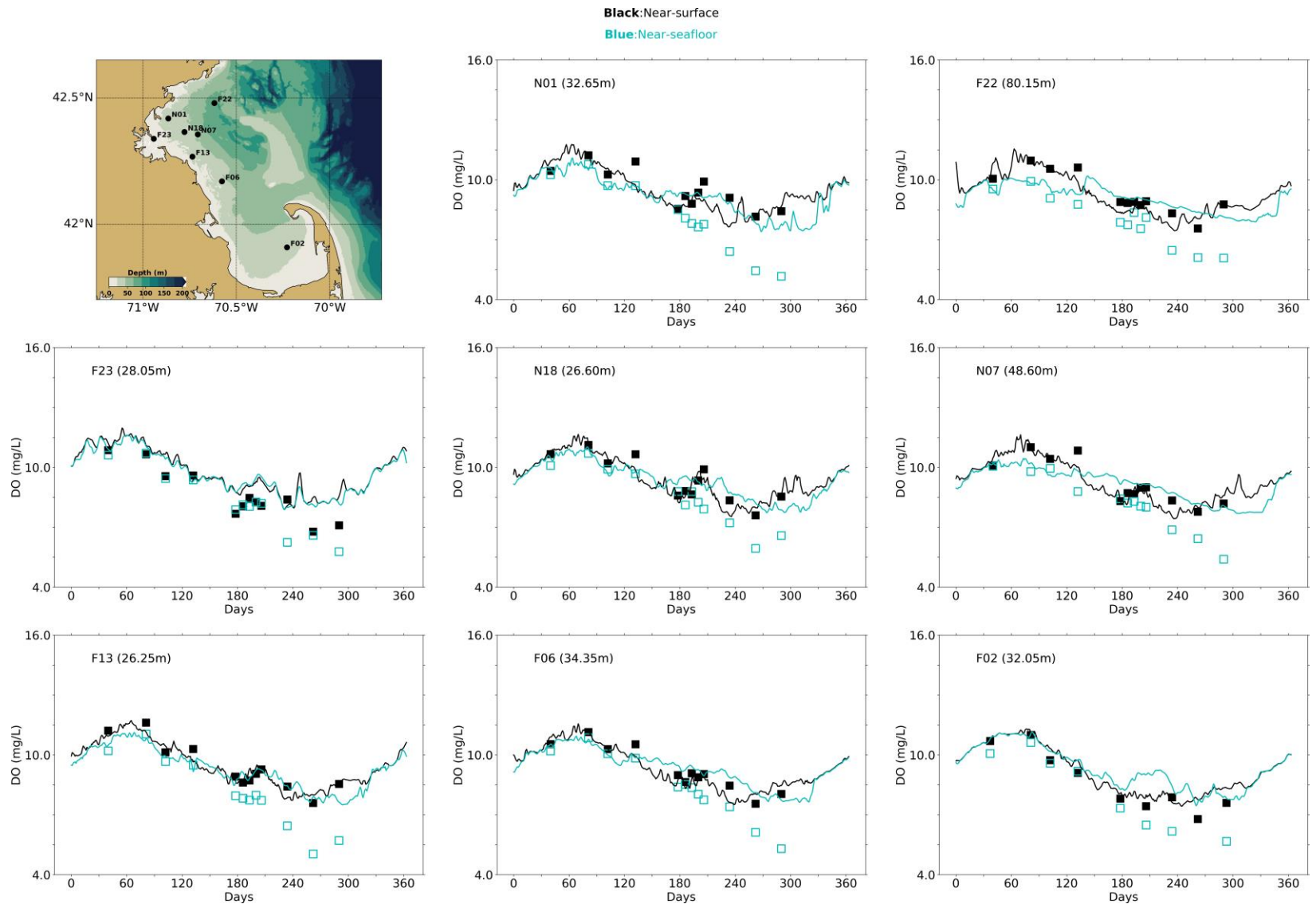


Figure 5-13 Dissolved Oxygen time series, model-observation comparison near surface and seafloor. Model results: lines. MWRA vessel-based survey observations: symbols.

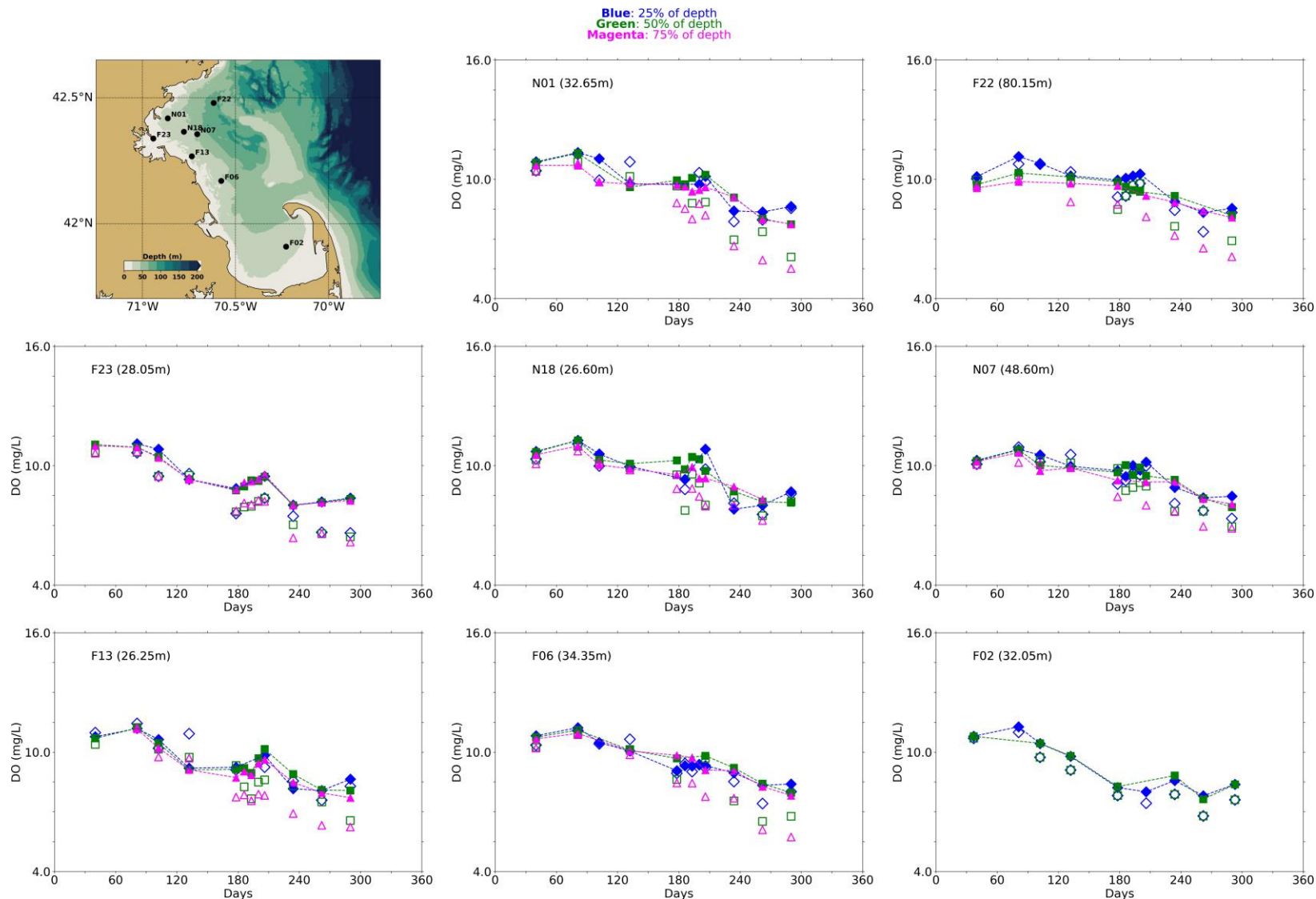


Figure 5-14 Dissolved Oxygen time series, model-observation comparison in water column. Model results: lines and full symbols. MWRA vessel-based survey observations: open symbols.



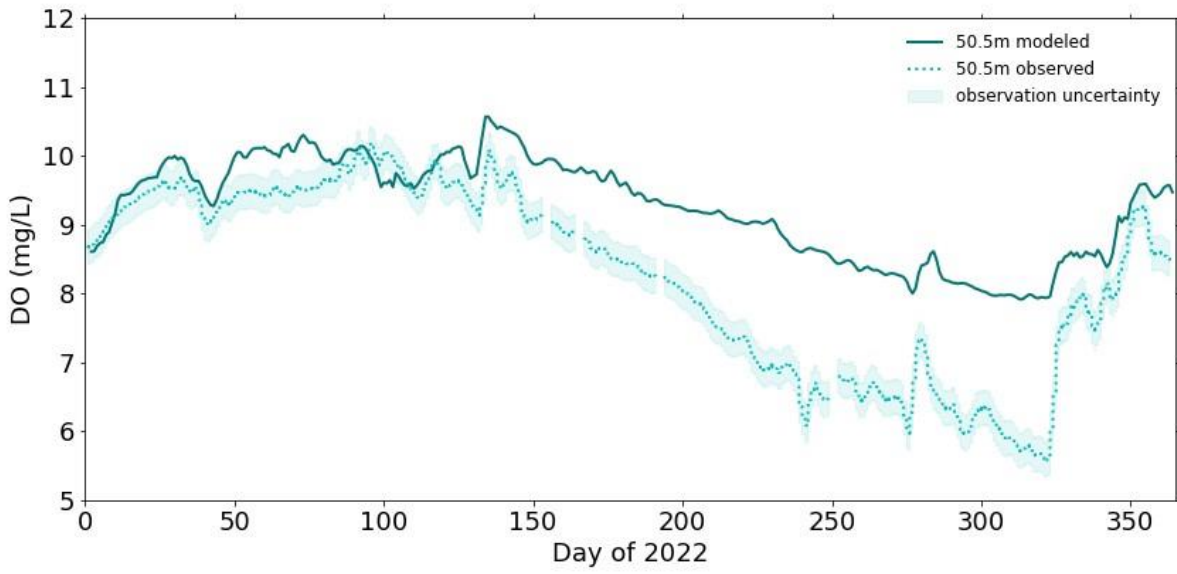


Figure 5-15 Dissolved Oxygen time series 50.5m deep at A01 mooring site, model-observation comparison for 2022.

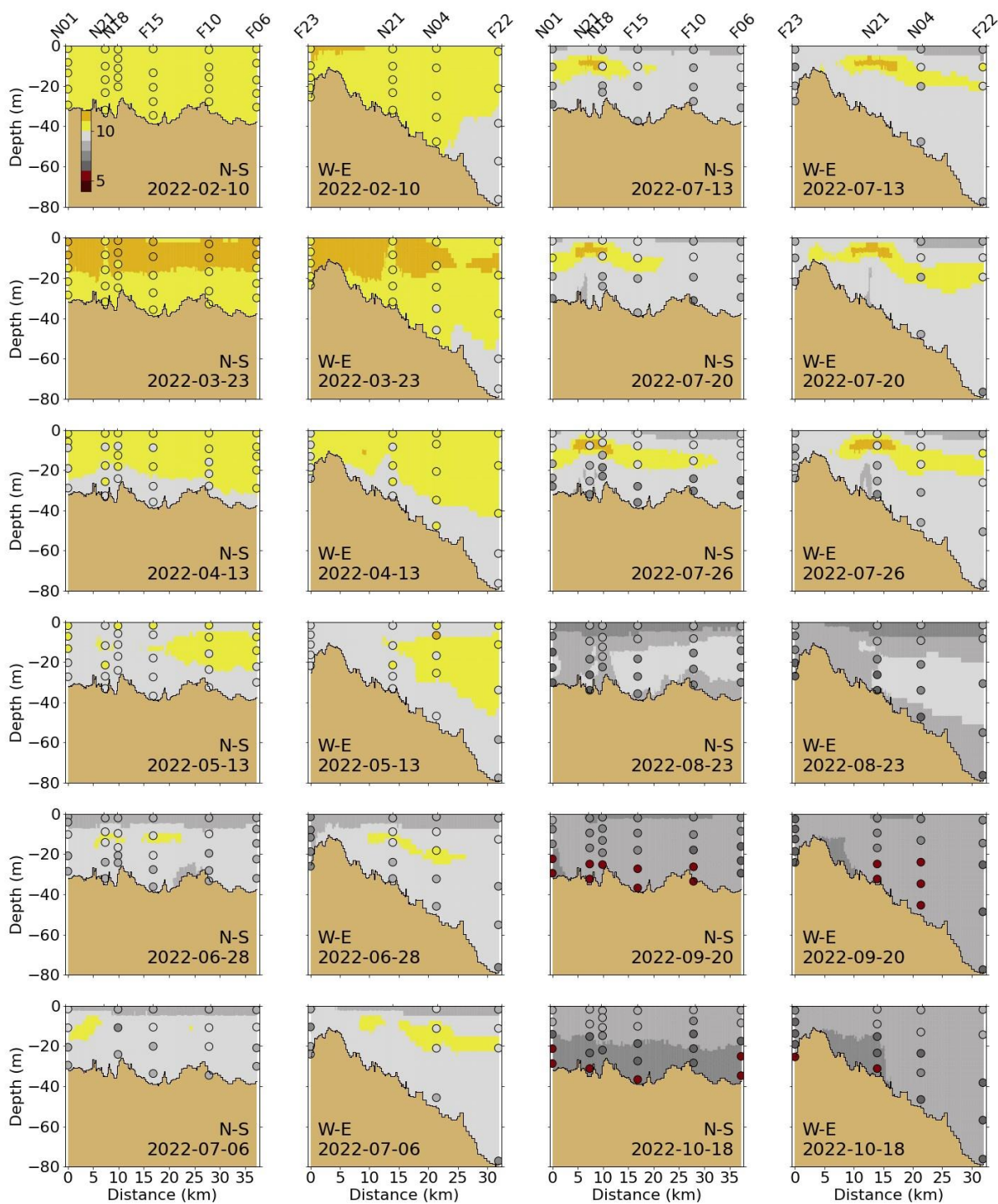


Figure 5-16 Dissolved Oxygen (mg/L) for 2022 along North-South (N-S) and West-East (W-E) transects (Figure 2-4). MWRA measurements are plotted with round symbols. Model results are 5-day averages around the sampling date.

## 5.2.6

### **Primary production**

Simulated primary production was compared to historical measurements at three monitoring locations (Figure 5-17). Box whiskers represent the 9th, 25th, 50th, 75th, and 91st percentiles of primary production observations over the period 1995-2010 (Keay et al., 2012). Primary production was in the range of historical measurements for the entire year 2022 at stations N04 and N18. Simulated primary production at station F23 was lower than historical measurements in the summer period. Highest simulated primary production at F23 occurred in September, similar to 2021 and slightly later than for previous years.



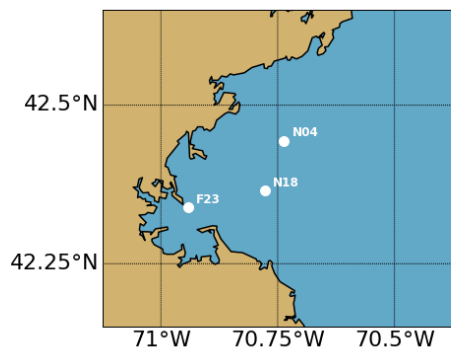
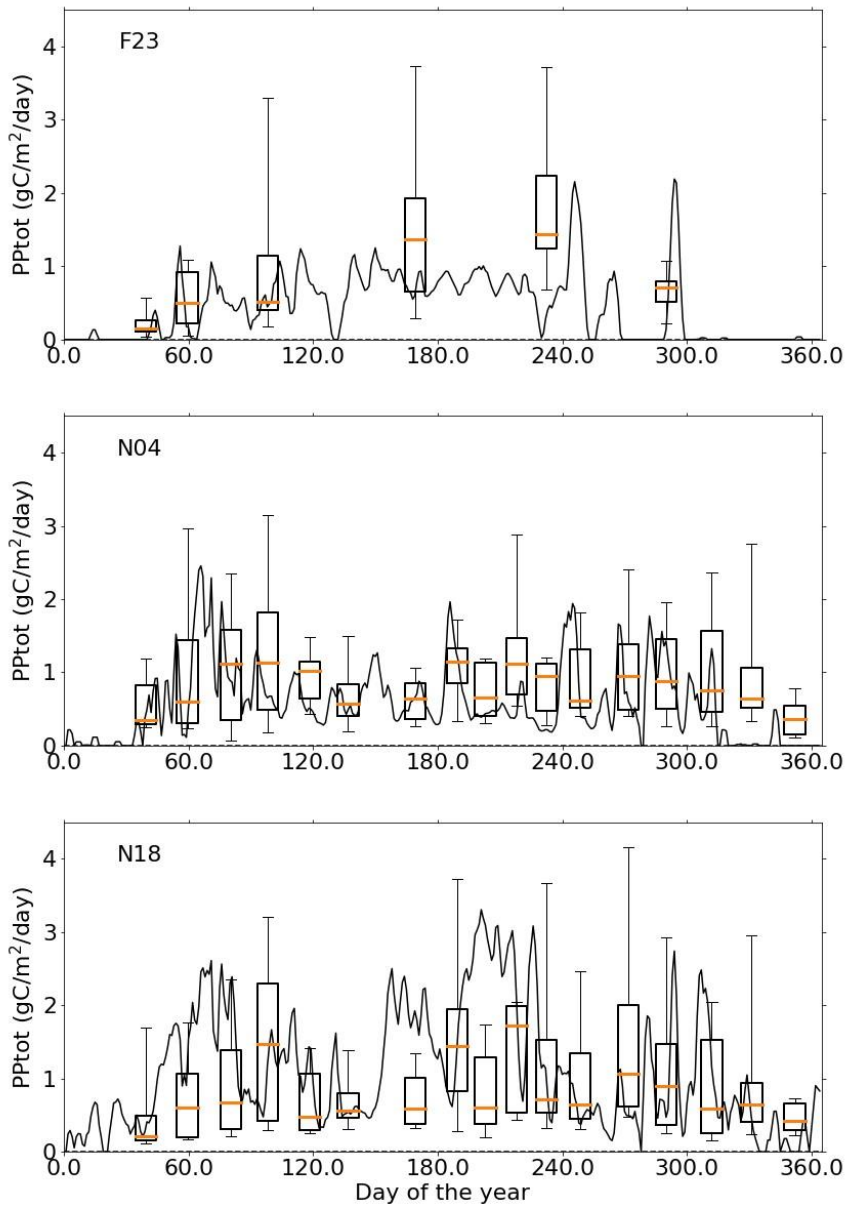


Figure 5-17 Simulated (lines; 2022) and observed (box-whiskers; 1995-2010) primary production.

### 5.2.7 Fluxes to and from the sediment

Sediment NH<sub>4</sub> fluxes (Figure 5-18) and sediment oxygen demand (Figure 5-19) outputs from the model were compared to measurements from the 2001-2010 period from Tucker et al. (2010) at stations located in Boston Harbor and Massachusetts Bay using plots in the same format as Figure 5-17.

Simulated sediment fluxes were low in winter and peaked in the summer due to higher temperatures favorable to biogeochemical activity, which mineralizes organic matter in the sediment. Sediment fluxes were higher in the harbor area than in Massachusetts Bay, which was captured by the model. Results for the year 2022 were similar to those from the individual years 2012 to 2016. These were mostly in the range of historical measurements, except for NH<sub>4</sub> sediment fluxes at the Mass Bay stations (MB01, MB03 and MB05). This discrepancy is related to the simplified representation of sediment biogeochemical processes (see Deltares, 2021).

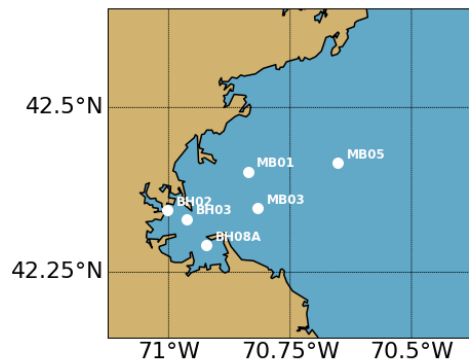
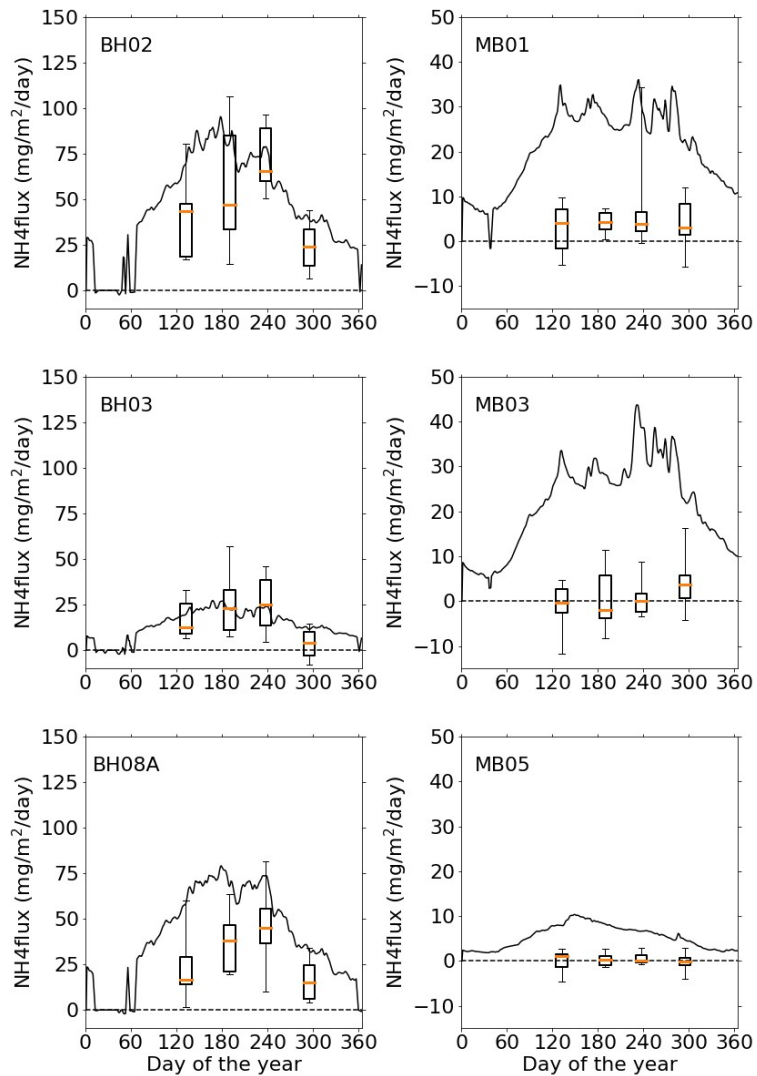


Figure 5-18 Simulated (line; 2022) and observed (box-whiskers; 2001-2010) sediment flux of ammonium. Note change of scale between the Boston Harbor stations (left) and Mass Bay stations (right).

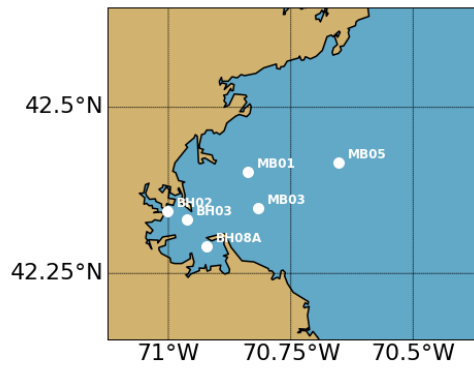
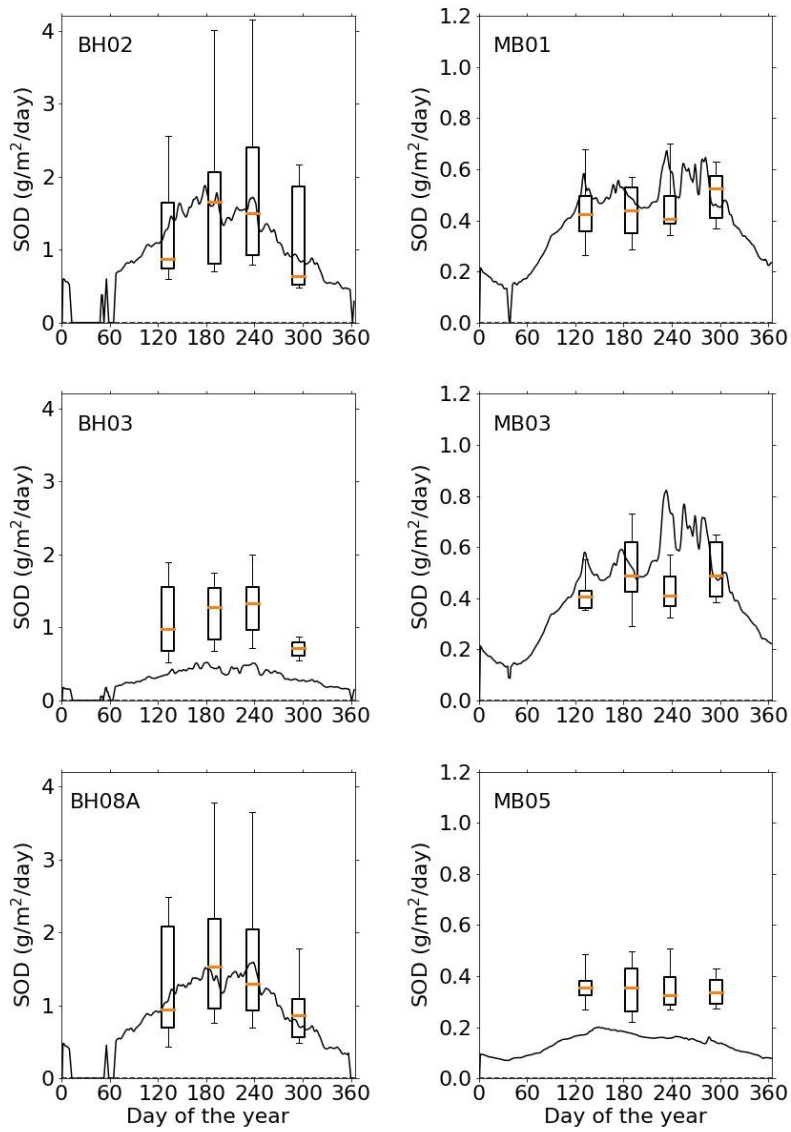


Figure 5-19 Simulated (line; 2022) and observed (box-whiskers; 2001-2010) sediment oxygen demand. Note change of scale between the Boston Harbor stations (left) and Mass Bay stations (right).

### 5.3 Phytoplankton community composition

Model phytoplankton community/species composition was not validated against field observations during model setup and calibration/validation. However, it is of interest to verify that its main characteristics in the model are consistent with general patterns known to characterize the bays, based on monitoring observations.

The phytoplankton sub-module (BLOOM) simulated the dynamics of 4 functional groups and their adaptation to changing environmental conditions (i.e., light and nutrient limitation). BLOOM simulates the rapid shifts in phytoplankton communities due to these changes, using linear programming to optimize whole-community net primary production (Los, 2009). Simulated phytoplankton groups include: diatoms, dinoflagellates, other marine flagellates, and the genus *Phaeocystis*. Their parameterization was initially based on that used in the North Sea eutrophication model (Blauw et al., 2009) and tuned during the BEM calibration process to better represent chlorophyll a as well as observed PON:POC ratios at MWRA monitoring locations (see Appendix B of Deltares, 2021).

Figure 5-20 shows the share of the different simulated phytoplankton groups in the total phytoplankton biomass near the water surface. Although total phytoplankton biomass temporal dynamics differed from station to station for the year 2022, phytoplankton composition showed similar temporal patterns. Marine diatoms dominated in the winter period and were succeeded in spring by marine flagellates. Dinoflagellates clearly dominated from June to October. This is similar to the simulated successions in communities for the previous years (2017-2021).

In 2022, increases in spring chlorophyll were observed, which, along with changes in nitrogen and silica concentrations observed in surveys from March to May, suggests a possible *Phaeocystis* bloom. However, the *Phaeocystis* abundances were relatively low (Libby et al., 2023). The simulated *Phaeocystis* biomass in the model showed a noticeable increase in levels during the spring flagellate bloom period (March-April) in Cape Code Bay and a minor increase in levels at multiple stations further north in late-May.

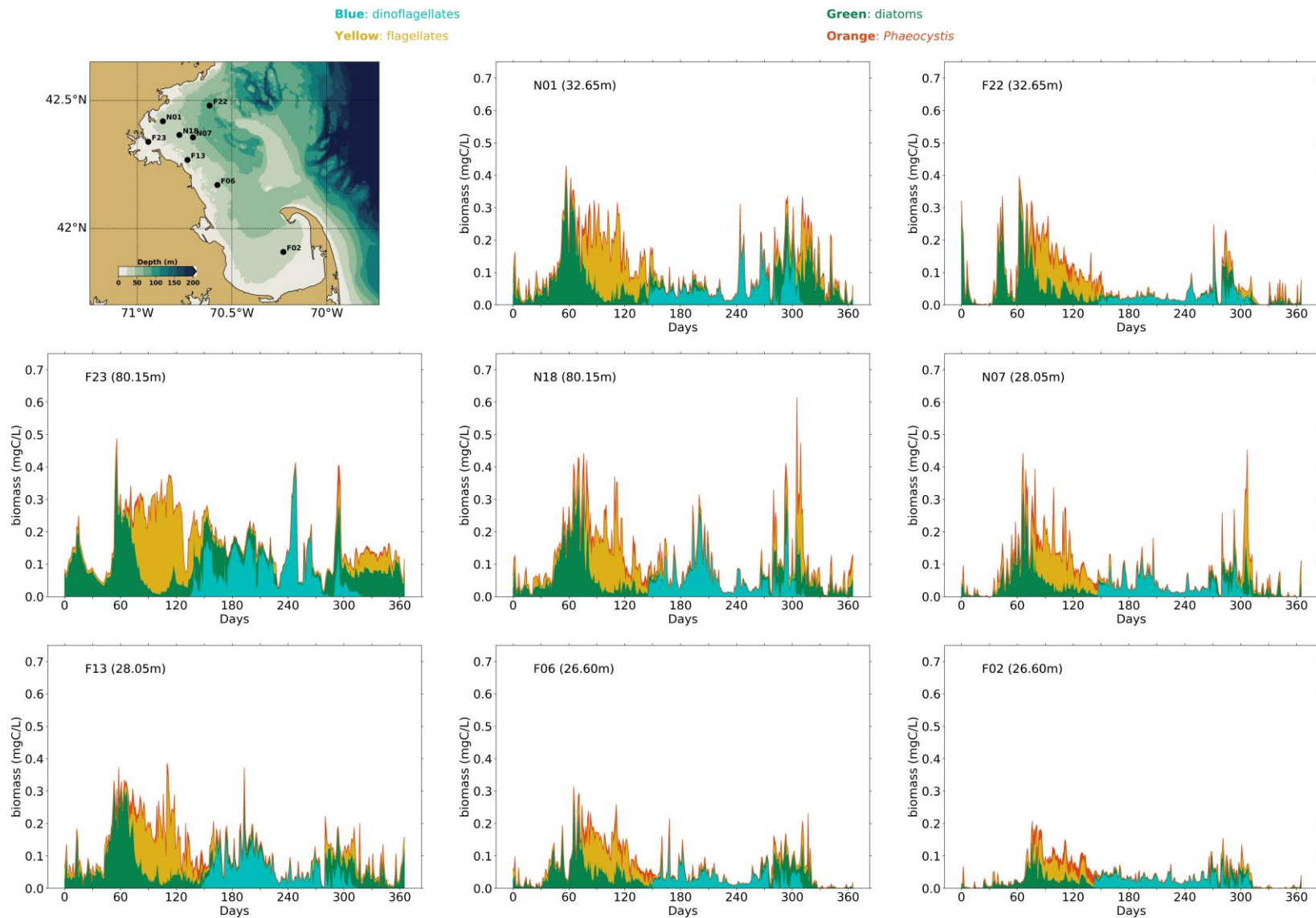


Figure 5-20 Simulated phytoplankton biomass time-series. Biomasses of the 4 simulated species groups (dinoflagellates, other flagellates, diatoms and *Phaeocystis*) are stacked.

## 5.4 Conditions on West-East transect through outfall

The signature of the outfall in terms of DIN concentrations was visible all year round, with increased concentrations up to a distance of about 10 km (Figure 5-21). The increased DIN was trapped in the lower layers of the water column in the period of stratification (April-September/October). During the other months, the effluent led to an increase in surface DIN concentrations. These temporal patterns were similar to those observed in previous years.

Except for a few summer months (June to August), chlorophyll a concentrations were higher nearshore (Figure 5-22). This was most likely due to the nutrient inputs from rivers to the harbor area, promoting algal growth (even though these discharges were lower than average in the period May-December). Further offshore, highest chlorophyll a concentrations were simulated in late winter/early spring near the surface. In summer months, maximum chlorophyll a concentrations occurred at a depth of ~10-20 m, approximately at the edge of the photic depth and consistent with the availability of DIN limited predominantly to the bottom waters under stratified conditions. These patterns were mostly similar to those simulated for previous years. However, for June to August a chlorophyll a maximum was simulated near the outfall at a depth of around 10m, right at the upper limit of the outfall plume. These simulated higher concentrations were most likely enabled by specific 2022 summer environmental conditions, such as weaker wind and less circulation than previous years (Figure 4-13 and Figure 4-14). It cannot be excluded that this simulated local maximum is connected to the models's underestimation of the light extinction coefficient; both phenomena were not present in simulations for earlier years. Note that the simulated conditions of high summer chlorophyll near the outfall were not reflected in the field observations.

The vertical cross-sections of DO concentrations for 2022 showed similar temporal and spatial patterns as for previous years, but slightly shifted in time (Figure 5-23). The highest concentrations occurred near the surface in February and March, similar to 2021. The highest concentrations between May and July occurred slightly under the surface, which corresponded to the depths at which chlorophyll a was the highest. No clear effect of the outfall on DO concentrations was visible in the plotted cross sections.



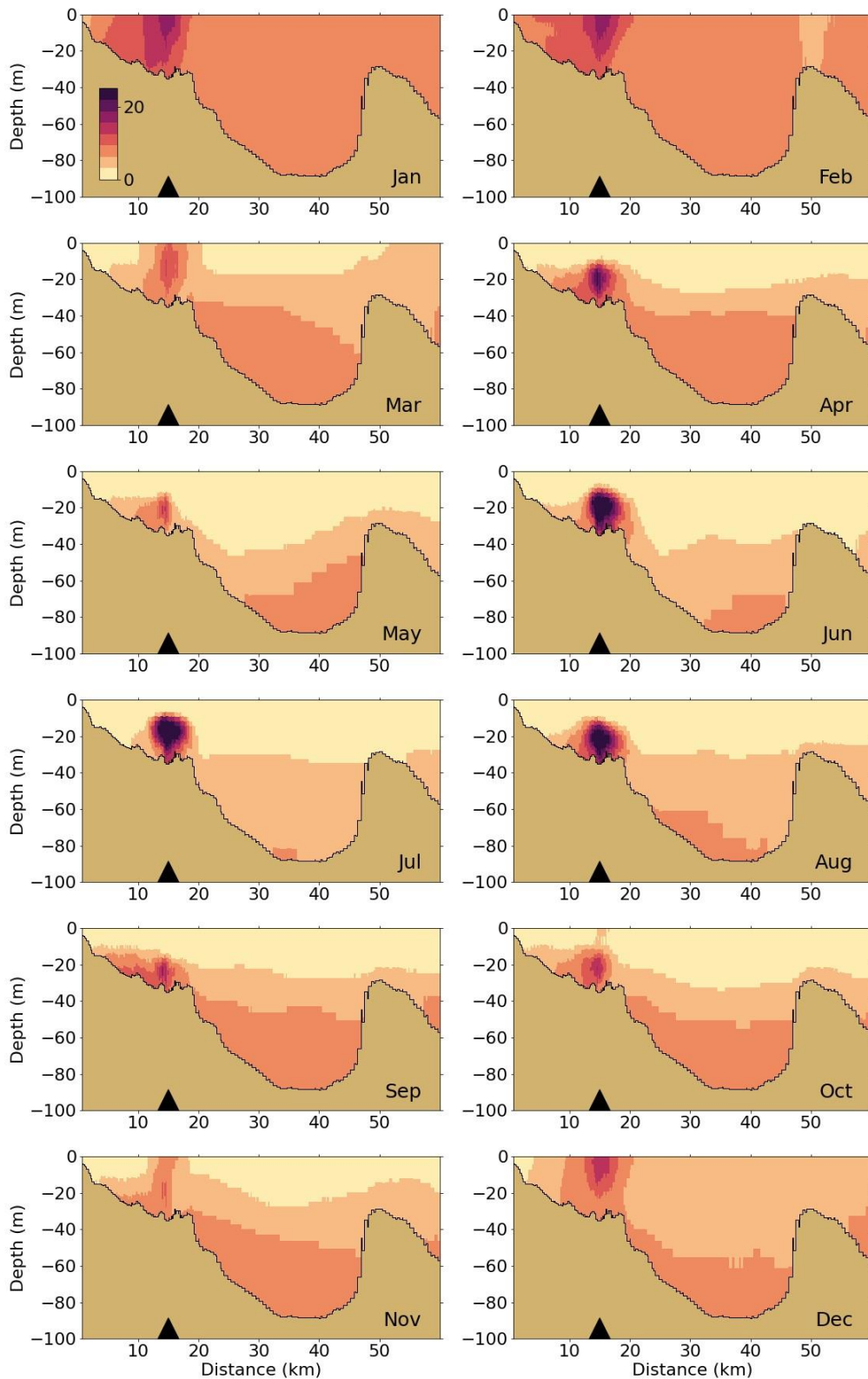


Figure 5-21 Dissolved Inorganic Nitrogen ( $\mu\text{M}$ ) for 2022 along west-east transect (Figure 2-4). Horizontal axis is distance eastward from coast; black triangle indicates the location of the outfall on the seafloor.

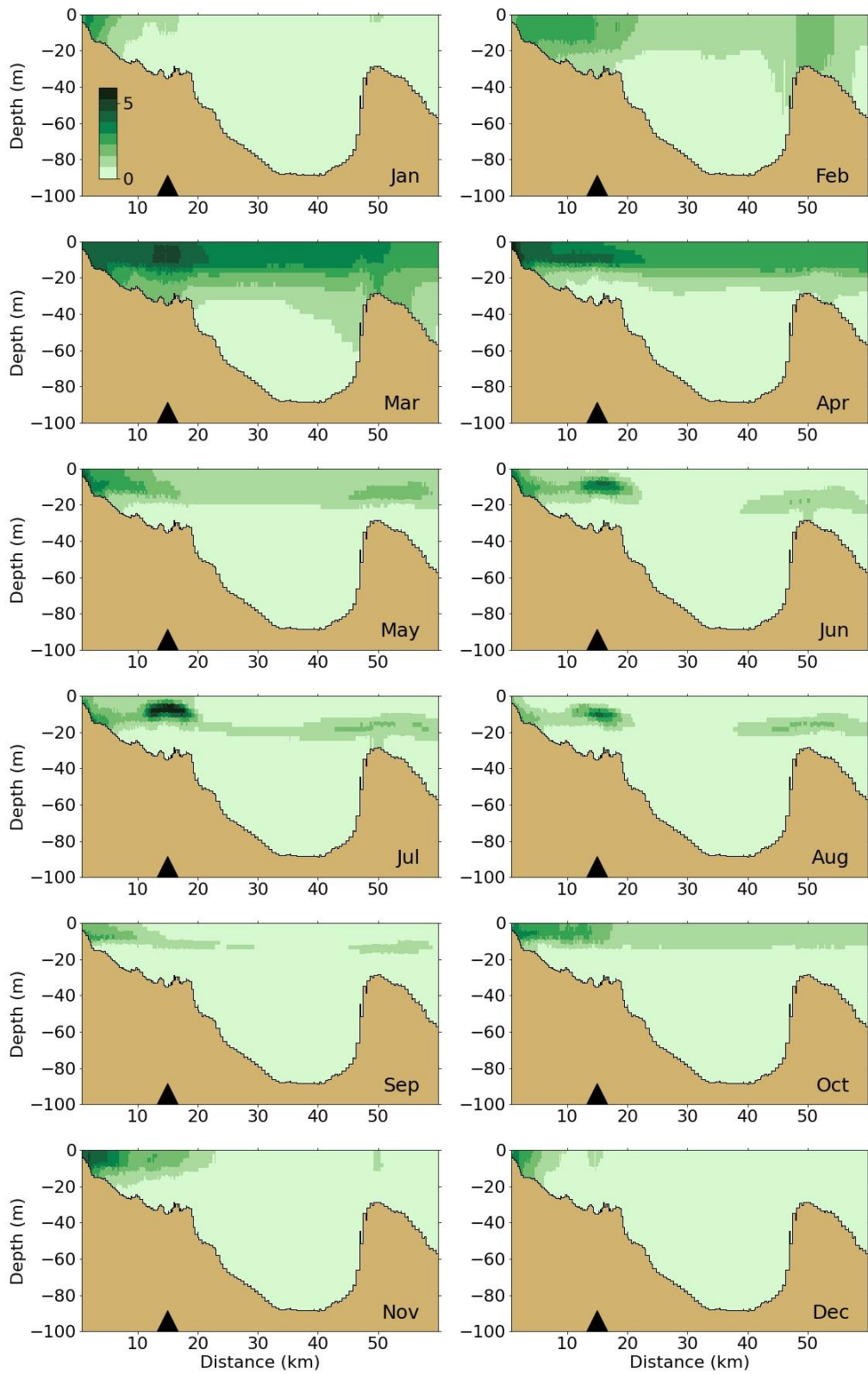


Figure 5-22 Chlorophyll a ( $\mu\text{g/L}$ ) for 2022 along west-east transect (Figure 2-4). Horizontal axis is distance eastward from coast; black triangle indicates the location of the outfall on the seafloor.

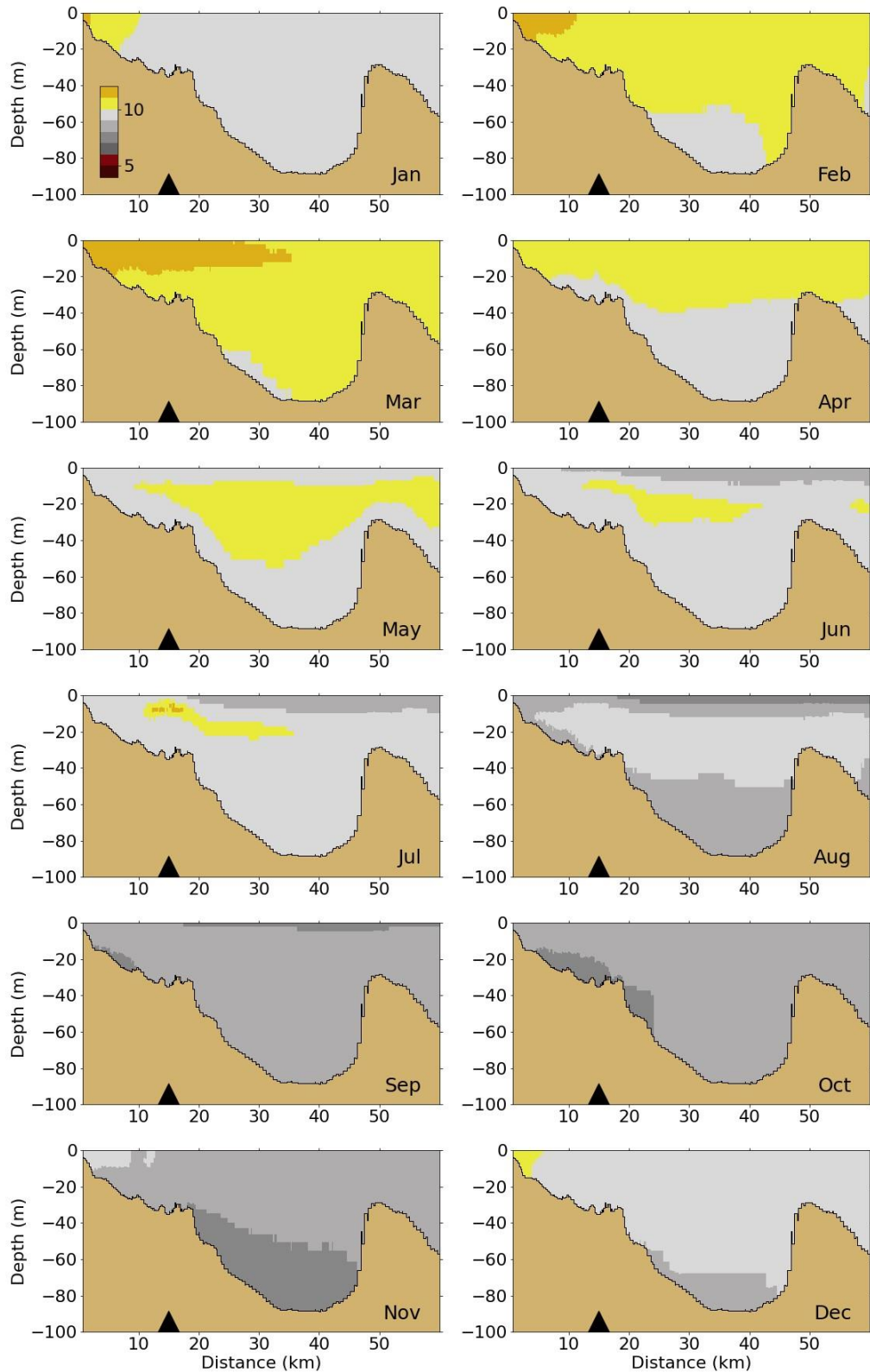


Figure 5-23 Dissolved Oxygen for 2022 along west-east transect (Figure 2-4). Horizontal axis is distance eastward from coast; black triangle indicates the location of the outfall on the seafloor.

## 6 Synthesis/Application

There are no synthesis/application simulations focused on the year 2022.

## 7 Conclusion

The performance of the hydrodynamic model was comparable to previous years. Temperatures were reproduced accurately, especially at the surface, even considering that the observed summer surface water temperature were generally above historical levels (Libby et al., 2023). The quality of modeled salinity was comparable to previous years at most stations.

At most stations, temperature stratification was present from April until mid-November with its maximum in July and August. Observed and modeled temperature stratification were similar. The surface salinity in 2022 summer was high in response to the unusually low river flow (Libby et al., 2022). As a result, in line with observations, only very limited salinity stratification was modeled.

Modeled non-tidal current patterns were similar to observations, but the temporal variability was slightly smaller. Magnitudes near the surface were largely similar to observations, with the exception of the underestimation in mid-August. At the bays-wide scale, the expected circulation pattern driven by the Western Maine Coastal Current was visible in the model. In general, the agreement between the hydrodynamic model and the observations was sufficient to conclude that the representation of processes was adequate to support water quality modeling.

Light extinction for the year 2022 was within similar ranges than previous years, even though on average slightly higher. The model slightly underestimated extinction at most stations, but represented variability well. Seasonal variations of surface and bottom DIN concentrations in 2022 were similar to those observed and simulated for previous years. Surface and bottom were comparable in winter, when the water column was well mixed. Surface DIN concentrations declined at the end of winter and were depleted from April to October, before increasing again mid-fall. Bottom concentrations remained stable or declined to a much lesser degree than surface concentrations, in spring and summer. The model generally reproduced these observed seasonal variations and vertical differences throughout the water column.

Seasonal variations of chlorophyll a observations in 2022 were similar to previous years except that there was no significant dinoflagellates (*Karenia mikimotoi*) bloom observed in late summer 2022. The model simulated the higher chlorophyll a peaks in early spring and in late summer. As for previous years, near surface simulated concentrations were in the same range as observations. Temporal variability was generally reproduced but the corresponding chlorophyll a peak concentrations were often underestimated, due to an underestimation of the phytoplankton biomass and/or of the community's chlorophyll-to-carbon ratio. Simulated chlorophyll a concentrations mostly decreased eastward from the coast. Early spring increases occurred throughout the relatively well-mixed water column. During the more stratified months, simulated bottom chlorophyll a remained low and highest values occurred near surface in the nearshore locations, and at the subsurface at the edge of the photic zone farther offshore where nutrients were depleted near the surface.

Particulate organic carbon (POC) concentrations at the observation stations showed generally higher levels in summer months and were generally consistent with biomass production at the offshore locations. Measured POC concentrations were highest closer to the harbor, likely due to the high river POC inputs. Concentrations were significantly lower near the bottom than at the surface. The model generally captured these POC variability and vertical gradients, but underestimated near-surface summer concentrations at most stations and overestimated concentrations near the harbor. As for

extinction, the underestimation by the model is specific to the year 2022 and has not been noted for previous years. It is probably the consequence of specific environmental conditions in 2022, i.e. high temperatures, low runoff inputs and low wind and currents over prolonged periods. As for chlorophyll a, simulated POC concentrations decreased from the coast eastward.

The vertical cross-sections of DO concentrations for 2022 showed similar temporal and spatial patterns as for previous years, with the highest concentrations occurring near the surface between January and April. The 2022 seasonal variations of DO concentrations were overall well reproduced in the model, with maximum concentrations observed at the end of winter or early spring and decreasing until fall before rising again. While winter concentrations at the surface and the bottom were comparable, bottom concentrations dropped lower at the end of the summer and beginning of fall. As for previous years, the model tended to overestimate summer bottom concentrations. Some of this may be attributed to the fact that the field measurement campaign observed historic minima of DO at many stations in 2022 summer and some unusually low DO concentrations in deep waters in late summer. The model-observation comparison at intermediate water depths showed similar behavior: in fall, the decrease in DO throughout the water column was slightly underestimated. The North-South and West-East cross-section plots show that DO generally had weak vertical gradients. Concentrations were higher at the end of winter and early spring and decreased until fall. Slightly higher concentrations were observed and simulated in the subsurface, where phytoplankton biomass is located, at the end of spring or early summer. The observed vertical gradients in DO concentrations were underestimated by the model in summer and fall.

Although total phytoplankton biomass temporal dynamics differed from station to station, phytoplankton composition showed similar temporal patterns across stations. Diatoms dominated in the winter period and were succeeded in spring by flagellates. Dinoflagellates clearly dominated from June to the end of October. These were typical characteristics of community composition seen in monitoring observations. Simulated *Phaeocystis* biomass in the model showed noticeable levels during the spring flagellate bloom period (March-April). This is similar to the timing of a possible *Phaeocystis* bloom as suggested by observed chlorophyll increases and changes in nitrogen and silica concentrations (Libby et al., 2023).

The signature of the MWRA outfall in terms of DIN concentrations was visible all year round, with increased concentrations up to a distance of about 10 km. The increased DIN concentrations were trapped in the lower layers of the water column during the period of stratification (April to October). During the other months, the effluent led to an increase in surface DIN concentrations as well. These temporal patterns were similar to those observed in previous years. For all year round except for the summer months (June-August), chlorophyll a concentrations were higher nearshore. This was most likely due to the nutrient inputs from rivers to the harbor area, promoting algal growth. For June to August, the highest chlorophyll a concentrations were around the outfall, potentially indicating an impact of the outfall. This impact was not visible in previous years, but may have been sparked in the model because both local non-residual current velocities and the Western Maine Coastal Current at Cape Ann were on the low side in the 2022 summer. It cannot be excluded that the local and temporal chlorophyll a maximum near the outfall is an artefact of the model's underestimation of the light extinction coefficient. It is further noted that these higher concentrations cannot be confirmed from the field data.



# References

- Alessi, Carol A., Beardsley, Robert C., Limeburner, Richard, Rosenfeld, Leslie K., Lentz, Steven J., Send, Uwe, Winant, Clinton D., Allen, John S., Halliwell, George R., Brown, Wendell S., Irish, James D., 1985. "CODE-2: moored array and large-scale data report", Woods Hole Oceanographic Institution Technical Report 85-35, DOI:10.1575/1912/1641. (<https://hdl.handle.net/1912/1641>)
- Blauw AN, HFJ Los, M Bokhorst and PLA Erftemeijer, 2009. GEM: a Generic Ecological Model for estuaries and coastal waters. *Hydrobiologia* 618: 175-198.
- Deltares, 2019a. D-Flow Flexible Mesh, Technical Reference Manual. Released for: Delft3D FM Suite 2020. Version: 1.1.0 SVN Revision: 63652. December 4, 2019.
- Deltares. 2019b. Delft3D Flexible Mesh Suite, D-Flow FM in Delta Shell, User Manual, Version 1.5.0, December 5, 2019 ([https://content.oss.deltares.nl/delft3d/manuals/DFlow\\_FM\\_User\\_Manual.pdf](https://content.oss.deltares.nl/delft3d/manuals/DFlow_FM_User_Manual.pdf))
- Deltares, 2021. Demonstration of the updated Bays Eutrophication Model. Boston: Massachusetts Water Resources Authority. Report 2021-02. 138 p. plus appendices. ([www.mwra.com/harbor/enquad/pdf/2021-02.pdf](http://www.mwra.com/harbor/enquad/pdf/2021-02.pdf))
- Deltares, 2022. Simulations of 2017 Hydrodynamics and Water Quality in the Massachusetts Bay System using the Bays Eutrophication Model. Boston: Massachusetts Water Resources Authority. Report 2021-12. 107 p. <https://www.mwra.com/harbor/enquad/pdf/2021-12.pdf>
- Deltares, 2023. Simulations of 2021 Hydrodynamics and Water Quality in the Massachusetts Bay System using the Bays Eutrophication Model. Boston: Massachusetts Water Resources Authority. Report 2023-07. 82 p. <https://www.mwra.com/harbor/enquad/pdf/2023-07.pdf>
- Hunt CD, RK Kropp, JJ Fitzpatrick, P Yodzis, and RE Ulanowicz, 1999. A Review of Issues Related to the Development of a Food Web Model for Important Prey of Endangered Species in Massachusetts and Cape Cod Bays. Boston: Massachusetts Water Resources Authority. Report ENQUAD 99-14. 62 p. (<http://www.mwra.state.ma.us/harbor/enquad/pdf/1999-14.pdf>)
- Keay KE, WS Leo, and PS Libby, 2012. Comparisons of Model-Predicted and Measured Productivity in Massachusetts Bay. Boston: Massachusetts Water Resources Authority. Report 2012-03. 11 p. plus Appendix. (<http://www.mwra.state.ma.us/harbor/enquad/pdf/2012-03.pdf>)
- Libby PS, Borkman DG, Geyer WR, Turner JT, Costa AS, Goodwin C, Wang J. 2023. 2022 Water Column Monitoring Results. Boston: Massachusetts Water Resources Authority. Report 2023-11. 69p. <https://www.mwra.com/harbor/enquad/pdf/2023-11.pdf>
- Los, FJ, 2009. Eco-hydrodynamic modeling of primary production in coastal waters and lakes using BLOOM. Ph.D. Thesis, Wageningen University, 2009.
- Taylor KE, 2001. Summarizing multiple aspects of model performance in a single diagram. *J. Geophys. Res.*, 106(D7), 7183–7192, doi:10.1029/2000JD900719.



- Tucker J, S Kelsey, and AE Giblin, 2010. 2009 benthic nutrient flux annual report. Boston: Massachusetts Water Resources Authority. Report 2010-10. 27 p.  
(<http://www.mwra.state.ma.us/harbor/enquad/pdf/2010-10.pdf>)
- Xue, P, C Chen, J Qi, RC Beardsley, R Tian, L Zhao, and H Lin, 2014. Mechanism studies of seasonal variability of dissolved oxygen in Mass Bay: A multi-scale FVCOM/UG-RCA application. Journal of Marine Systems. 131, 102-119.
- Zhao L, Beardsley RC, Chen C, Codiga DL, Wang L, 2017. Simulations of 2016 Hydrodynamics and Water Quality in the Massachusetts Bay System using the Bays Eutrophication Model. Boston: Massachusetts Water Resources Authority. Report 2017-13. 111p.  
(<https://www.mwra.com/harbor/enquad/pdf/2017-13.pdf>)

Deltares is an independent institute for applied research in the field of water and subsurface. Throughout the world, we work on smart solutions for people, environment and society.

**Deltares**



**Massachusetts Water Resources Authority**

**Deer Island**

**33 Tafts Avenue • Boston, MA 02128**

**[www.mwra.com](http://www.mwra.com)**

**617-242-6000**